Central Aerohydrodynamic Institute

TsAGI International, Inc.

EXPERIMENTAL AND THEORETICAL INVESTIGATION OF THE WEAKLY IONIZED

NON-EQUILIBRIUM PLASMA INFLUENCE ON A FLOW OVER BODIES OF SIMPLE

FORMS

Contract No. F61775-99-WE046
Final Report

Zhukovsky
August 2000

REPORT DOCUMENTATION PAGE

Form Approved OMB No. 0704-0188

1. REPORT DATE (DD-MM-YYYY)	2. REPORT TYPE	3. DATES COVERED (FROM - TO)
01-09-2000	Final	xx-xx-2000 to xx-xx-2000

4. TITLE AND SUBTITLE
Experimental And Theoretical Investigation Of The Weakly Ionized Non-Equilibrium Plasma Influence On A Flow Over Bodies Of Simple Forms
Unclassified

5a. CONTRACT NUMBER
F61775-99-WE046

5b. GRANT NUMBER

5c. PROGRAM ELEMENT NUMBER

6. AUTHOR(S)
Makachev, Nicolai ;

5d. PROJECT NUMBER

5e. TASK NUMBER

5f. WORK UNIT NUMBER

7. PERFORMING ORGANIZATION NAME AND ADDRESS
TsAGI
Zhukovsky-3
Moscow 140160, Russiaxxxxx

8. PERFORMING ORGANIZATION REPORT NUMBER

9. SPONSORING/MONITORING AGENCY NAME AND ADDRESS
EOARD
PSC 802 BOX 14
FPO, 09499-0200

10. SPONSOR/MONITOR'S ACRONYM(S)

11. SPONSOR/MONITOR'S REPORT NUMBER(S)

12. DISTRIBUTION/AVAILABILITY STATEMENT
APUBLIC RELEASE
,

13. SUPPLEMENTARY NOTES

14. ABSTRACT
This report results from a contract tasking TsAGI as follows: The contractor will investigate the effects of plasma discharge on aerodynamic bodies. He will perform experiments in the supersonic and subsonic wind tunnels at TsAGI. His proposed investigation will answer fundamental questions such as: 1) Nature of the observed behavior of shock waves in (or after) clouds of gas-discharge plasma; 2) The possible influence of gas-discharge plasma on aerodynamic characteristics of simple bodies; 3) Influence of gas molecules vibrational excitation on boundary layer flow properties. He will also perform numerical investigation using algorithms of non-stationary two- and threedimensional Euler equations and two-dimensional Navier-Stokes equations for vibrationally excited gas. Level-by-level kinetic model and appropriate turbulence model to account for turbulent transfer of excited components will also be developed. The technical approach is outlined in his proposal. Payment will be made upon receipt and acceptance of first preliminary report. Due no later than 4 months after contract award.

15. SUBJECT TERMS
EOARD; Weekly Ionized Plasma

16. SECURITY CLASSIFICATION OF:			17. LIMITATION OF ABSTRACT	18. NUMBER OF PAGES	19. NAME OF RESPONSIBLE PERSON
			Public Release	77	Fenster, Lynn lfenster@dtic.mil
a. REPORT Unclassified	b. ABSTRACT Unclassified	c. THIS PAGE Unclassified			

19b. TELEPHONE NUMBER
International Area Code
Area Code Telephone Number
703767-9007
DSN
427-9007

Standard Form 298 (Rev. 8-98)
Prescribed by ANSI Std Z39.18

REPORT DOCUMENTATION PAGE

Form Approved OMB No. 0704-0188

1. AGENCY USE ONLY (Leave blank)	2. REPORT DATE	3. REPORT TYPE AND DATES COVERED
	1-September -2000	Final Report

4. TITLE AND SUBTITLE	5. FUNDING NUMBERS
Experimental And Theoretical Investigation Of The Weakly Ionized Non-Equilibrium Plasma Influence On A Flow Over Bodies Of Simple Forms	F61775-99-WE046

6. AUTHOR(S)

Dr Nicolai Makachev

7. PERFORMING ORGANIZATION NAME(S) AND ADDRESS(ES)	8. PERFORMING ORGANIZATION REPORT NUMBER
TsAGI Zhukovsky-3 Moscow 140160 Russia	N/A

9. SPONSORING/MONITORING AGENCY NAME(S) AND ADDRESS(ES)	10. SPONSORING/MONITORING AGENCY REPORT NUMBER
EOARD PSC 802 BOX 14 FPO 09499-0200	SPC 99-4046

11. SUPPLEMENTARY NOTES

12a. DISTRIBUTION/AVAILABILITY STATEMENT	12b. DISTRIBUTION CODE
Approved for public release; distribution is unlimited.	A

13. ABSTRACT (Maximum 200 words)

This report results from a contract tasking TsAGI as follows: The contractor will investigate the effects of plasma discharge on aerodynamic bodies. He will perform experiments in the supersonic and subsonic wind tunnels at TsAGI. His proposed investigation will answer fundamental questions such as: 1) Nature of the observed behavior of shock waves in (or after) clouds of gas-discharge plasma; 2) The possible influence of gas-discharge plasma on aerodynamic characteristics of simple bodies; 3) Influence of gas molecules vibrational excitation on boundary layer flow properties. He will also perform numerical investigation using algorithms of non-stationary two- and three-dimensional Euler equations and two-dimensional Navier-Stokes equations for vibrationally excited gas. Level-by-level kinetic model and appropriate turbulence model to account for turbulent transfer of excited components will also be developed. The technical approach is outlined in his proposal. Payment will be made upon receipt and acceptance of first preliminary report. Due no later than 4 months after contract award.

14. SUBJECT TERMS		15. NUMBER OF PAGES
EOARD, Weakly Ionized Plasma		
		16. PRICE CODE N/A

17. SECURITY CLASSIFICATION OF REPORT	18. SECURITY CLASSIFICATION OF THIS PAGE	19. SECURITY CLASSIFICATION OF ABSTRACT	20. LIMITATION OF ABSTRACT
UNCLASSIFIED	UNCLASSIFIED	UNCLASSIFIED	UL

CONTENT

1. ABOUT SIMULATION OF THE ELECTRIC DISHARGES INFLUENCE ON FLOW OVER BODIES IN THE REGIME OF THE BOUNDARY LAYER.

The data of numerous numerical and experimental investigations are well known and published which confirm that, with help of the electric discharges created in the neighborhood of a streamlined body, it is possible to change the aerodynamic forces acting on the body. These investigations often relate to the problem of search of methods of the drag reduction with help of the volume heat generation evoked by the electric discharges that is organized in an enough large area in front of the body or near of it. In this case, as rule, the highly considerable expenditures of energy, large values of voltage and currents are required for reaching of the essential effect. As a result, the wish is explained to take attempts to realize the electric discharge influence on the flows overbuilding of which in the desirable direction does not require large electric powers because of the small space dimensions of the process and a low velocity of gas.

A simple examination of possible situations shows the boundary layer on the surface of an enough thin body for which the viscous friction gives the essential deposit in the drag can be a perspective candidate for such role by force of small thickness and a relatively low velocity of gas in the depth of the boundary layer.

Let us add to these considerations the known fact [1.1, 1.2] of the skin friction reduction in the turbulent boundary layer achieved with help of arrangement of the micro nonuniformities, so called, "riblets" on the streamlined surface. At the determine choice of the geometric parameters of riblets relative to ones of the boundary layer, these riblets exert such influence on the vortex structure of the arising boundary layer that evoke relaminarization of it and reduction of the skin friction force acting on the streamlined surface.

In this connection, it is of interest to investigate possibility of the skin friction control with help of the electrical discharge system that forms the periodical one of "heat" riblets arranged over the streamlined surface, extended along the flow and arising, in particular, because of displacing action of the air heated by the discharges on the flow.

Since the well verified technology of the near surface discharge system creation was absent at the start of the work, the estimation of the effectiveness of such method of influence on the flow in the boundary layer was possible only in modeling conditions without the discharges ignition and at imitation of action of them on the flow with help of artificial hard "heat" riblets or other near surface elements that would be considered in some details below. It will be noted that, in case of such "cold" experiments, the real heat mechanism of the discharge influence on the flow in the boundary layer is simulated crude enough because of the practically homogeneous field of the gas temperature and the different mechanisms of the artificial riblets action on the stream when it is possible to talk only about the simulation on order of magnitude of disturbances that arise in the flow.

The peculiarities of the discharges extended along the flow do not allow to hope on

reproduction of the optimal geometric characteristics of the real riblets in the experiments. In particular, the "thermal riblets" created by the discharges will have, most probably, a greater effective cross section and absolutely different (rounded but not sharp) form of the effective outside surface. However these riblets can give positive effect since they do not increase the total surface of a streamlined surface.

At the first stage of the work (in absence of the technology of the near surface discharges forming), the necessary existed in the preliminary tuning of the equipment and models prepared for tests in the plasma aerodynamic experiment. From the point of view of the skin friction reduction, the desirable purpose also consisted in elucidating of the perspective places of applying of influences investigated on the boundary layer. It should be remarked that considerable part of the models for experiments of the last stage of the contract was worked out and manufactured during this stage since the primary program of the contract did not foreseen the tests with heating and plasma generators use in the aerodynamic experiments.

2. QUALITATIVE ESTIMATES

The characteristic sizes of the artificial unevenness can be estimated from the following considerations. Let us take the hypothesis that, in conditions of interest, the electric discharge influences on the flow as a local zone of the heat output into the moving gas. In doing so, the outer stream has to flow over this zone of heated and displacing gas. Let us make some simplifications in considered task supposing the heat output is continuos and steady-state in time.

1. Assume that the process takes place in the laminar boundary layer or the laminar sublayer of the turbulent boundary layer.

2. Let us also suppose that one can neglect of the pressure change in the flow at heating of it; in result, a velocity of gas can be believed to be steady along a flow line.

In the section 1 of the incident flow (Fig. 2.1), the density and the gas temperature are supposed to be constant both along the coordinate y and that of z. Let us also believe that a velocity of the incident flow linearly increases along the coordinate y:

$$U(y) = K_1 y ; \quad K_1 = C_f \, r \frac{U_\infty^2}{2} \, m = C_f \operatorname{Re}_1 \frac{U_\infty}{2} .$$

The standard designations are used here which do not require special explanations.

The heat Q is supplied to the gas between cross sections of 1 and 2. At these sections, the gas has got the temperatures of T_1 and T_2, correspondingly. The temperature T_2 is constant on the section 2 and depends on values of Q and T_1. It is supposed that the extreme border of the considered field tube in the sections 1 and 2 is limited by half circumferences of radii R_1 and R_2.

For the parameters relation in the sections 1 and 2, the laws of conservation of energy, mass, momentum and the equation of state are used. Besides, it is believed that the gas velocity in the section 2 also linearly changes on coordinate y.

$$U(y) = K_2 y$$

Fig. 2.1.

In result, the relations are obtained that allow to estimate the heat displacement area and the corresponding displacement thickness

$$\delta^* = \frac{\Delta S}{2R_2}, \quad \Delta S = S_2 - S_1 = \frac{3\pi Q}{4C_p\rho T_1 R_1 K_1} = \frac{3Q}{4C_1\rho_1 T_1 U_1}$$

Here $U_{1,2}$ are the velocities of the gas movement in the sections 1 and 2 at the points where $y = R_{1,2}$.

The border of the heated gas displaces in the transverse direction relative to the cold gas because of the heat transfer and the turbulent mixing. Taking for simplification that a velocity of this displacement relative to the cold gas is constant, the following expression for the value ΔR of increase in the radius of the considered field tube can be obtained:

$$\Delta R = C \, \Delta X$$

where C is the constant and ΔX is the distance from the section 1.

In Fig. 2.2, the results of calculation of the flow parameters in section 2 are shown for the following conditions:

$$T_1 = 288K, \ \rho_1 = 1.225 \text{ kg/m}^3, \ Re = 3 \cdot 10^6, \ C_f = .0025, \ U_\infty = 30\text{m/s}, \ U_1 = 5.65\text{m/s}, \ C = .1$$

The heat is supplied on the portion from 0 to .4 mm.

It is seen that, after cessation of the heat input, the temperature T, the area of the displacement ΔS and the displacement thickness δ^* sharp reduce along the coordinate X at a distance of about some millimeters.

Fig 2.2.

The fulfilled estimations also show that in the case of the local heat input in the laminar

sublayer of the turbulent layer of .05mm – thickness, the heat input of .01W per one unevenness is sufficient that the height of it will be more than .05 mm. In case of the modelling experiments the thickness of the artificial riblets (the strings stretched along the flow) was close to this value, namely, .15 mm.

It should be however noted that the theoretical consideration gives an enough optimistic estimation of the energy expenditures necessary for the discharge ignition that can be related with the simplified model of the effect. Really, at the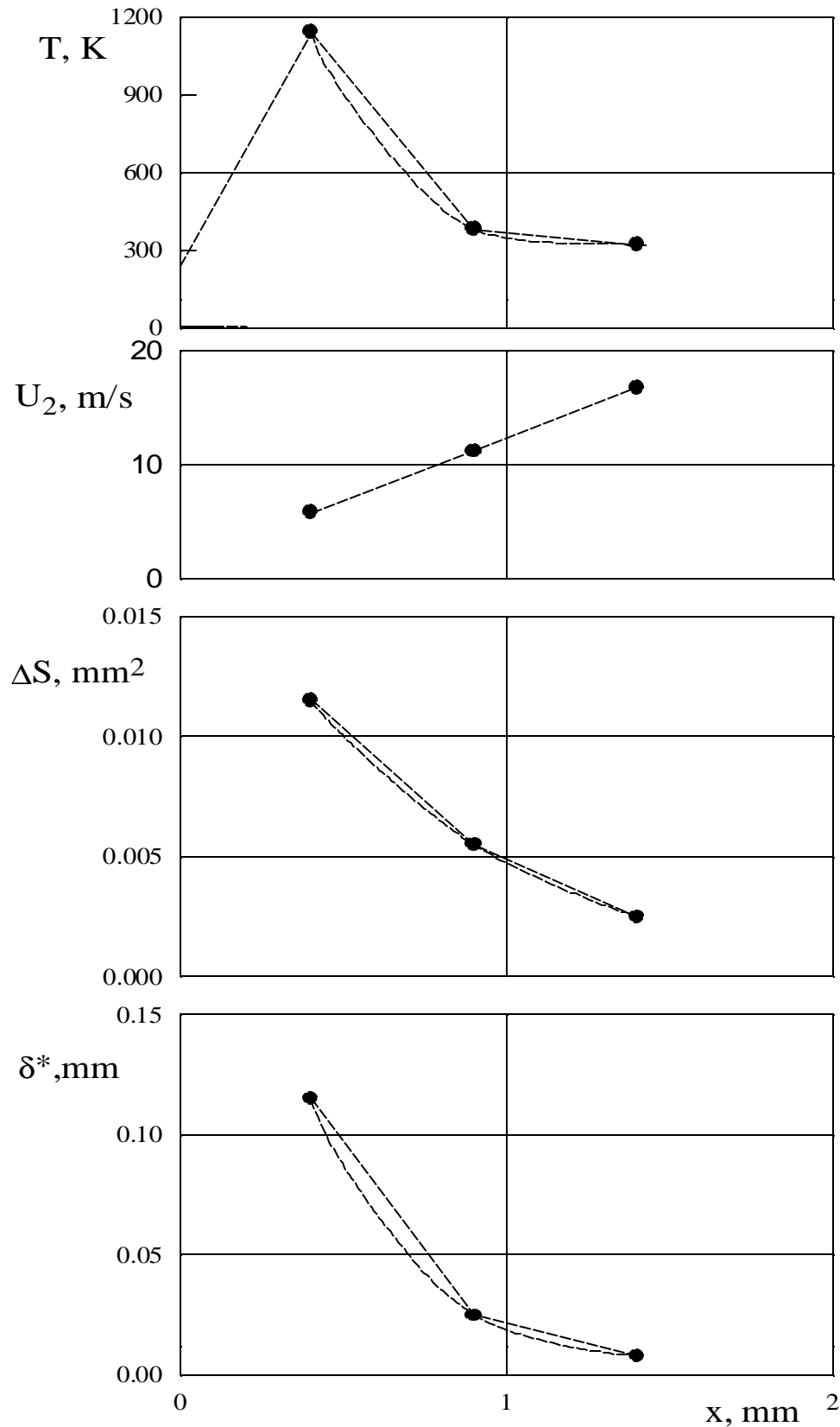 fulfillment of the work, the trial tests were carried out to elucidate possibility of the complex near surface discharges ignition. At the power of generator of about 100 W, the ignition of about 200 discharges was realized. In doing so, the frequency of pulses was 10 kHz, the pulse voltage was about 6 kV and the surface density of the points in which the discharges were realized was up to 5 cm^{-2}.

3. SIMPLIFIED NAVIER-STOKES APPROACH TO THE "THERMAL RIBLETS" AND THEIR SIMULATORS. STEADY AND UNSTEADY CASES.

3.1. Theoretical examination of flow properties near a "thermal riblet" and its "cold" imitator.

In precise statement the problem of numerical simulation of considered flows is rather difficult and requires for the solution of application of the non-stationary three-dimensional equations of Navier-Stokes. Therefore the reception even approximate, but qualitatively correct results now can become really achievable only at diminution, at the expense of the justified simplifications, dimensionality of solved problems.

The used further simplifications follow from such proved later assumptions: the cross size of a band of a gas heated in the discharge is much less than its size in a longitudinal direction; the reference time of longitudinal flow near "thermal riblet" is much greater of reference times of gas flow in orthogonal directions..

Let's designate a coordinate axis directional along the exterior stream as an axis $?$, and orthogonal to it axes, as Y and Z. The relevant orthogonal components of gas velocity are designated further as U, V, W, and by virtue of the made assumptions the inequalities $U \gg V \approx W$ are valid.

The discharges and relevant by them "thermal riblets" form near a surface of a body in a normal to axis ? plane periodic structure with two symmetry axes, that allows considerably to reduce the sizes of area, where the calculations (see plan on Fig.3.1) are produced. On the plan the shaped curve show the stationary contour of thermal source. At the solution the power of this heat source, stationary value or variable on time is set depending on a solved problem. In case of non-stationary statement at the initial time the fields of temperature and velocity of gas, and also its pressure are set. On a streamlined surface of a body are set temperature or requirements of heat exchange of a surface with a stream, and also conditions of zero normal and tangential velocities . On symmetry axes we have zero derivatives of macroparameters in a direction of local normal lines to these axes. "On infinity" we set pressure, temperature and quantity of

velocity U - interior limits of the exterior solution for a flow of a surface of a considered body.

Briefly we shall stop on simplified gas dynamics equations for problems, solved at numerical simulation.

Fig. 3.1.

3.2. Stationary case

Let's assume, that the formulated above requirements on components of gas velocity, time and geometrical scales of examined flow are carried out. Then in a stationary case we have the following simplified equations for the description of flow and thermal processes in "thermal" riblets neighbourhood:

1)Continuity equation

$$\nabla_y \rho V + \nabla_z \rho W = 0$$

2) Equation of impulses in a projection to an axis ?

$$\rho V \nabla_y U + \rho W \nabla_z U = -\nabla_x P - \nabla_y \tau_{xy} - \nabla_z \tau_{xz}$$

3,4) Equations of impulses in projections on an axis Y and Z

$$\nabla_y P = 0, \nabla_z P = 0$$

5) Equation of energy

$$\rho?_v (V\nabla_y T + W\nabla_z T) = P(\nabla_y V + \nabla_z W) + \nabla_y q_y + \nabla_z q_z + Q(y/y_0, z/z_0)$$

Here τ and q are the tensor of viscous stresses and vector of heat flux, $Q-$ some heat source with stationary power and geometry

6) Equations for Y_i - components concentrations

$$\rho V \nabla_y Y_i + \rho W \nabla_z Y_i = \nabla_y \rho D_{ij} \nabla_y Y_j + \nabla_z \rho D_{ij} \nabla_z Y_j + R_i$$

where D_{ij} – diffusion coefficients, R_i-macroscopic rates of inelastic processes in gas.

The derivation of simplified equations may be produced more strictly. Really, at known value of Q - volume density of heat release by "thermal riblets" - we may determine the scale of normal to X-axis components of gas velocity V or W.

$$P = 2\pi r L \lambda \delta T / r, \quad W = \pi r^2 L, \quad Q = 2\lambda \delta T / r^2 \approx \rho c V \delta T / r, \quad V \approx \mu / \rho r$$

As a consequence we obtain the value of flow scale in X-direction

$$L_0 = r \bullet U / V >> r$$

It is evidently that in case $L >> L_o$ we may omit the all terms with X-derivatives and obtain the above showed equations.

Calculated quantity is the frictional force acting on a streamlined surface and varying the value depending on a relations between geometrical parameters of a problem: a step between axes of "thermal riblets" and their diameter. At the known solution the force of drag is calculated under the formula

$$F_D = \iint \mu(T_S)(\partial U(y,z)/\partial y) dxdz$$

The viscosity of gas and derivative from its velocity are calculated near to a streamlined surface.

The results of these calculations are planned to be compared with data "of «cold" experiments using imitators of thermal riblets. Let's underline, that such variant of experiment at lack of generators of the electrical discharges with necessary properties is a single possible one, though the simulation of actual properties of real "thermal" riblets in viewed experiments is not exact. For example, in case of a used experiment the mechanism, effective in a reality, - motion of heated in the discharge gas - is not reproduced exactly. Further, in experiments and calculations with riblets imitators on their surface are assumed the requirements of zero tangential and normal velocity, missing in real conditions. Similarly, the trials to investigate with simulators the action on a flow pulse-periodic and non-stationary discharges generally are impossible.

The manifold errors of model phenomena simulation lead to change of explored effects. However it is possible to hope, that the model phenomena simulation is capable to give approximate, but qualitatively correct information, especially, how the change of geometrical parameters influences character of change of aerodynamic forces.

Let's note, that the mathematical simulation of properties of considered flow at "cold" trials, can not use the equation of energy and consider temperature of gas as a constant value.

3.3. Non-stationary and multi-pulsed discharge conditions.

In a non-stationary case the above mentioned system of equations should be complemented by partial derivatives on time from density, velocity, gas temperature and gas mixture components concentrations. The above used name "multi-pulsed" discharge here refers to a mode, at which elementary volume of gas during its motion together with a stream through the region of the discharge is supposed having action of large number of electric impulses with large ratio of time period to pulse duration

At a formulation of mathematical models the specified distinctions in the featured phenomena can be essential. For example, let's introduce labels: $r, a, l, \Delta t -$ a cross-dimension of a band of the discharge, velocity of a sound, molecular free path length and pulse duration (real time scale). If the requirements on value of this duration are gained, at first diffusion and then convective mechanisms of gas transport lose the value on gauge of a pulse length Δt.

Really, if the inequality $\Delta t << r^2/al$ is carried out, there is a unimportant diffusion transport of molecules across region of discharge; if the restriction on quantity of a pulse length is more essential, namely, $\Delta t << r/a << r^2/al$, decreases value of convective transport mechanisms.

It is important that all these modifications are contained in system of above developed simplified gas dynamic equations.

4. EXPERIMENTAL FACILITIES AND SCHEDULE

4.1. Experimental conditions

The analysis of the aerodynamic task that we stated in this work resulted in that for obtaining more reliable results it is very desirable to carry out the experiments in a wind tunnel which has lower intensity of the flow turbulence than we would have in the wind tunnel T–129. We took an opportunity of fulfilling the experimental investigations in the wind tunnel that has the initial degree of turbulence less than about 0.06% instead 0.3% in the wind tunnel T–129.

A schematic drawing of the wind tunnel is presented in Fig.4.1. This subsonic wind tunnel T-36I is a fan-driven test facility of open cycle. The velocity of the flow is varied in the range of about from 2 to 60m/s. The set up has a closed test section the dimensions of which equal 350×500×2600mm. The total pressure in the wind tunnel is atmospheric and the stagnation temperature equals about 300K. The maximum Reynolds number per 1 meter is equal to $4.2 \cdot 10^6$. At the entrance in the test section, the air flow can be artificially made turbulent by means of auxiliary devices.

Following types of the measurements can be carried out in this wind tunnel: 1) balance measurements, 2) skin friction measurements for the flat plates in the laminar and turbulent flows, 3) static pressure distribution measurements over the model surface with the help of point to point gauges, 4) investigations of laminar/turbulent transition for different conditions including

influence of riblets, micro–roughness and heating of various zones of the models and near surface flow, 5) determination of the velocity profiles in boundary layers, 6) measurements of the level of the velocity pulsations and distributions of it in boundary layers and a number of other measurements. Registration of the outlet signals of most measuring devices, processing of these signals and the graphing design of the results are carried out with the help of the wind tunnel computer.
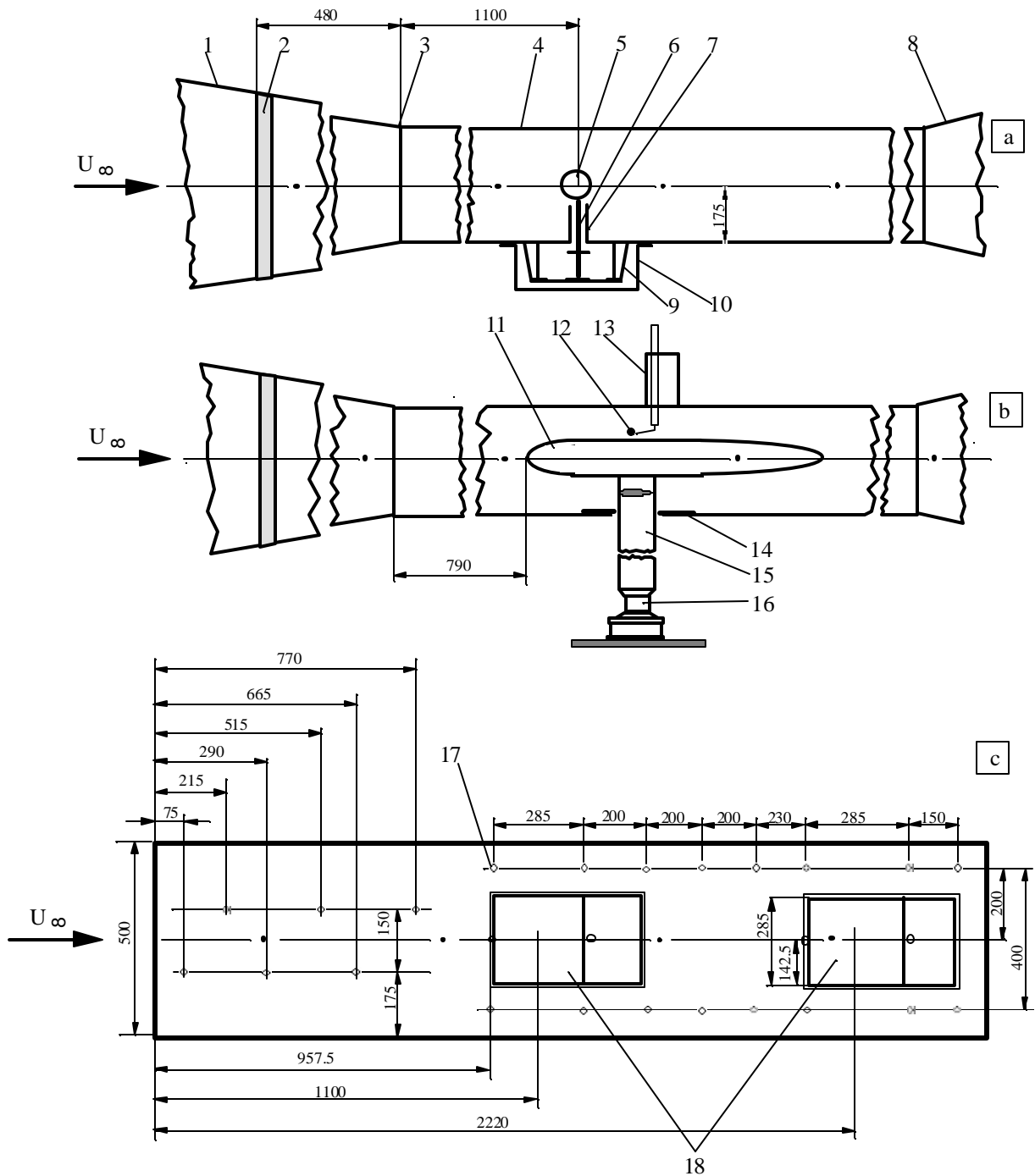

Fig.4.1.

1 - nozzle; 2 - turbulizator; 3 - origin of test section; 4 - test section; 5 - spherical model; 6 - strut of sphere; 7 - cowl; 8 - diffuser; 9 - floating element; 10 - casing; 11 - model of fuselage; 12 - probe of anemometer; 13 - micro-traverse arrangement; 14 - cover plate; 15 - strut; 16 - tensometric balance; 17 - drain orifices; 18 - floating element.

At the entrance in the test section, the flow cross section is pressed in ratio 12:1 due to the nozzle. For realization of the velocity pulsation in the range of 0.03-0.06 %, four deturbulizing grids are installed in the setting chamber of the wind tunnel. The grid has the filling coefficient equal 0.6. The possibility is foreseen to regulate the position of the lateral walls of the wind tunnel to the goal of the flow velocity gradient control and the boundary layer growing compensation along the test section. The check of the flow velocity is carried out on the base of evidences of the total pressure tube installed in the setting chamber and of the static pressure measurements at a distance of 30mm upstream from the edge of the nozzle. The fields of the flow velocity and parameters of turbulence are measured by the two component constant - temperature anemometer of DISA. The probe of the anemometer has a diameter of 5μm and 1.2mm - length. In vertical direction, it is displaced with a step of 0.1mm by a mechanism of traverse. This device is arranged on the upper wall. Along of X–axis (i.e. along the flow), the probe can be displaced in the range of 50...2400 mm from the edge of the nozzle by a tape–traction mechanism.

For the direct measurement of the skin friction, the lower wall of the wind tunnel has a floating element with a semiconductor tensometric converter. The streamed around area of the floating element equals 285×285mm^2. The center of the floating element is arranged at a distance of 1100mm from the nozzle edge. The mean–square error of the measurement by the floating element equals about 0.3 %. In fulfilled experiments, the lower wall represented one variant of the model.

The lateral walls have seven couples of windows. The windows of the test section are closed by optical glasses. The diameter of each of them equals 200mm.

Some details of the wind tunnel and the arrangement of the models in the test section are shown in Fig. 4.1*a* and Fig.4.1*b*.

In Fig. 4.1*a*, the arrangement of sphere in the test section is presented. The sphere had a diameter of 70mm and was installed on the hard strut of 6mm diameter which was mounted on the balance of the floating element of the wind tunnel. For the reduction in the force that acts on the strut from the flow, the strut placed inside a defending screen that was a tube of 12mm inner diameter and 14mm outer one. The screen was fixed on the lower wall of the test section. The construction of the floating element was covered by a hermetic casing. It was intended for harmful outer air flow did not penetrate into the test section. The gap between the sphere and the casing was about 3mm. It practically ensured the measurement of the forces that acted only on the sphere.

In Fig.4.1*b*, the arrangement of the model in form of a fuselage is shown. The model of duralimin has the maximum diameter of 100mm; the length of it is equal to 1m. The nose part of the model is a half–ellipsoid with half–axes equal 50mm and 200mm. The tail part of the model is also a half–ellipsoid with half – axes of 50mm and 300mm. The nose part of the model and the tail one are hollow and can be taken off at the preparation to the various variants of experiments. In the preliminary experiments, the model was installed in the test section of the wind tunnel at

equal distances from the lateral walls of the wind tunnel; the axis of the model was arranged at a distance of 180mm from the lower wall. A vertical strut of the model had a wing profile of 200mm - chord and 35mm - thickness. Only 130mm of the strut height was in the air flow, the rest part of it was out of the wind tunnel. The gap between the wing profile and the opening in the wind tunnel wall (about 0.5mm - width) was covered by special profiled plates. The aerodynamic drag of the model was measured by an one-component flange tensometric balance of cylinder type. It was manufactured of high–strength alloy steel. The elements of this balance sensitive to the deformations were wire tenso-resistors. They were glued to the lateral wall of the cylinder and combined in an bridge scheme. Supply of the scheme was carried out from a stabilized source of voltage. The voltage signal from the bridge proportional to the deformation of the resilient element of the balance was subjected to current amplification and registered by the personal computer of the wind tunnel.

4.2. Results of preliminary experiments

4.2.1. Tests of the spherical model

The main goal of the tests for the sphere was to verify the method of measurement of the forces that act on this model from the flow and comparison the results obtained with known literature ones.

It is known that, at a flow over a sphere, so called crisis effects take place that connect with sharp change of the character of a stream. These effects accompany by separation of the flow and, as a result, by pulsations of loads on the balance. The separation of the flow has laminar character in the range of number Re_d equal $3 \cdot 10^4$-10^5, where $\mathrm{Re}_d = u_\infty D/\nu$, D is the diameter of sphere. In this case, the drag coefficient keeps approximately constant $C_d = 0.48$-0.52 and the total drag arises , in the main, in result of influence of the pressure force integral. The laminar separation point arranges at $\varphi \approx 90°$ (where φ is the angle counted from the stagnation point in the meridian plane). At the numbers Re_d more than 10^5, the stream in the boundary layer becomes turbulent, and the separation point displaces down stream approximately up to $\varphi \approx 110°$. The region of the weak shorten essentially in comparison with the case of the laminar flow separation and, correspondingly, the drag, that is the result of influence of the pressure force integral, decreases. The drag reduction coefficient reduces to about 0.1. The interval of the critical numbers Re has comparably small range equal $1.5 \cdot 10^5 \leq \mathrm{Re}_c \leq 4 \cdot 10^5$ [4.1].

In case of a sphere, crisis effects arises the faster (at lower value of Re_d) the more the initial value of u'_∞ of the turbulent flow. A sphere, in result of the large sensitivity of the character of a flow around it to the initial turbulence, is used in the experimental aerodynamics as an standard pattern of the surface at the determination of the value of this turbulence. It is approximately considered that reduction in C_d arises at the critical number Re_c which one can believe equal Re_d corresponding to $C_d = 0.3$. At the atmospheric turbulence ($u'_\infty/u_\infty \to 0$), $\mathrm{Re}_c \to (3.6–3.7) \cdot 10^5$.
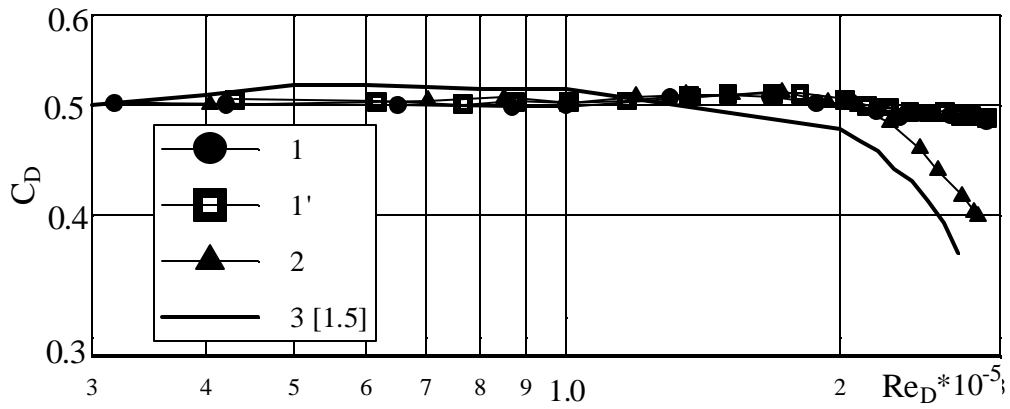
Fig.4.2

Some results of the fulfilled experiments are shown in Fig.4.2., where the dependence of $C_d(R_d)$ is plotted. In this tests, (D=70mm, u_∞=62m/s) the number Re_d was equal or less than 3 10^5. In Fig.4.2, the results signed by lines 1 and 1' were obtained at the "right" course of tests (increase in u_∞) and "reverse" one (decrease in u_∞). It is seen that results are practically reproduced. The solid line 3 in this figure shows the dependence taken from [4.2]. Some divergence in the results at $\mathrm{Re}_d \geq 1.7\ 10^5$ is probably connected with distinction in the test conditions of our work in comparison with those described in [4.2] (particularly, in values of u'/u_∞). The indirect verification of this supposition was carried out in the following manner. The wire ring diameter D_r of which equaled 35mm was installed on the front part of the sphere. The diameter of the wire d_w was 0.2mm. The ring turbulized the flow in the boundary layer and had to be cause of the transition to the turbulence stream and to decrease C_d at lower values of Re_d. From the results presented in Fig.4.2 (points 2), it is seen the decrease in C_d really takes place in this case at $\mathrm{Re}_d \geq 2\ 10^5$.

In conclusion, one can note that for conduction of the tests in all the range of the critical numbers $1.5\ 10^5 \leq \mathrm{Re}_c \leq 4\ 10^5$, it is necessary to use the sphere of diameter 100–120mm.

4.2.2. Experimental study of the fuselage-like model

On the first stage of investigations for the model in the form of fuselage, the character of a flow over the model was studied at the flow velocity values in the range of 20–60m/s. The position of laminar/turbulent transition was determined with help of the anemometer on the relative mean- square values of the velocity pulsation ε. The probe was displaced along X–axis on the height from the model surface corresponding to the value of the relative local velocity $u/u_\infty \approx 0.5$ in the range of X=130mm–1050mm from the origin of the model.

In Fig.4.3, the results of measurements of the laminar/turbulent transition are presented for the speed equal 20, 30, 40, 50 and 60m/s. It is seen that at a velocity of 60m/s the transition took place at X=300mm from the origin of the model. At a velocity of 20m/s, a flow over the model was laminar along almost all the length of the model. However in the last case, a sharp

transition to the turbulent regime was observed in the tail part of the model ($X = 960$mm). It is possible it was connected with separation of the flow in this zone.
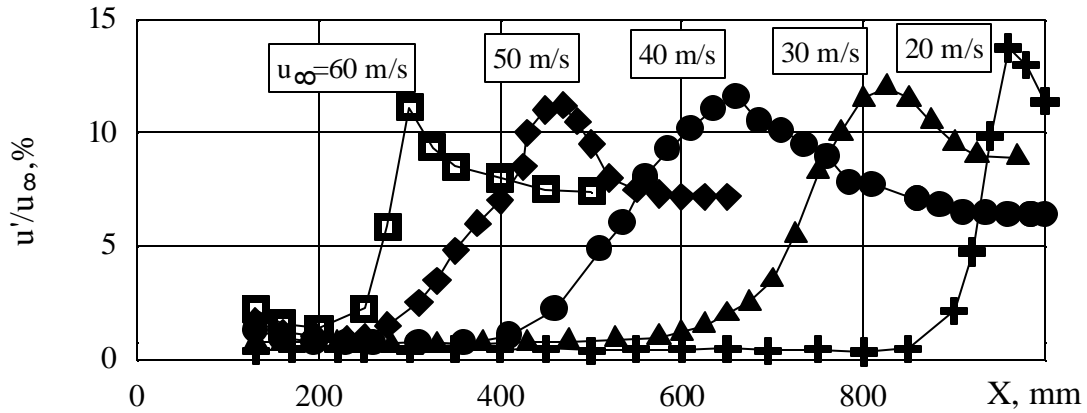

Fig.4.3.

Fig.4.4.

At laminar zones of a flow over the model, the profile of the mean velocity and pulsation of it were measured in the sections X =130, 240, 380, 600, 800mm. The integral parameters of the stream were also determined: the boundary layer thickness δ, the displacement one δ^*, the momentum one δ^{**}, and formparameter $H = \delta^*/\delta^{**}$.

In Fig.4.4, profiles of the relative velocity were plotted as a function of the relative coordinate y/δ^*. Blasius' theoretical profile was also plotted there. It is seen that experimental points are closed enough to the theoretic profile. Thus, for this model, the formulae of Blauses' theory obtained for the flat plate can be used for estimations of the characteristics of near surface stream.

Fig.4.5.

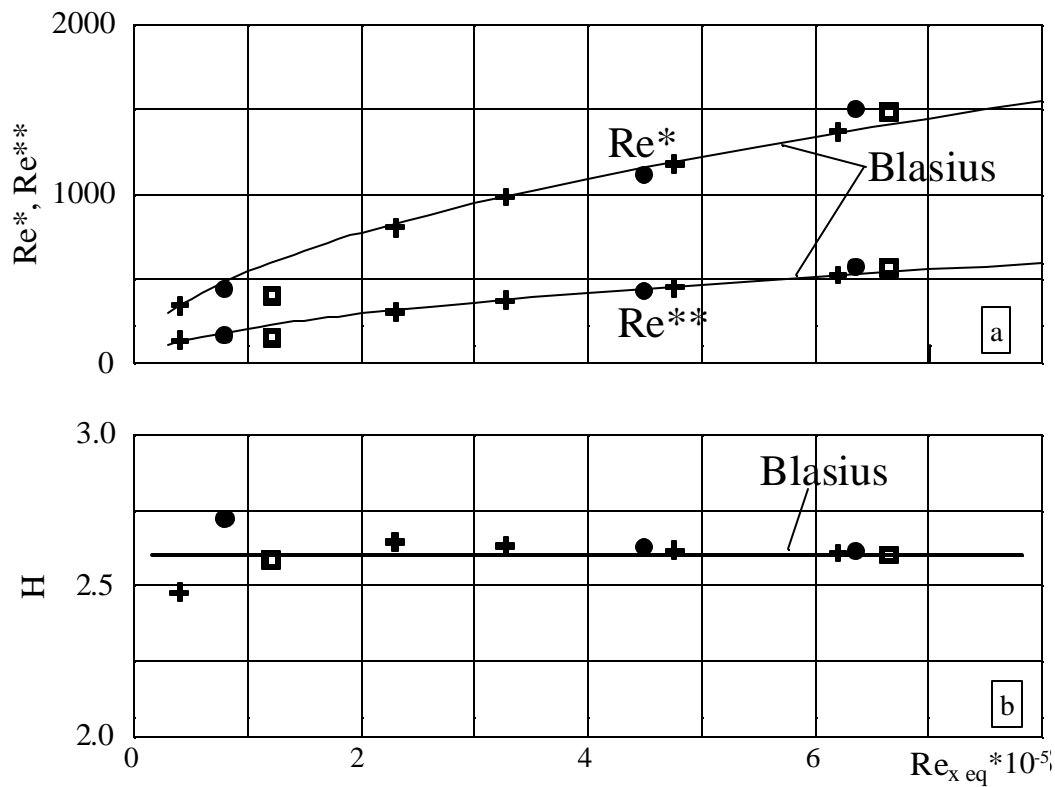In Fig. 4.5*a*, the dependence of number Re^* calculated on the experimental values of the displacement thickness and Re^{**} defined on the data of the momentum thickness on the number Re_{xeq} is presented. The last number was calculated on the distance x_{eq} which was defined on the integral parameters δ^* and δ^{**} for the laminar boundary layer on a flat plate. In this figure, Blasius' curves are also given. It is seen that divergence of the theoretical data and experimental ones is insignificant. Accordingly, in the wide range of number Re_{xeq}, the value of formfactor H is close to the theoretical one, that is 2.6 for laminar regime of a flow over a plate.
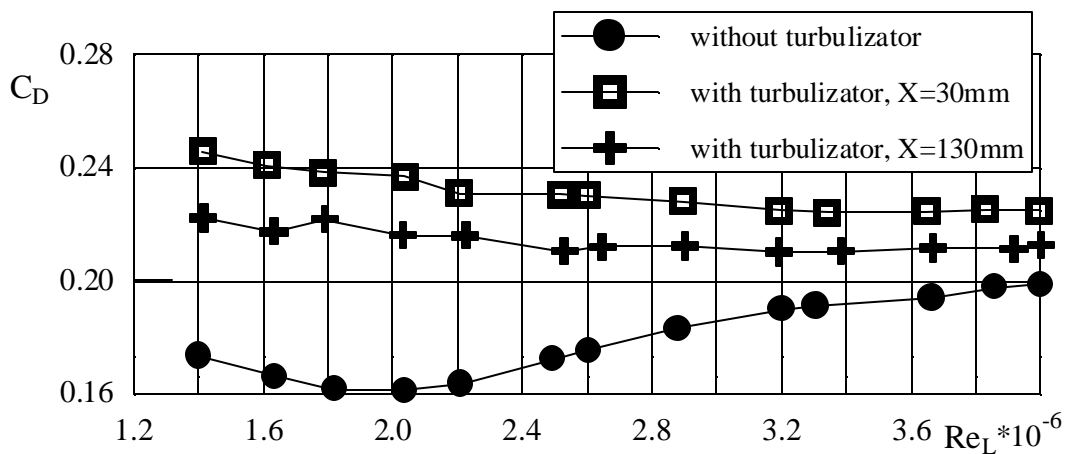

Fig.4.6.

The measurements of the drag of the model were carried out with help of the tensometric balance at the free stream velocity varied from 20m/s to 63m/s that corresponded to the values of number Re_d in the range $(1.4–4.1)\cdot10^5$. In these conditions, the drag of the model changed from 40 to 400G.

In Fig.4.6, the dependence of the drag coefficient of the model C_D on number Re_L is shown for two variants of tests. In the first of them, the model did not have a turbulizator (a wire ring of 0.24mm - diameter) and it was installed on the model at the second variant of the tests. It is seen that, at the turbulizator absence, the dependence of C_D on Re_L has a smooth maximum at $Re_L \approx 2 \cdot 10^6$. At increase in number Re_L above $2 \cdot 10^6$, it is observed a line rise in C_D that, probably, connects with increase in the length of the turbulent zone of the stream (see Fig.4.3). Presence of the turbulizator on the model led to increase in the coefficient C_D in all the range of number Re. This increase in C_D depended on the place where the turbulisator was arranged relatively the origin of the model (X =30mm and 130mm).

4.2.3. Experiments on the a flat plate model

One of the goal of the preliminary work was elucidation of opportunity to use the lower wall of the test section of the wind tunnel as a surface that simulates a flat plate at a longitudinal flow over the model. For realization of this goal, in the first series of experiments, the character of the stream regime was studied at the smooth surface of the contour of the wind tunnel (without turbulizating devices). In the second series, on the walls of the nozzle, a turbulizator was glued in view of a streak of abrasive paper with approximately one degree of the graininess.

4.2.3.1. Parameters of the flow at the smooth surface of the contour of the wind tunnel

The parameters of the laminar/turbulent transition were measured at some distances from the test section origin in the range of 160–2500mm and at u_∞ =12–64m/s. One component probe of the anemometer was arranged on the axis of the test section symmetry and on the height y equal 0.5mm from the wall surface. The filament of the probe was oriented parallel to the surface and normal to the flow velocity. The distributions of the longitudinal velocity pulsation u' and the mean speed $\bar{u}$ were measured at the fixed point of x in dependence on the free stream velocity $u'(u_\infty, x = const)$ as well as a number of profiles of distribution of u' along the wall at u_∞ being fixed, i.e. $u'(u_\infty, x = const)$. The position of the laminar/turbulent transition was determined in this work as the position of the longitudinal velocity pulsation maximum, i.e. $\max[u'(u_\infty, x = const)]$ or $\max[u'(u_\infty = const, x)]$. The results of the tests are presented in Fig.4.7–4.10.
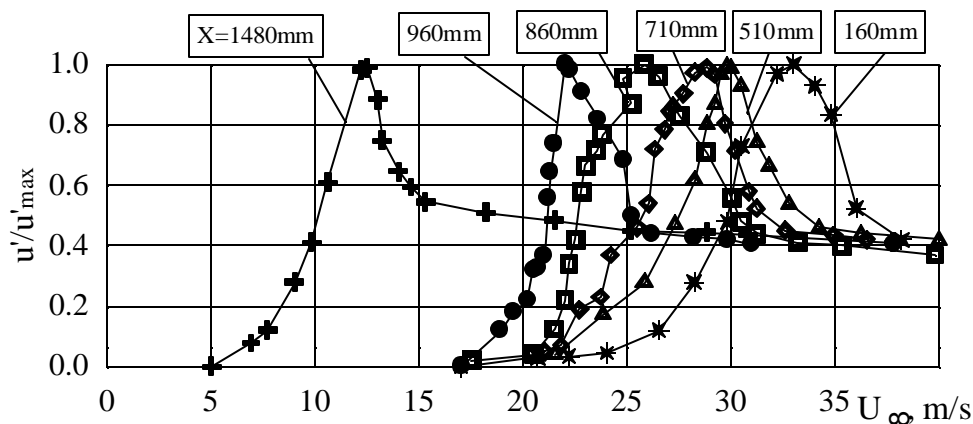

Fig.4.7.

In Fig.4.7, the distribution of the longitudinal pulsation normalized on the maximum value of it in dependence on u_∞ is shown at the different positions of the anemometer probe. It seen that the distributions of u'/u'_{max} are practically similar with each other in the different sections x. At that, the value of u' after the end of the transition area equals about 40% of u'_{max} (in the transition zone).
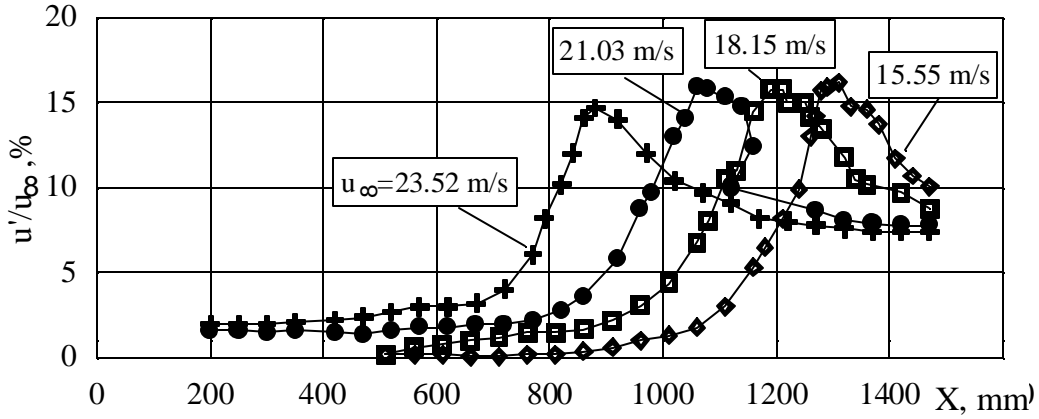

Fig.4.8.

In Fig.4.8, the distribution of relative pulsation $u'/u_\infty(u_\infty, x = const)$ along the surface of the lower wall is given at different values of the flow speed. It is seen that the character of the $u'/u_\infty(u_\infty = const, x)$ dependence is analogous to the $u'/u_\infty(u_\infty, x = const)$.

Comparison of the distributions considered above is presented in Fig.4.9 where the experimental dependence of Reynolds numbers $\mathrm{Re}_{\Delta x} = u_\infty \Delta x / \nu$ and $\mathrm{Re}_{\Delta u} = x \Delta u / \nu$ on Reynolds number Re_{ctr} of the transition is shown (the points 1 and 2, correspondingly). The number $\mathrm{Re}_{\Delta x}$ was calculated on the length of the transition $\Delta x = x_T - x_L$. The number $\mathrm{Re}_{\Delta u}$ was calculated on the value of $\Delta u = u_T - u_L$. The number Re_{ctr} was calculated on the equivalent distance from "the leading edge of a plate" to the end of the transition area $\tilde{x}_{eq}$ (the definition of $\tilde{x}_{eq}$ will be given below). In Fig.4.9, the data are also shown that were taken from [4.2, 4.3]. It is seen that the results of estimation of the transition length on the distributions $u'(x, u_\infty = const)$ and $u'(u_\infty, x = const)$ coincide with each other and well conform with the data [4.2, 4.3]. This allows to do conclusion that the laminar/turbulent transition can be determined on the profile $u'(u_\infty, x = const)$ as well as the conception of equivalent length $\tilde{x}_{eq}$ can be used.

The equivalent number Re was calculated as Re_x of the boundary layer on a smooth flat plate which had the origin of the laminar regime of the stream on the leading edge and the integral parameters δ, δ^*, δ^{**} equaled values that were taken from this work. The value $\tilde{x}_{eq}$ was determined as the arithmetic mean one of values x_{jeq} calculated from the relations that followed from Blasius' law: on the boundary layer thickness $x_{\delta eq} = (\delta/5)^2 \, \mathrm{Re}_1$, on the displacement thickness $x^*_{eq} = (\delta^*/1.73)^2 \mathrm{Re}_1$, and on the momentum thickness $x^{**}_{eq} = (\delta^{**}/0.664)^2 \mathrm{Re}_1$. The analysis of experimental data showed that the origin of the equivalent laminar boundary layer was placed at the distance of 200–600mm from the nozzle edge and could be calculated by the relation $\Delta x_{eq} = (20 u_\infty - 30)$ [mm].
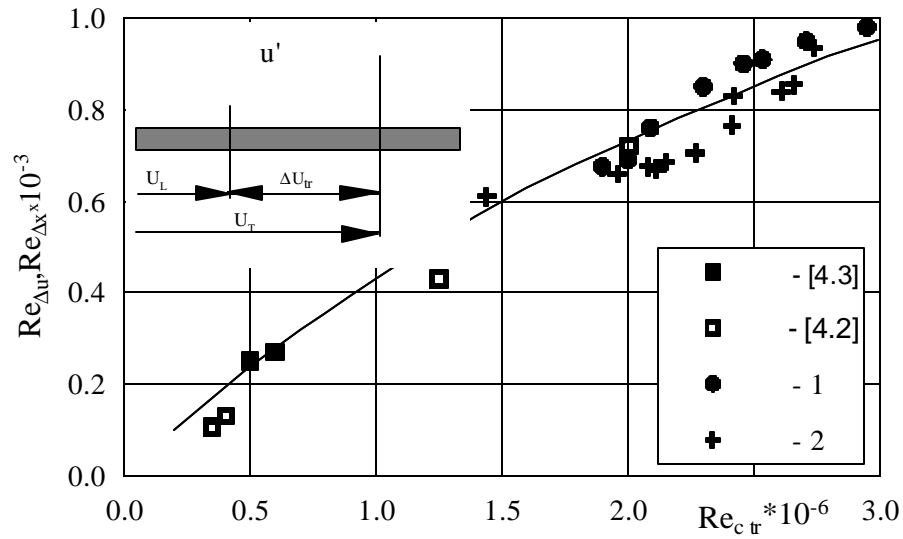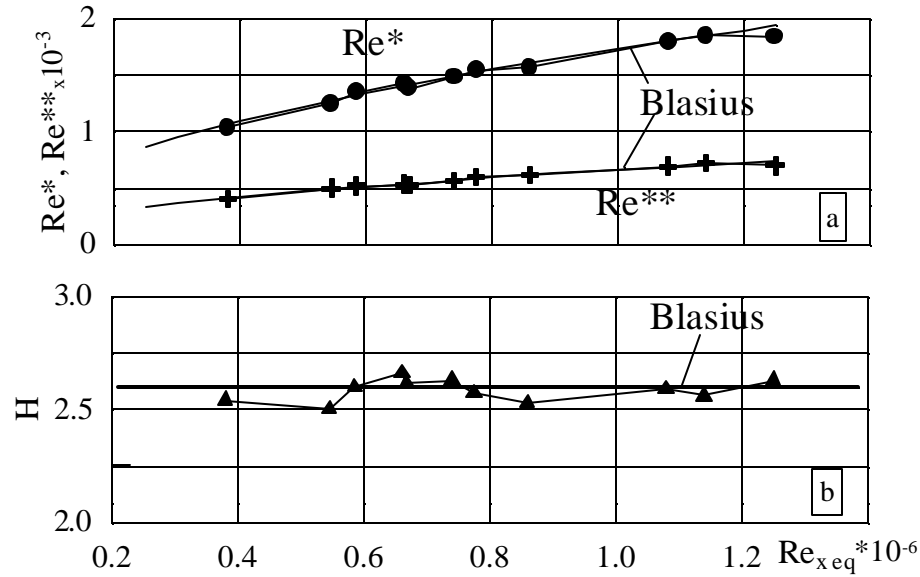
Fig.4.9.

Fig.4.10.

The empiric dependence of $Re^* = \delta^* u_\infty/\nu$, $Re^{**} = \delta^{**} u_\infty/\nu$ and formparameter H on the number Re calculated on the equivalent length $Re_{xeq} = (x_P + \Delta x_{eq})u_\infty/\nu$ (x_P is coordinate of the probe) are shown in Fig.4.10. It is seen that experimental data is satisfactory described by Blasius' relations. The analysis of measurements of the laminar/turbulent transition parameters (some of which are presented in Fig.4.7–4.10) allowed to make conclusion that on the lower wall of the wind tunnel test section, the laminar boundary layer took place at the velocity of the flow in the range of 12m/s–30m/s and number $Re_{tr} \approx (1.6$–$2.3) \, 10^6$ (at turbulizator absence).

In the second series of the tests, the turbulizator was installed on all four walls of the nozzle of the wind tunnel. It had uniform graininess (mean size of the grain equaled 32μm) and was deposited on the plates that had a thickness of about 1mm. The distance from the leading edge of the turbulizator to the test section origin was $X_T = 480$mm, the width of the turbulizator h_T equaled about 40mm.

The measurements of the integral parameters of the boundary layer were carried out with

help of a total pressure tube that had the reception orifice form of which was close to rectangular one at the outer sizes of 0.42mm×1.26mm. The thickness of its wall was 0.1mm. The static pressure was being taken at the section of X that was the nearest to the coordinate of the reception orifice of that tube (see Fig.1.1c). Apart from correction coefficients that took into account the peculiarities of the total pressure tube and the inclined – tube gauge, the humidity of air was taken into consideration at the calculation of the flow velocity $u(y)$.

Fig.4.11.

4.2.3.2. Simulation of the turbulent regime of a flow over the walls of the test section of the wind tunnel with help of the turbulizator

Fig.4.12.

Some results of the integral parameters measurements are presented in Fig.4.11. In particularly, in Fig. 4.11a,b, empiric dependence of Re^* and Re^{**} on Re_x is given. The last number was calculated on the distance from the leading edge of the turbulizator. Nicuradse's

dependence [4.4] $\mathrm{Re}^* = (\mathrm{Re}_x/110.682)^{0.861}$ is shown in Fig.4.11a. The relation of Sivels–Pain $\mathrm{Re}^{**} = 0.044\,\mathrm{Re}_x\big/(\lg \mathrm{Re}_x - 1.5)^2$ is plotted in Fig.4.11b as curve 1 and Prandtl's dependence [4.4] $\mathrm{Re}^{**} = \mathrm{Re}_x^{0.8}\big/66.13$ is given there as curve 2. It is seen the experimental points well correlate with these relations. In Fig.4.11c, the values of the first formfactor H are plo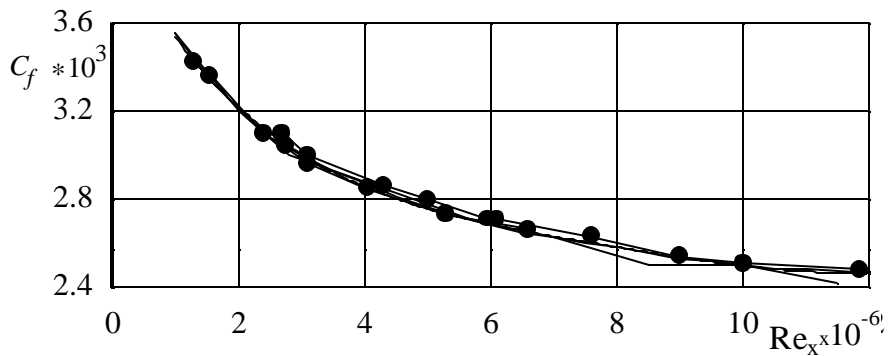tted as a function of Re_x. It is seen that both values of $H \approx 1.38$–1.36 and smooth decrease in $H(\mathrm{Re}_x)$ at increase in Re_x conform to a developed turbulent boundary layer.

In Fig.4.12, the dependence of the local friction coefficient C_f on Re_x is shown. The estimation of C_f was calculated as arithmetic mean one of values C_{fi} defined on the empiric parameters of the boundary layer δ^*, δ^{**}, H on the base of known relations of Ludwieg–Tilman, Karman–Shehner, Sivels–Pain, Spalding–Chi, Falkner and etc. (in sum about 18 relations were used). The values of C_f were also determined by indirect method that based on the universality of the $u(y)$ profile on the logarithm plot (method of Clauser and Osaropogly [4.4, 4.5]). Apart from estimation of C_f on the base of the $u(y)$ profiles, the approximating dependence of the direct balance measurements that were carried out with help of the floating element is presented in Fig.4.11 (the solid line). At these measurements, the center of the floating element was at the distances $X_{fe}=1100$mm and 2370mm from the edge of the nozzle. The results of the tests showed that estimations of C_f on the $u(y)$ profiles and on the balance measurements practically coincided. On the whole, the analysis of the results presented in Fig. 4.11, 4.12 allowed to make conclusion that use of the turbulizator of this type gave opportunity to simulate the turbulent boundary layer in this wind tunnel in the range of number Re equal $(1$–$12)\ 10^6$.

Thus, the results of the preliminary experiments show that the set up is prepared to fulfillment of the second stage of investigations.

4.3. Program of models of "thermal'' riblets planed testing at "cold" conditions

Wind tunnel:	T36I TsAGI
Cross-section	$0.35\mathrm{X}0.5\ \mathrm{m}^2$
Length of working section	2.8 m
Used flow velocity	<60 m/s
Dimensions of tested models:	1 – 0.1 m
Intensity of flow turbulence	0.03-0.06%
Cross-dimensions of tested "cold" nets	0.15-1 mm
Investigated models:	plane plate; round fuselage sphere

INVESTIGATED PHENOMENA (WITH AND WITHOUTE IMITATORS).

Plane plate	laminar/turbulent transition (LTT)
Fuselage forward part	LTT
back part	flow separation (FS)
Sphere	FS

MEASUREMENT PROCEDURES

Determination of drag force and its changing

Determination of the level of turbulent pulsations in various flow points and its changing.

5. "COLD" TESTS OF FUSELAGE-LIKE MODELS

The basic goals of the fulfilled tests were study of "aerodynamic characteristics" of obstacles which were installed on the surface of the investigated bodies and imitated the geometry of electrodes of some plasma generators (in this work the body investigated were a model of a fuselage and a flat plate)

The following "aerodynamic characteristics" were considered:

a) for the model in the form of a fuselage, they were: the coefficient of the total drag C_D, the distribution of the excessive pressure along the tail part, the deformation of the fields of $\overline{u}(y)$ and $u'(y)$ in the wake of the body.

b) for the model in the form of a flat plate, they were: the coefficient C_f of the local skin friction, the position of the laminar/turbulent transition, the integral parameters δ^* and δ^{**} determined in the boundary layer after the obstacles and over them;

The following types of the obstacles were tested:

a) for the model in the form of a fuselage, they were: 1) strings with a circular cross section which were stretched on the surface along the flow, 2) steel rings across the flow in the boundary layer (an analogy of Large Eddies Break Up (LEBU) elements), 3) thin plates with a teeth edge that were directly accommodated on the surface.

b) for the model in the form of a flat plate, they were strings along the flow and riblets of V – type;

The types of the obstacles were chosen on the base of the concept of the plasma use for the drag reduction (see above). Apart from that, the following circumstances were taken into consideration.

According to the literature data (see, for example, [5.1]), it is known that, at the optimal parameters, V-riblets and LEBU –elements can reduce the skin friction by about 6-10 %. These optimal parameters for riblets are $h_{opt}^+ \approx 10 - 15$, $s_{opt}^+ \approx 15 - 25$. For the LEBU of the scheme of tandem, they are $l_{opt} \approx (1 - 1.5) \cdot \delta_0$, $h_{opt} \approx (0.5 - 0.8) \cdot \delta_0$, $t_{opt} \approx (0.005 - 0.01) \cdot \delta_0$, $\Delta s_{opt} \approx (10 - 20) \cdot \delta_0$. It will be noted these results have relation to conditions without energy supply and for Reynolds numbers in the range of $R_{ex} \approx 10^6$ - $6 \cdot 10^6$ that conforms to conditions of our tests. The other reason of choice these types of obstacles was the preliminary experiments with some types of electrodes of the plasma generator fulfilled in this work (see below).

5.1. Results of experiments for the fuselage-like model

In this work, the attempt was undertaken to investigate some possible variants of the plasma generators electrodes configurations (without initiation of the discharges) from the point

of view of influence of them on the aerodynamic drag change both at the turbulent regime of flow over a body and at the laminar one. Three constructive types of electrodes were tested in combination with the basic model of a fuselage (also see above): 1) electrodes of the riblet type in form of longitudinal strings accommodated on the surface of the model, 2) electrodes in form of Large Eddies Break-Up (LEBU)– configurations for distraction of eddy structures, 3) electrodes in form of rings projections of the small height which arrange on the surface.
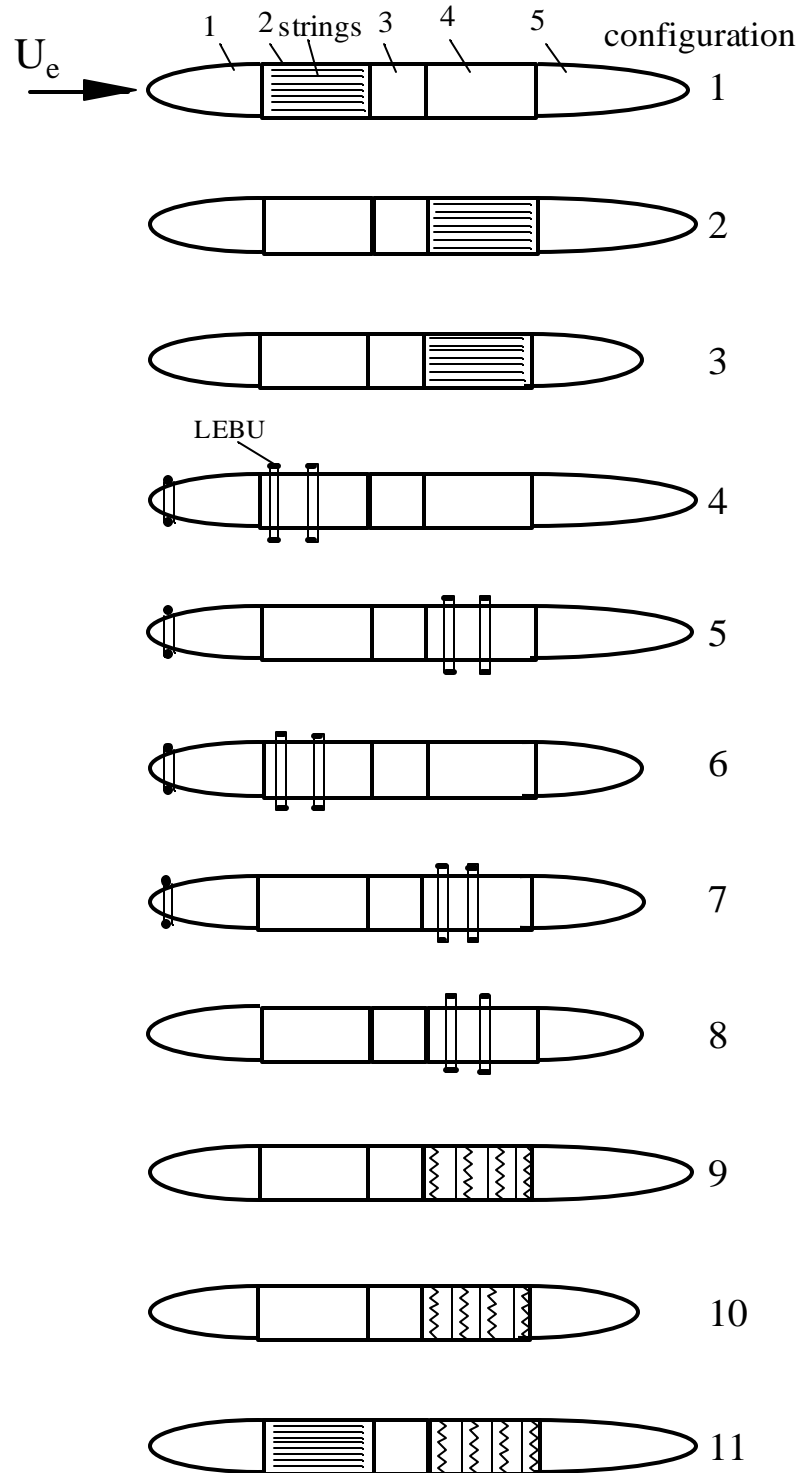

Fig.5.1

The basic type of tests were comparative balance measurements of the integral drag of the

model at presence of electrodes and without them. The model consisted of five basic parts (Fig.5.1): 1 – the nose elliptic part that had the length l=200mm and ratio of $d/l=1:2$ (here d is the diameter of the cylindrical part of the model), 2 – the front cylindrical part of the model of 197mm – length, 3 – the central cylindrical part of 106mm – length, 4 – the tail cylindrical part that had the length equal 197mm and 5 – the tail elliptic part of 300mm–length and the ratio of $d/l=1:3$. The general length of the model equaled 1000mm. The variant of the model assembly with more blunt tail part was also tested. In this case, the ratio d/l equaled 1:2 and the length of the model was 900mm.

At this stage of the work, the model was modernized. For measurements of the static pressure distribution on the model surface, the receiving openings of .05mm - diameter were drilled (six openings were made in the nose part, one opening was in the front cylindrical part and ten openings were drilled in the tail part of the model). The measurement of this distribution was carried out at the velocity of the flow equal 10, 20, 30, 40, 50 and 60m/s. It was ascertained that the character of the relative distribution of the pressure $\overline{p}_{st}$ did not practically depend on the flow velocity. This situation is illustrated by Fig. 5.2 in which the distribution of $\overline{p}_{st}$ is given for the velocity of 10 and 60m/s without them.
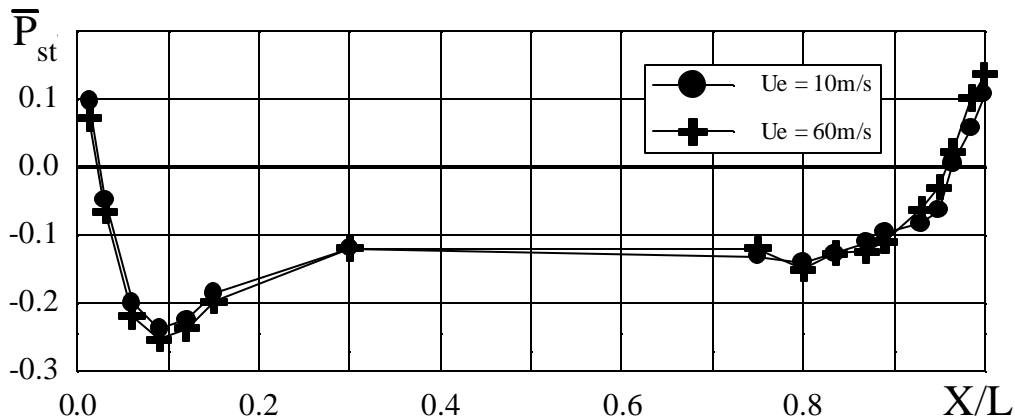

Fig. 5.2

Apart from that, the model was equipped by rings imitating some types of the plasma generator electrodes for creation of the near surface discharge. Two types of ring "electrodes" were used. The first of them was the cardboard ring of 0.3mm – thickness and 12mm - total width in which small teeth of 6mm-height and 6mm –step were cut on the tail side of the ring edge. The rings (usually four pieces) were installed at some distance (about 40mm) from each other directly on the front or tail cylindrical parts of the model. The second type of "electrodes" was manufactured in view of two metal rings of 0.2mm – thickness and 6mm – width. One of the rings had the diameter equal 104mm, the other – 105mm. The rings were installed on the cylindrical part of the model at some distance, one after the other. This distance equaled half of the boundary layer thickness.

The study was also carried out with the third variant of the system that imitated a plasma generator. That was a number of strings of 0.15mm – diameter which were accommodated on the cylindrical part of the model. The strings were fastened with help of openings that were drilled in

the cylindrical part at the distance of 30mm from the butts regularly on the circumference with the step of 2mm. The length of strings was 120mm.

The strut of the model was closed by the cowl. The gap between the lower wall of the wind tunnel and the strut was also closed by a film of polyethylene to expel the influence of the harm flow of air on the results of measurements.

The study of influence of the various configurations of electrodes on the drag was carried out both at laminar and at turbulent regimes of flow over the model. In the last case, a turbulizing wire ring of 0.24mm – diameter was mounted close to the surface of the model at the distance of about 30mm from the nose apex of the model.

In the first stage of the investigations, the profiles of the velocity were measured with help of the hot-wire anemometer at presence of the turbulizator and without it and the integral parameters of flow over the model such as the boundary layer thickness δ, the displacement one δ^*, the momentum one δ^{**}, and formparameter $H = \delta^*/\delta^{**}$ were determined.

The second stage of the experiments consisted in the measurements of the integral drag of the model in the range of velocity from 15 to 60m/s at accommodation of "electrodes" of different configuration in turn on the model. The total number of configurations investigated were eleven if one took into account the possibility of various arrangement of three basic variants of "electrodes" relative to the nose of the model and also took into consideration the different state of the incident flow.

The schemes of configurations of the model with various types of "electrodes" that were tested are presented in Fig.5.1. In case of the model which had the tail part with the ratio $d/l =$ 1:3, six variants were investigated and five ones were studied in case of the tail part with that ratio equal 1:2. The results of experiments are illustrated by Figures 5.3-5.11. In particular, in Fig. 5.3, 5.6, 5.8, 5.10, the results of the balance measurements of the coefficient C_D of the total drag of the model for different variants of electrodes are given as a function of Reynolds number Re_d that was calculated on the diameter of the cylindrical part of the model. In Fig. 5.5, 5.7, 5.9, 5.11, the dependence of the relative coefficient $\overline{C}_D = C_D/C_{D0}$ on the Reynolds number Re_d is given (C_D and C_{D0} are the drag coefficients calculated with use the mid-section of the model at presence of electrodes and without it, correspondingly). Taking into consideration some scattering of the experimental points, the processing of the experimental results was carried out with use of approximating curves in form of polynomials of different degree n.

We will considerate in detail the results of influence of each of three basic configurations of electrodes on the value of $\overline{?}_D$.

5.1.1. Influence of the electrodes of riblet type

Two variants of arrangement of the strings that imitated electrodes of the riblet type were studied: on the front cylindrical part of the model (x=230-350mm) and on the tail one (x=530-650mm). In both cases, the stream line mid-section increased approximately by 3.4%.

The geometrical parameters of the riblet surfaces are characterized by dimensionless values

$$s+ = (su_\infty / \nu)\sqrt{C_f / 2} \text{ and } h^+ = (hu_\infty / \nu)\sqrt{C_f / 2}$$

where ρ+ is the distance between ribs (in our case, it is the distance between strings), and $h+$ is the height of ribs. For determination of parameters s+ and h^+, it is necessary to determine the local coefficient of friction. In case of the laminar stream, it equals $C_f = 0.664/\sqrt{Re_x}$ $= 0.664/(Re_1 x_{eq})^{1/2}$ where x_{eq} is the equivalent distance determined from the integral parameters of flow over the cylindrical model. In dependence on the regime of flow over a body, the estimations give for s+=54 - 330 and for h^+=4 - 25.
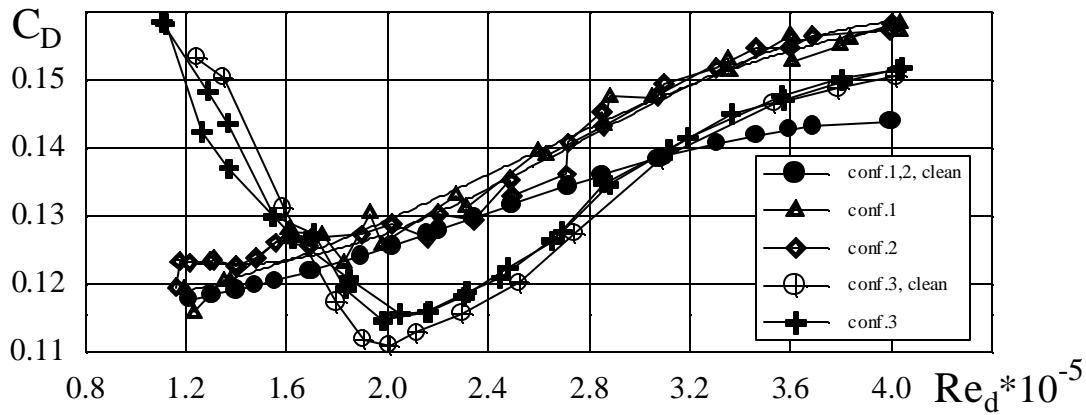

Fig.5.3

In Fig.5.3, the results of the balance measurements of the coefficient C_D for three configurations of the model (variants 1,2,3 in Fig. 5.1) are shown. The strings were arranged either on the front cylindrical part of the model or on the tail one. One can see that, in the range of $Re_d = (1.6-4.1) \cdot 10^5$, the drag smoothly increased both for the basic model and the model with the strings. This growth was conditioned by the increase in the length of turbulent zones of the flow. In particular, at the arrangement of the strings on the front part of the model, the laminar/turbulent transition displaced to the nose of the model (Fig.5.4) and the region of the turbulent flow increased.
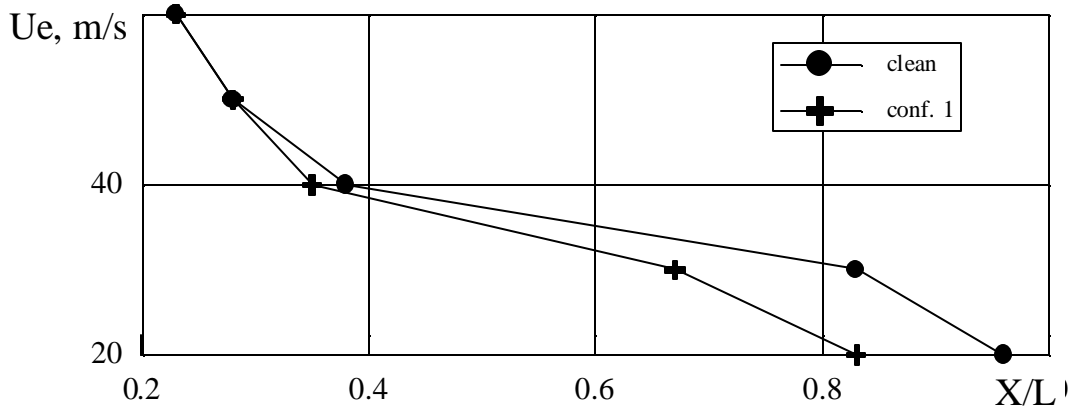

Fig. 5.4

In case of the model which had the shorter tail part (variant 3), a minimum of the coefficient C_D was distinctly observed at $\mathrm{Re}_d = 2\cdot 10^5$ probably conditioned by the length change of the laminar and turbulent zones of the flow.

For variants 1 and 2 the relative value of the drag coefficient $\overline{C}_D$ increased by 3% - 10% at the growth of Reynolds number Re_d but for variant 3, the decrease in the drag equal 1-2% was observed at $\mathrm{Re}_d < 1.5\cdot 10^5$ (see Fig. 5.5).
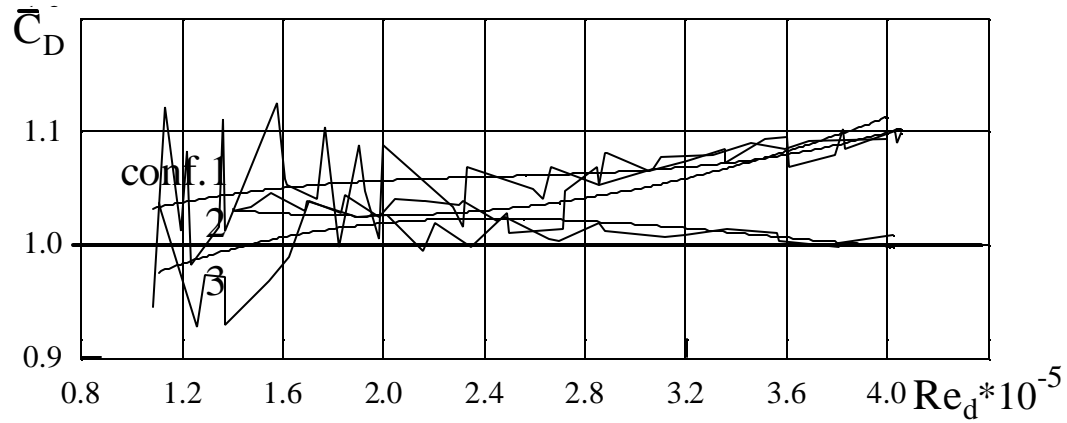

Fig. 5.5

5.1.2. Influence of electrodes manufactured in the form of LEBU - devices

In the variant 4, the electrodes in the form of the metal rings described above were installed on the front cylindrical part of the model. The ring of 104mm – diameter was arranged at the distance $x_1=220$mm and the ring of 105mm – diameter was at the distance $x_2=280$mm. The rings were mounted by eight small struts which had a thickness of 0.2mm and were arranged sharp along the flow. In the variant 5, the coordinates of the rings was $x_1=600$mm and $x_2=700$mm.

Table 1

Conf No.	d/L	Position of elements of LEBU		Relative geometry parameters of LEBU						
		X_1/L	X_2/L	h_1/δ_1	h_2/δ_2	l_1/δ_1	l_2/δ_2	t_1/δ_1	t_2/δ_2	S/δ_1
4	1:3	0.22	0.28	0.5	0.48	1.5	1.3	0.05	0.04	15
5	1:3	0.60	0.70	0.21-0.23	0.24-0.26	0.63-0.69	0.58-0.62	0.021-0.023	0.023	10.5-11.4
6	1:2	0.24	0.4	0.5	0.38-0.4	1.5	0.9-0.5	0.05	0.03	35-21
7	1:2	0.67	0.78	0.21-0.23	0.24-0.26	0.63-0.69	0.58-0.62	0.021-0.023	0.019-0.02	10.5-11.4
8	1:2	0.67	0.78	0.21-0.46	0.28-0.54	0.63-1.38	0.68-1.3	0.021-0.046	0.023-0.043	10.5-23

In experiments at the turbulizator presence on the nose part of the model, the profiles of the velocity and pulsations of it were measured by the anemometer in the cross-sections x=195, 400 and 650mm in the range of velocities u_∞ =20 – 60m/s and also the integral parameters of the boundary layer were determined. The relative parameters of LEBU changed in dependence on the flow velocity and the position of rings. The compass of them is presented in Table 1, where: h_1, h_2 -height of installation; l_1, l_2 - width; t_1, t_2 – thickness of LEBU elements; s - distance between the elements; δ_1, δ_2 – thickness of the boundary layer at the place of the elements installation, L – the total length of the model.
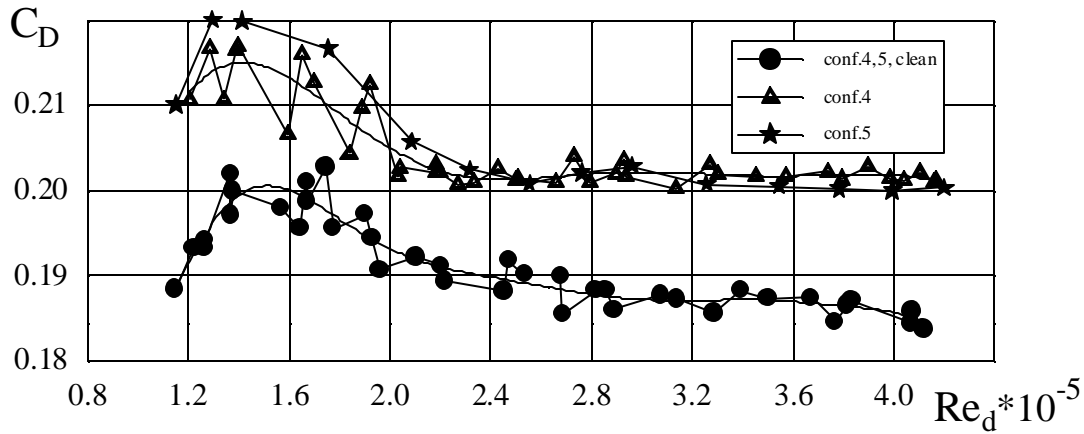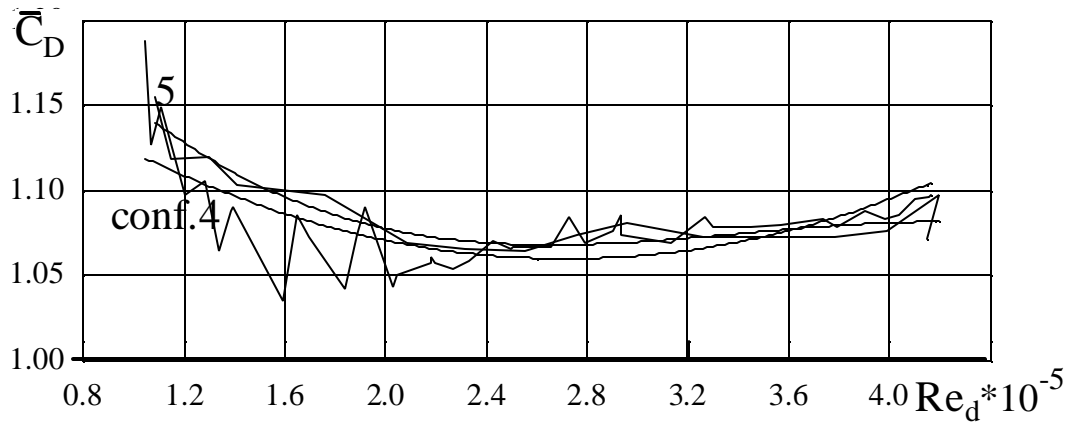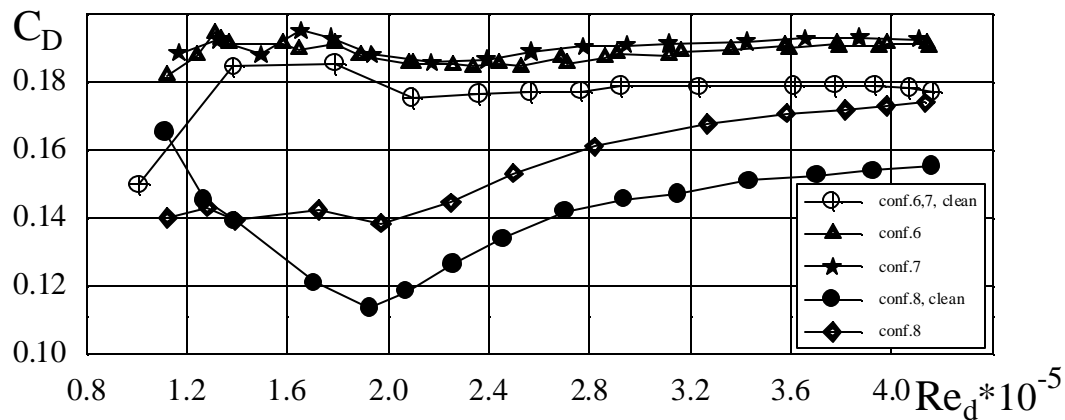
Fig. 5.6

Fig.5.7

Fig. 5.8

The results of the tests for the model having different configurations of LEBU are given

in Fig. 5.6 and in Fig.5.7. It will be noted some peculiarities in the dependence of the drag coefficient of the model on Reynolds number Re_d. In particular, the drag of the model with the longer tail part (d/l=1:3) had the maximum at $Red \approx 1.3 \cdot 10^5$ both on the model without LEBU and on the model with them (Fig. 5.6, configurations 4 and 5). The values of drag did not practically depend on the position of LEBU on the cylindrical parts of the model (i.e. on the front part or on the tail part). The relative increase in the drag value at the presence of LEBU equaled 6–13% in dependence on Re_d (Fig. 5.7).
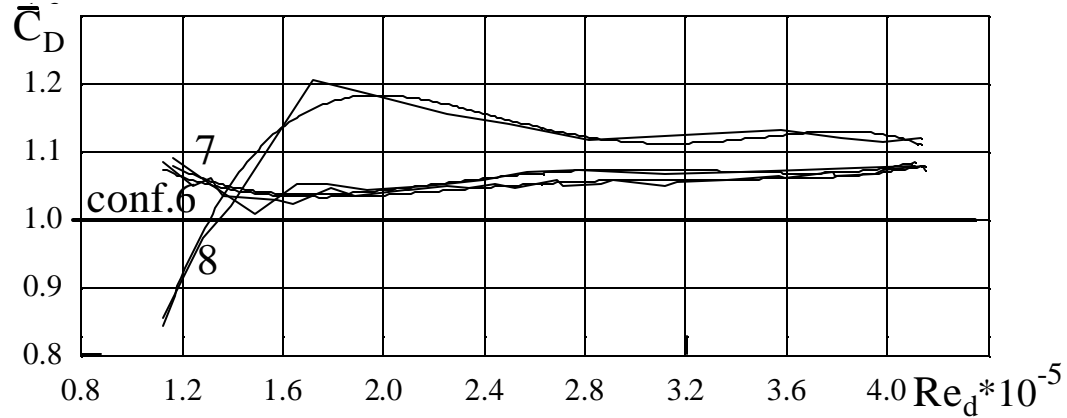

Fig. 5.9

The drag of the model that had the shorter tail part (d/l=1:2) (Fig. 5.8, configurations 6 and 7) at the turbulizator presence changed insignificantly in all the range of Re_d=(1.1 – 4.2)$\cdot 10^5$. The alternation of the LEBU position relative to the nose of the model weakly influenced on the value of C_D (it was seen from comparison of data for configurations 6 and 7 in Fig. 5.8). In the both cases, the drag increase turned out to be 3 – 7 %. However without turbolizator, the character of dependence of the drag coefficient on the Reynolds number was quite another. The arrangement of the LEBU on the model led to the drag decrease by 12% at the low values of Re_d =(1.1 - 1.3)$\cdot 10^5$ (Fig. 5.8 and Fig. 5.9, configuration 8). At the increase in Re_d from $1.4 \cdot 10^5$ to $4.2 \cdot 10^5$, the drag at first increased by 18% and then smoothly decreased by 12%.

Such character of the LEBU influence on the drag was probably conditioned by the shorten of the separation stern region because of the action of the LEBU on the stream at the low velocities of a flow over the model.

5.1.3. Influence of the ring protrusions of small height

The system of four ring protrusions that had the thickness of .3mm was used. They were installed on the tail cylindrical part of the model at a distance of 40mm from each other (Fig.5.1, configurations 9,10,11). The distance from the nose apex to the first ring was 573mm. In dependence on the regime of flow over the model, the relative height of the protrusion h/d changed in the range of 0.033–0.075. The results of the drag measurements are presented in Fig.5.10,a,b,c.

The arrangement of the protrusions on the model with the longer nose part (d/l=1:3) led to the drag increase by 7–10% (Fig. 5.10,a, configuration 9).
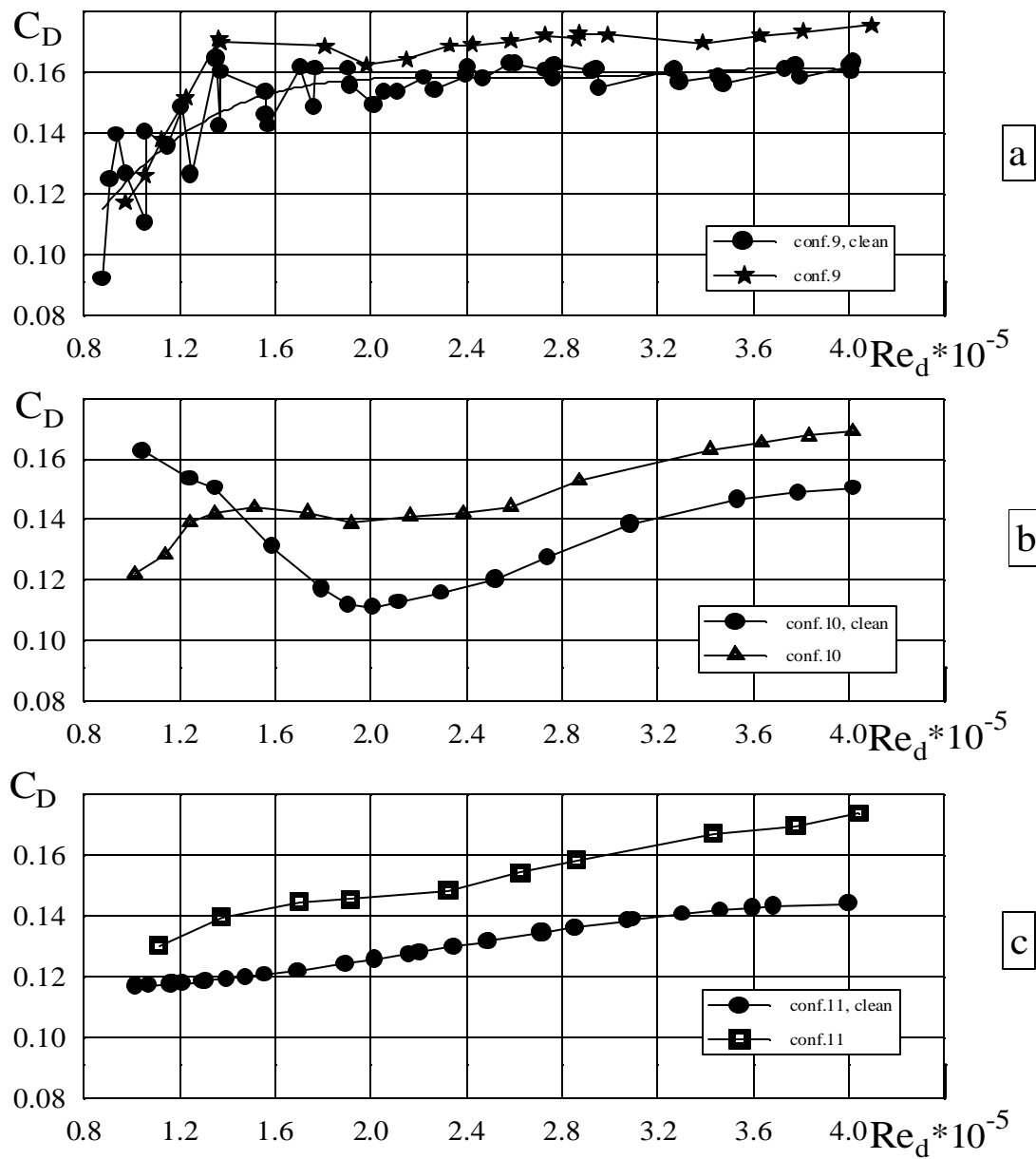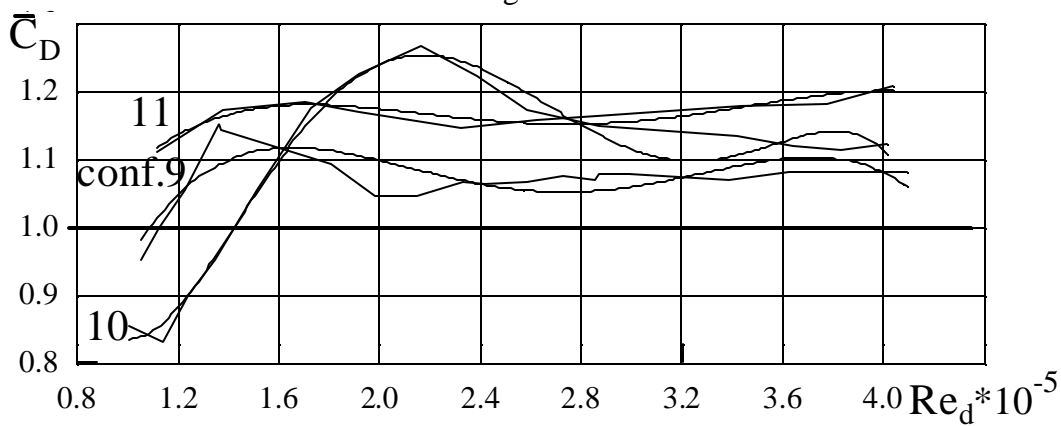
Fig. 5.10

Fig. 5.11

The presence of protrusions on the model with the shorter tail part (d/l = 1:2) gave significant decrease in the drag (by 17%) at $Re_d \approx (1–1.4) \cdot 10^5$. At the same time, at Reynolds number more than $1.4 \cdot 10^5$, the drag sharply increased (by 25%) at $Re_d = 2.2 \cdot 10^5$ and then

decreased by 10% at $Re_d=4\cdot10^5$ (Fig. 5.10,b and 5.11, configuration 10). All the values of effects are given in compare to the drag of the model without rings.

In Fig. 5.10,b and Fig.5.11, the results of measurements of the drag are shown for the model that had the protrusions and strings that were accommodated on the front cylindrical part of the model (the strings had the diameter of .15mm, the length of 120mm and the step between them was 2mm). The presence of the strings led to the additional increase in the drag by 5–10 % (Fig.5.11, configurations 11 and 9).

At the configurations of the model No 11 and also at No 1, the profiles of the velocity and pulsations of it in the wake of the model were measured. The probe of the hot-wire anemometer was displaced in the vertical main plane crossing the central axis at a distance of 5mm from the model. In Fig. 5.12,a,b, the results of these measurements are given for the velocity of the flow equal 20 and 50m/s. It is seen that, at the different velocity, the character of the profiles was alike. The small decrease of the flow velocity (about 10%) in the low part (at the negative values of y) was conditioned by the influence of the model strut cowl on the flow.
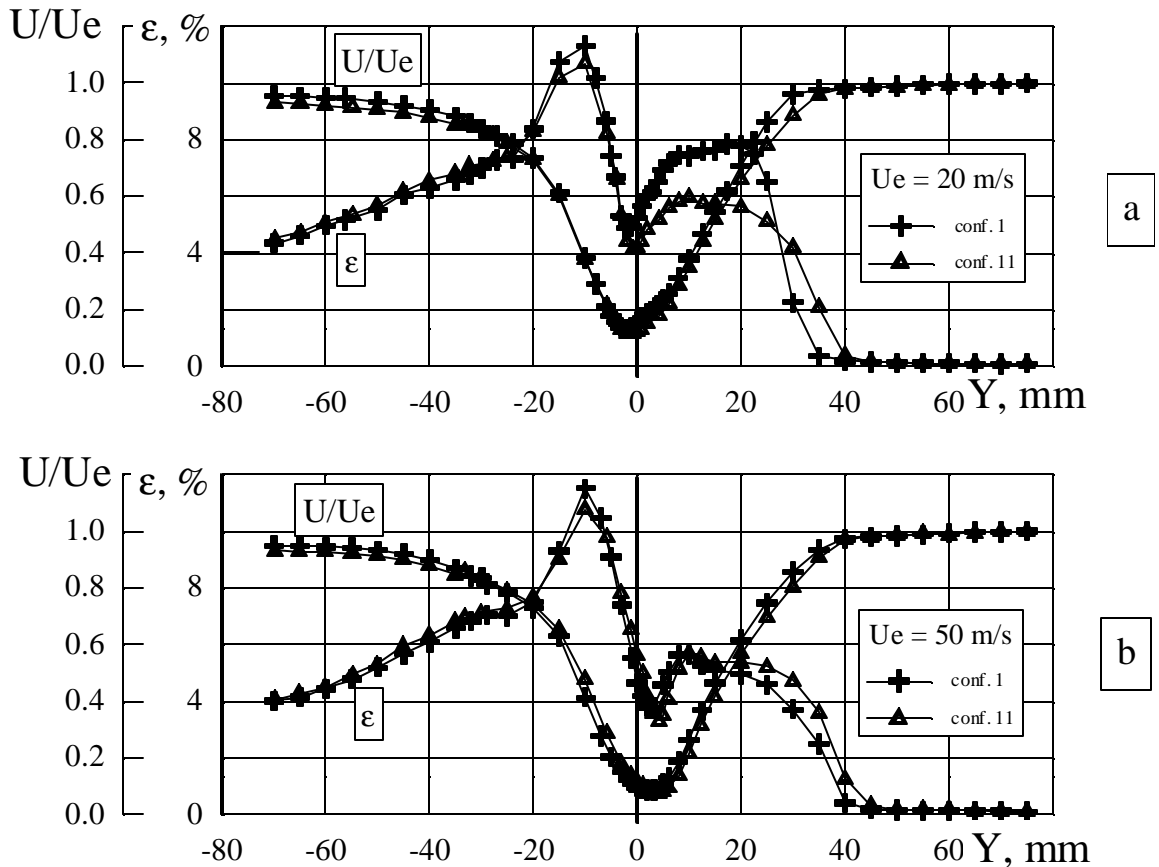
Fig. 5.12

The relative pulsations of the velocity ε reached 11% and were conditioned by the influence of the cowl. At the same time, the maximum level of the velocity pulsations in upper part of the flow was about 6% at the velocity equal 50m/s (Fig.5.12,b). At the flow velocity of 20 m/s, the level of the pulsations depended on the configuration of the model. In particular, at y in the range of 0–30mm, the value of ε was larger by 2% for the configuration No.1 in which the

strings were accommodated on the model than for the configuration No.11 (Fig.5.12,a). It was probably conditioned by the turbulizing influence of the protrusions arranged on the tail cylindrical part of the model in the latter configuration.

In conclusion it may be marked the investigations of eleven configurations of the model fulfilled in the range of Reynolds number equal $(0.8–1.2)\cdot10^5$ showed that presence of obstacles of the studied types on the surface of the axisymmetric model in the form of a fuselage led, as rule, to increase of the drag by 2–20 %, in dependence on the regime of flow over the model, configuration and geometrical parameters of the obstacles imitating electrodes of plasma generators. However, for the model with the tail part having l/d=2:1, there were the regimes at Re_d=$(1–1.3)\cdot10^5$ for which the installation of the electrodes of the certain configuration led to decrease in the drag of the model by about 5–10%.
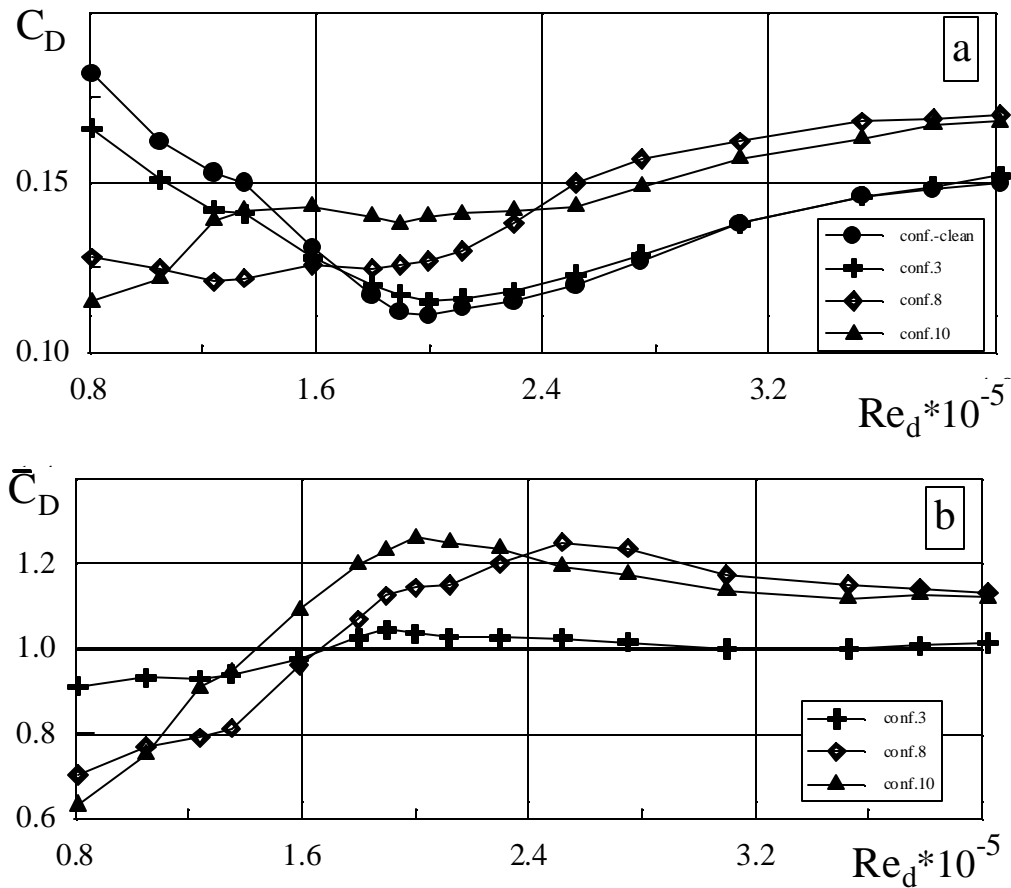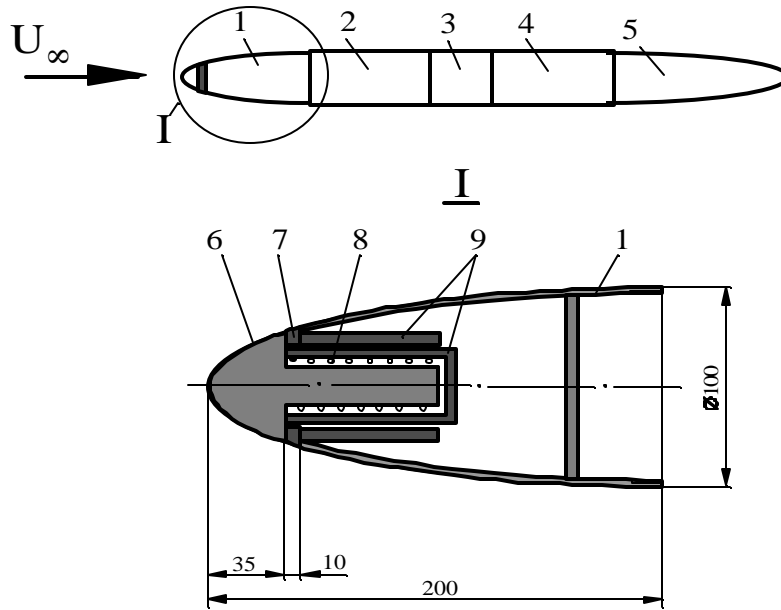

Fig. 5.13

5.2. Summary of the "cold" experiments

The experiments with obstacles showed that they could not only increase the aerodynamic drag of the models but in the case of the model of fuselage also decreased this drag at the define configuration of the obstacles, geometric parameters of the nose and tail parts of the model and the regimes of flow over the model. Thus the idea of expedience of the experiments with the obstacles as the preliminary stage of the experiments on the investigation of the electric discharge influence on the drag justified itself. The additional data in this direction for the model of a

fuselage are given in Fig.5.13 where the values of C_D and $\overline{C}_D$ as functions of Re_d are given for the configurations of the model No 3, 8, 10 (Fig. 5.1). It is seen that, at the obstacles arrangement on the rear cylindrical part of the model with the short tail part, the regimes of flow over the model could exist at which the effect of the drag decrease reached 30-37 % at $\mathrm{Re}_d \sim .8 \cdot 10^5$ for the configurations of the obstacles 8 (single LEBU) and 10 (system of four rings that had teeth). It was about 9 % for configuration 3 (strings). At the increase in the number Re_d up to $1.6 \cdot 10^5$, the gain in the drag decreased independently on the obstacles configurations. At $\mathrm{Re}_d > 1.6 \cdot 10^5$, the presence of "electrodes" led to the drag increase. Such peculiar character of the obstacles influence was probably caused by the turbulizing action of them on the stern separation of the flow at the low numbers Re_d when, at the obstacles absence, the regime of flow around all the model was laminar.

If we consider the heat concept of the electric discharge influence on the drag as the basic one then it is important to definite right those areas on the body surface at which supply of the heat leads to the effect of the drag reduction. The theory [5.2, 5.3] gives the definite forecast in this direction. In fulfilled work, it was verified for the case of the model of fuselage.

1 - nose part; 2 - front cylindrical part;
3 - central part;4 -rear cylindrical part;
5 - tail part; 6 - tip of the model;
7 - heat insulation insertion; 8 - electrical heater;
9 - heat insulation screens

Fig. 6.1

6. EXPERIMENTS WITH HEATED FUSELAGE-LIKE MODEL

One of the positive factors of the discharge influence on flow around a body can be heating of the body surface in that zone where the discharge electrodes are arranged. The theoretical and experimental investigations fulfilled earlier [5.2, 5.3, 6.1] showed that heating of the surface of the flat plate near the leading edge of it led to increase in stability of the laminar

boundary layer downstream, increase in a laminar zone of the flow and, ultimately, to decrease in the wall shearing stress. In this part of the report, the results of experimental investigations are described for the model of fuselage (Fig.6.1) the nose part of which was manufactured of copper and had the elongation of 1.5 for the nose part and 3 for the tail one. The total length of the model L was equal to 1000 mm.

The simulation of the heat influence on the aerodynamic drag was carried out by means of local or total heating of the nose part with help of electrical heater that was arranged inside the nose part of the model. In the first case, directly the tip of the nose of 35 mm – length was heated. It was insulated in heat relation from the rest of part of the model by an insertion of the material with the low coefficient of the heat conductivity. The constructive scheme of the nose part for this case is shown in Fig. 6.1. In the second case, all the nose part of the model of 200 mm – length was heated. The elongation of the nose part in this case was also 1.5.

The measurement of the temperature distribution along the nose part surface was carried out by the system of six thermocouples. For measurement of the boundary layer parameters, the two component constant – temperature anemometer of DISA was used. The probe of the anemometer had diameter of 5μm and 1.2mm - length. In vertical and horizontal directions, it was displaced by a tape–traction mechanism.

Let us consider the results for the first variant of the experiment. The following method of tests was used. At a steady velocity of the incident flow, the drag of the model and the values of the temperature on the surface of it were measured. Then heating was switched on at the power $N = 400$W and, in the definite intervals of time equal 30 sec, the values of C_D and the temperature distribution were simultaneously registered. As only the value of C_D reached the minimum, the electrical heater was switched off. Independently on the flow velocity, the temperature distribution had the view shown in Fig.6.2.
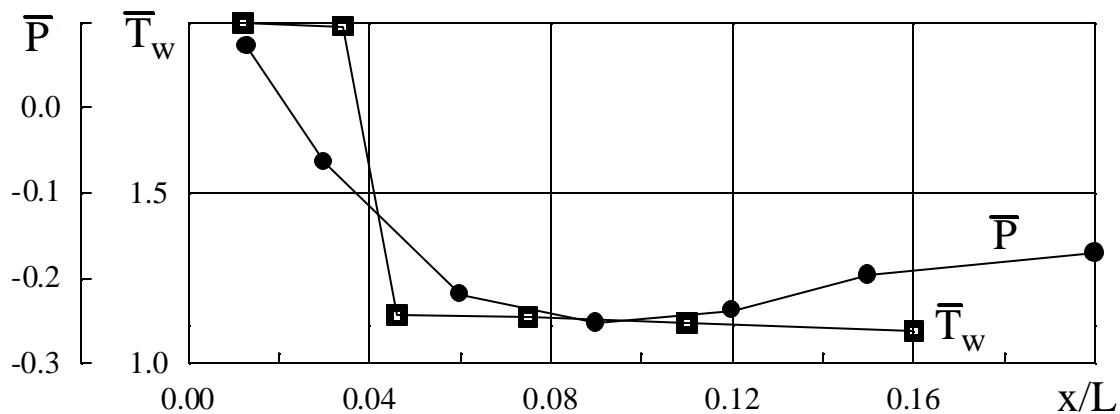

Fig. 6.2

Here $\bar{T}_W = T_W / T_{W0}$ where T_{W0} is the initial value of the temperature and T_W is the current value of it. In this figure, the distribution of static pressure $\bar{p}$ on the nose part of the model at a velocity of the flow of 50 m/s is also given (the static pressure was normalized to the dynamic head). It is seen that, at the heated portion of the model ($\bar{x} = x/L = 0 \div .035$), the pressure abrupt

drops, then reaches the minimum at $\bar{x} = .1$ and further begins to increase. Such pressure drop exerts stabilizing influence on the transition to turbulent regime of the flow at heating of the nose tip.
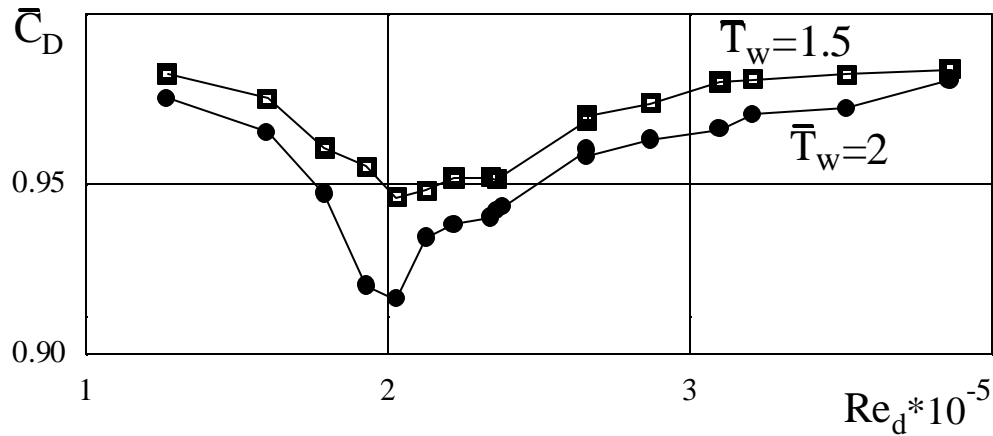

Fig. 6.3

In result of measurements of the coefficient C_D and the surface temperature, the dependence of the relative drag $\bar{C}_D$ on Reynolds number Re_d was plotted ($\bar{C}_D = C_{DH}/C_{DWH}$, C_{DH} is the coefficient C_D at heating of the nose part tip, C_{DWH} is analogous one without heating). In Fig.6.3, the dependence $\bar{C}_D$ on Re_d is presented for two levels of heating of the tip $\bar{T}_W$ equal 2 and 1.5. It is seen that at $Re_d = 2 \cdot 10^5$ the effect of the drag reduction had the maximum value. It turned out to be about 8 % at $\bar{T}_W = 2$ and about 5 % at $\bar{T}_W = 1.5$
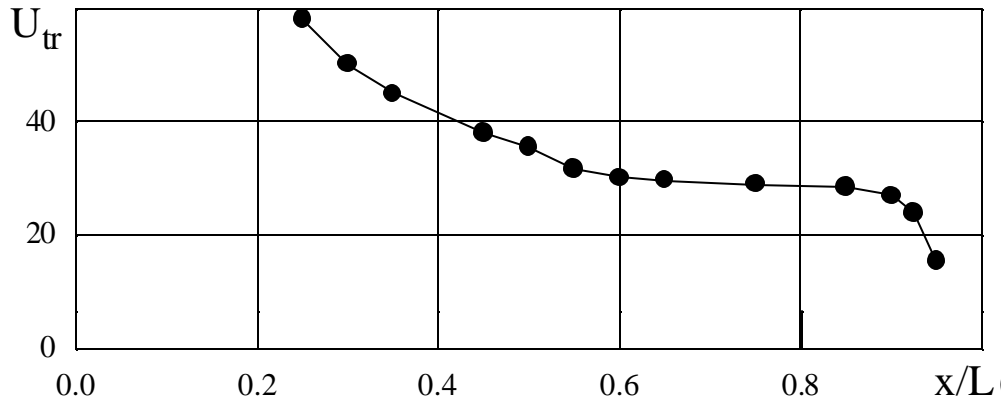

Fig. 6.4

The dependence $\bar{C}_D$ on Re_d where the minimum $\bar{C}_D$ reaches at $Re_d = 2 \cdot 10^5$ ($U_\infty \approx 30$ m/s) probably connects with that the small change of the number Re_d near indicated value of it leads to considerable displacement of the transition from $\bar{x} = .5$ to $\bar{x} = .95$ (Fig.6.4).

Therefore the increase in stability of the laminar boundary layer at heating leads to noticeable decrease in the total drag that connects with the laminar flow zone increase in the boundary layer. The process of the stream laminarization in result of heating of the tip is illustrated by Fig.6.5. Here the dependence of the relative temperature of the tip $\bar{T}_{W1}$ and those of the surface T_{W3} behind the insulating insertion, the relative pulsations u''/U_e and the coefficient $\bar{C}_D$ on the time of heating are given (the pulsations were measured near the upper envelope line

of the model at the point with coordinates equal $x = 500$ mm, $y = .3$ mm and at the velocity U_∞ at the velocity $U_\infty = 34$ m/s).
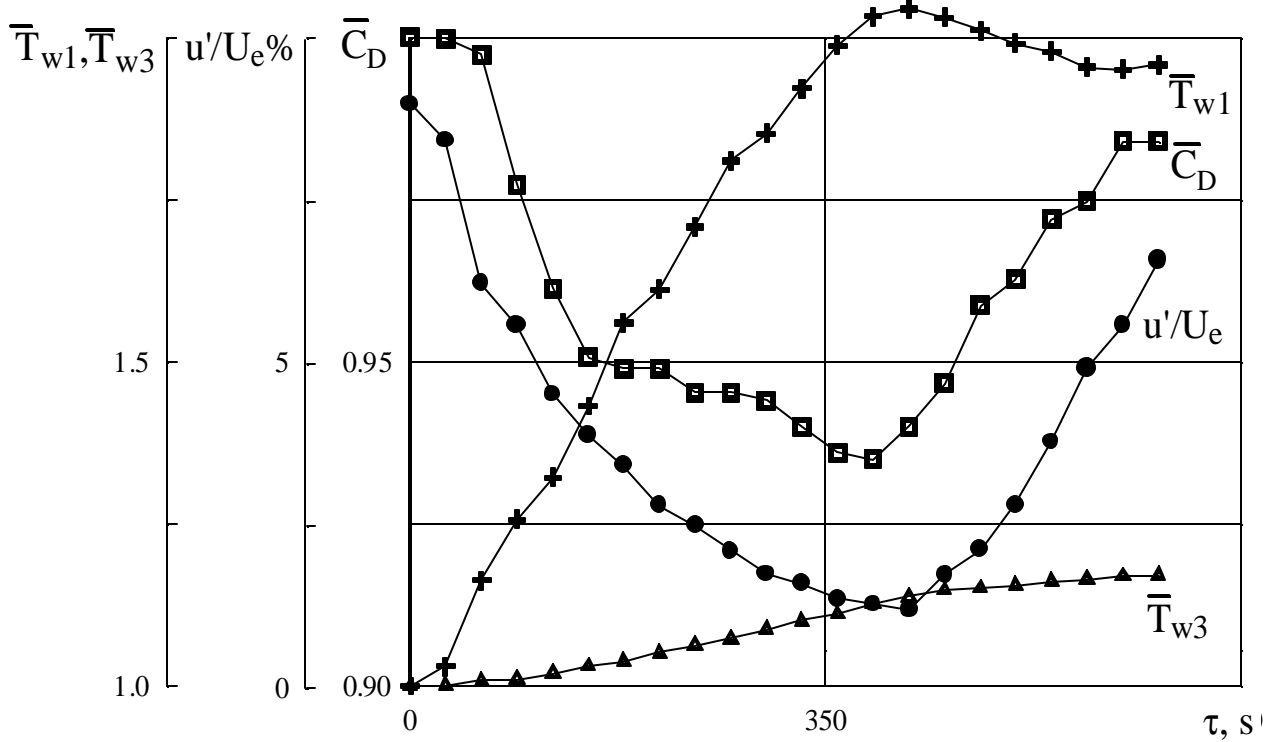

Fig. 6.5

At the growth of the tip temperature $\overline{T}_{1W}$ in the process of heating, the velocity pulsation decreases from 9 % to 1.2 % i.e. laminarization of the stream takes place. Simultaneously the drag coefficient $\overline{C}_D$ decreases and reaches the minimum in 400 sec after switching on of heating. Further, at $t > 420$ sec, the drag and the velocity pulsation begin to increase that connects with reaching of critical level $\overline{T}_{W3} = 1.14$ of the surface temperature behind the insulating insertion that exerts destabilizing influence. Heating of the last surface takes place, in basic, because of the heat transfer from the flow that has been warmed near the tip.

The fulfilled experimental investigations showed on importance of the heating zone localization in the area of the negative gradient of pressure. In particular, heating of all the nose part that had the length equal 200 mm along the axis x led to increase in value of the drag at all the levels of heating. This fact is illustrated in Fig. 6.6,a where the dependence of the relative coefficient $\overline{C}_D$ on Re_d is given for the different values of heating of the surface. The surface temperature distributions corresponding to these regimes (measured without flow) are shown in Fig 6.6,b. The distribution of the relative static pressure $\overline{p}$ on the nose part is also given in this figure.

It can be noted that destabilizing influence of heating which led to the drag increase was connected with putting the zone of heating on the area of unfavorable change of the pressure ($\overline{x} = .1 \div .2$) at the nose part (Fig. 6.6,b).

It will be also noted that, in these experiments, the analogous tests were carried out for the

model that had the short tail part ($\lambda_{tail} = 1.5$). In this case, heating both all the nose part of the model and the tip of it always led to the drag increase. It can be supposed that, at this configuration of the model, the negative effect of the increase in the stern separation zone at the laminarization of the flow on the cylindrical part of the model was putted on the positive effect of the transition delay at heating of the tip. However this question requires more detail additional investigations.
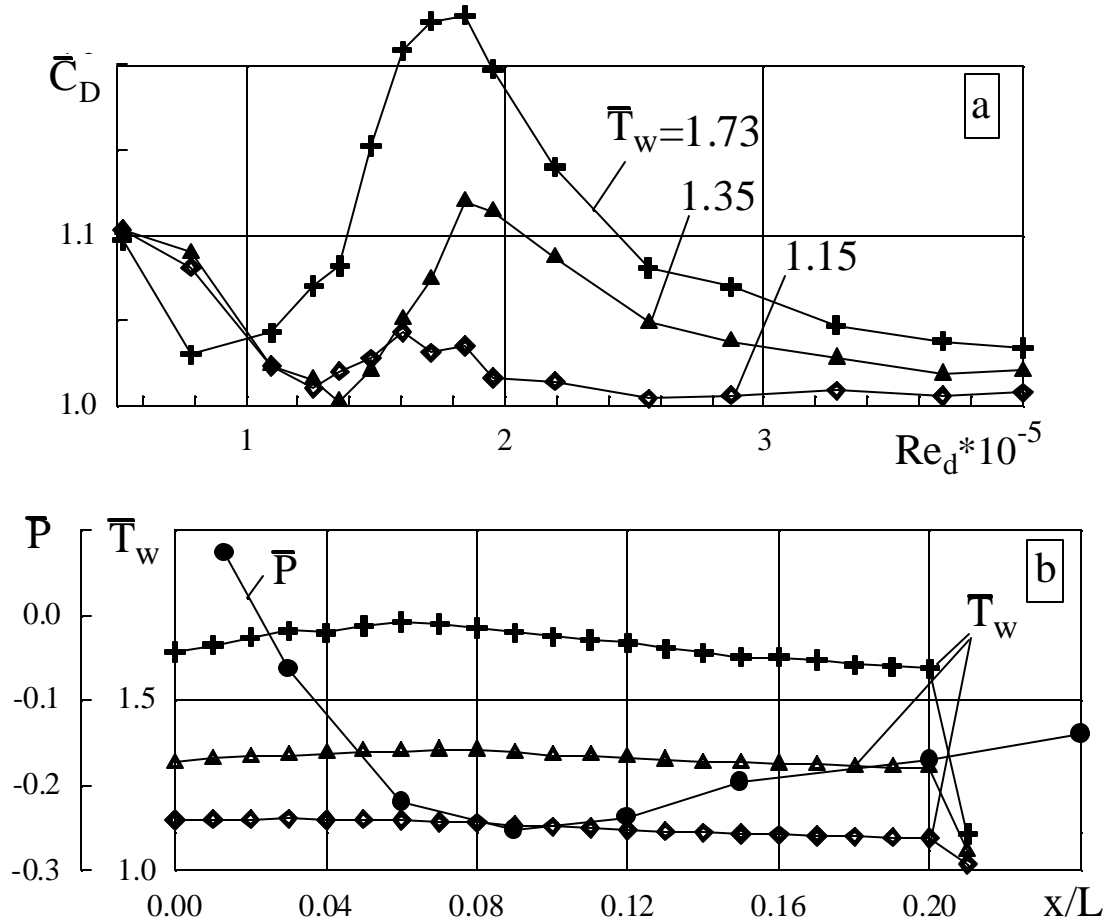

Fig. 6.6

The basic conclusion that follows from fulfilled tests consists in the result that not only the temperature level exerts essential influence on the drag of the model at use of this method of drag reduction but also the position and size of the heated zone which is necessary to tie with the pressure distribution on the model surface. As the fulfilled experiments showed, heating of the nose part of the model in area the negative gradient of pressure can lead to the noticeable decrease in the total drag.

7. EXPERIMENTS ON THE FLAT PLATE AND FLOATING ELEMENT.

As it was noted above, the role of the flat plate model in these tests played the lower wall of the wind tunnel T-36I. The tests were carried out in three series.

In the first series of the tests, the turbulizator was installed on all four walls of the wind tunnel. It had uniform graininess (mean size of the grain equaled 32μm) and was deposited on the

plates that had the thickness of about 1mm. The distance from the leading edge of the turbulizator to the test section origin was x_T=480 mm, the width of the turbulizator Δx_T was about 40mm.
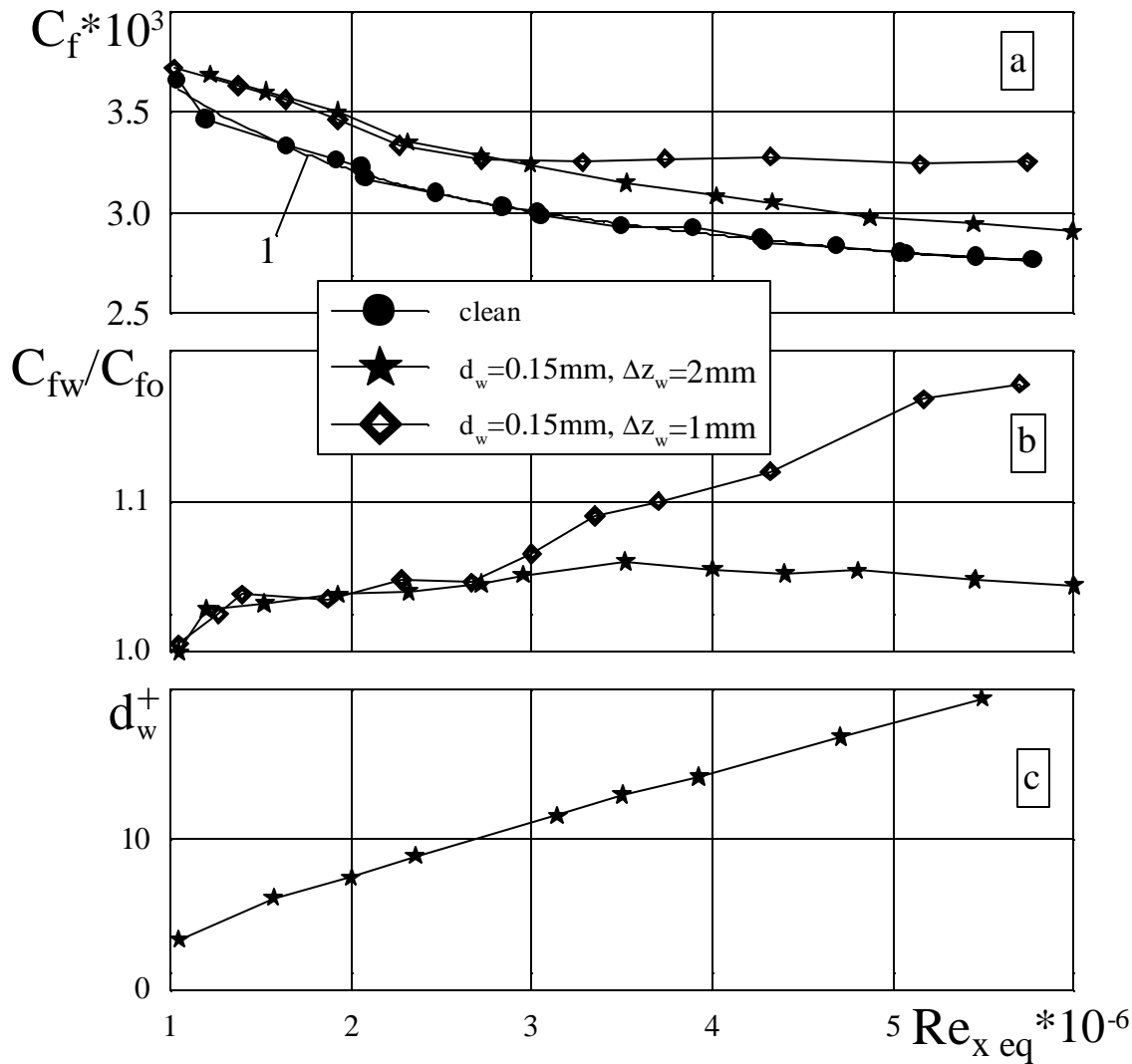

Fig. 7.1

The obstacles in the form of strings that had the diameter d_w=0.15mm, the length l_w=270mm and two values of the step Δz_w=1;2 mm were stretched along the surface of the floating element and fitted closely to it. The results of experiments are presented in Fig. 7.1 where the dependence of the coefficient of the local friction of C_f on Reynolds number $Re_{Xeq}=u_\infty x_{eq}/\nu$ (here x_{eq} is the distance from the leading edge of the turbulizator to the center of the floating element) is illustrated. For comparison, in this figure by the line 1, the dependence of the coefficient C_{f0} on Re_{eq} for a "smooth" plate is given. The last curve was obtained on the base of the mean velocity profiles $\bar{u}$ (y) and on the literature data for the coefficient C_{f0} as a function of δ^*, δ^{**} and etc. It is seen that estimations of C_{f0} on the profiles of $\bar{u}$ (y) and the analogous values measured with help of the floating element practically coincide. The installation of the strings of variant No.1 with d_w=0.15mm and Δz_w=2mm on the floating element led to increase in the value of the local friction by about 4–6 %.

At the more compact arrangement of the strings (variant No.2, d_w=0.15mm, Δz_w=1mm), the experimental function of $C_{f0}(Re_{Xeq})$ coincided with the analogous one for the variant No.1 in

the range of the Reynolds numbers $10^6 \leq Re_{Xeq} \leq 3 \cdot 10^6$ (Fig. 7.1,b). It may be noted that, in this range of Re_{Xeq}, the dimensionless diameter of strings

$$d+ = (d_w u_\infty / \nu)\sqrt{C_f \Big/ 2}$$

that was calculated in the coordinates of "the wall law" equaled 4–10 (Fig. 7.1,c). Thus the strings with the diameter $d_w^+ \leq 10$ were equivalent in the hydrodynamic meaning to each other, non dependently on the packing "density" of them.

At the values of $d+ \geq 10$, the density of packing influenced significantly on the increase in the friction drag. In particular, at $\Delta z_w = 2mm$, the value of C_{fw}/C_{f0} was practically constant and equal 1.05, but, at $\Delta z_w = 1mm$, it increased at the growth of Re_{Xeq} (up to the value of about 1.2 at $Re_{Xeq} \approx 6 \cdot 10^6$) (Fig. 7.1,b).

In the second series of tests, the turbulizator was removed from the wind tunnel walls. It gave possibility to measure the local friction coefficient at the laminar, transitive and turbulent regimes of flow in the boundary layer. In Fig. 7.2,a, the dependence of the coefficient C_f on the Reynolds number Re_1 is presented.
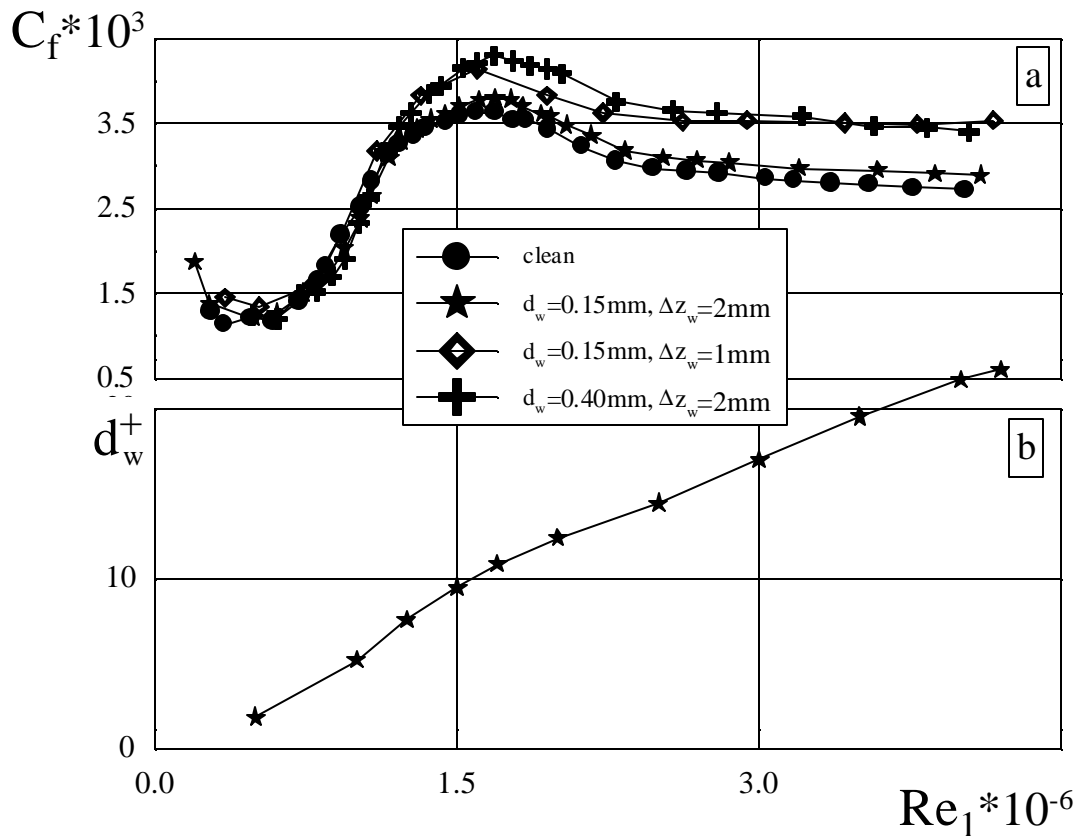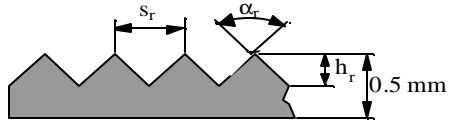

Fig. 7.2

It is seen that at $Re_1 \leq 1.6 \cdot 10^6$, the friction drag coefficient of the surfaces with strings ($d_w = 0.15mm$) at the laminar and transitive regimes of flow ($d_w^+ \leq 10$–12, Fig.7.2,b) practically coincided with C_{f0} of a smooth surface. At the transition to the turbulent regime of the flow, the value of C_{fw} increased and, at $Re_1 \approx (3.0 - 4.25) \cdot 10^6$ ($u_\infty = 45 - 60m/s$), the relative losses $\Delta C_f = (C_{fw} - C_{f0})/C_{f0}$ equaled about 6% for $d_w = 0.15$ ($d_w^+ = 18 - 22$), $\Delta z_w = 2mm$ ($\Delta z_w^+ = 220 - 300$).

They were about 25% both at d_w=0.4mm ($d_w^+ \approx 45 - 60$), Δz_w=2mm (Δz_w^+=220 − 300) and at d_w=0.15mm ($d_w^+ \approx 18 - 22$) but at Δz_w=1mm (Δz_w^+=110 − 150). Thus, from the point of view of the friction rise, the increase of the strings diameter in $d_{w2}/d_{w1} \approx 2.7$ times is equivalent to the reduction of the interval between the strings in the crosswise direction in 2 times.

Table 7.1

? plate	h_r mm	s_r mm	α_r	
? 1	0.07	0.26	112°	
? 2	0.1	0.25	53°	
? 3	0.22	0.26	53°	

In the third series, the laminar/turbulent transition was measured over the strings stretched on the surface of the floating element and also over riblets. The plates with riblets of material on the base of magnesium had the thickness of .5mm, the area equal 315x375mm and were directly glued on the lower wall. The total length of the region where the experiments were carried out was 945mm and 375mm – width. The origin of this region was at the distance of 500mm from the edge of the nozzle. The front edge of the plate with the ribs had the form of a half wedge. The geometrical parameters of the riblet plates are given in Table 7.1.

In the most works, the riblet coatings were being studied for the goal of the turbulent friction drag reduction. In [6.2, 6.3], for the first time it was experimentally shown that riblets can significantly delay the late stages of the transition to turbulence but can accelerate the initial phase of it. In our experiments, the first trial tests on study of the riblet parameters influence on the laminar/turbulent transition were fulfilled in conditions of the boundary layer of the wind tunnel T-36 I. It will be noted that recommends of [6.2, 6.3] (included the choice of the dimensionless parameters) were taken into account only particularly.

The measurements of the profiles of the mean velocity $\bar{u}(y)$ and the longitudinal pulsations $u'(y)$ were carried out by the hot-wire anemometer type of which and parameters were presented above. The probe of the anemometer was displaced along the X – axis on those height y where u=0.5 u_∞. The position of maximum of the longitudinal pulsations $\max[u'(u_\infty = const, x)]$ was considered as the position of the laminar/turbulent transition. The velocities u_∞ lied in the range of 10 – 30m/s.

The results of the tests are illustrated by Fig. 7.3. In particular, in Fig. 7.3,a, the values of Reynolds number of transition Re_{tr} are presented as a function of Reynolds number $\underline{\mathrm{Re}_1} = u_\infty / \nu$. In Fig. 7.3,b, the values of the relative change of Reynolds number of transition $\Delta \mathrm{Re}_{tr} = (\mathrm{Re}_{trw}-$

Re_{tr0})/Re_{tr0} as a function of Re_1 are given (here Re_{trw} and Re_{tr0} are Reynolds numbers of the transition for the surfaces with the obstacles and smooth ones, correspondingly). The Reynolds numbers of the transition were counted up with calculations that the origin of the "equivalent" boundary layer was arranged upstream from the cut of the nozzle and was described by the relation $\Delta x_{eq}=(20u_\infty-30)$mm.
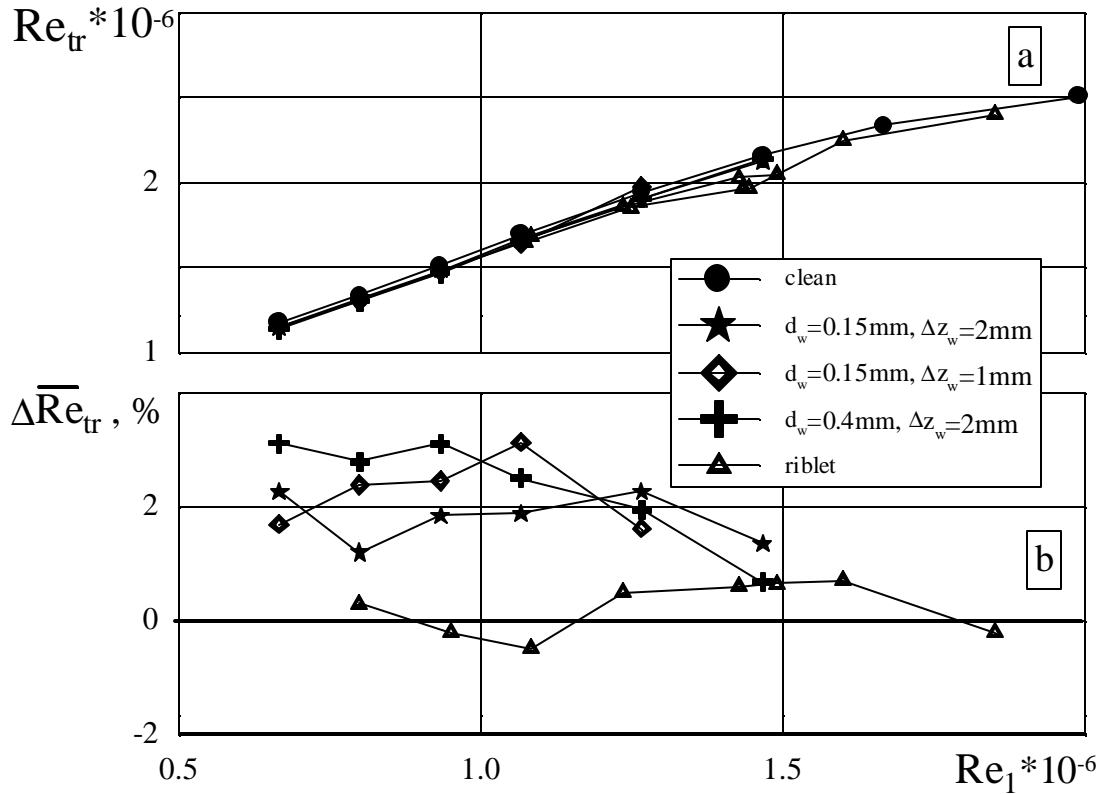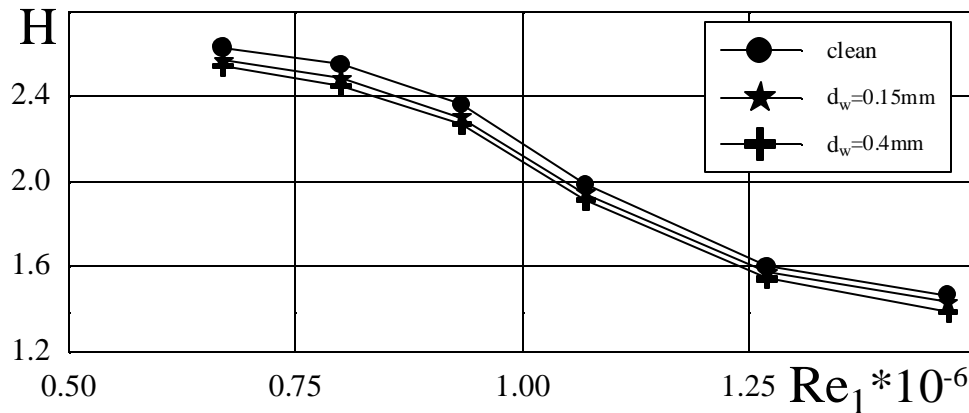

Fig. 7.3

Fig. 7.4

From the results presented, it is followed that the displacement of the transition upstream was insignificant and for strings did not exceed $\overline{\Delta \mathrm{Re}_{tr}}$ =2% at d_w=0.15mm and $\overline{\Delta \mathrm{Re}_{tr}}$ ≤3% at d_w=0.4mm. The displacement of the transition on the surfaces with riblets was not practically observed (Fig. 7.3,b). This fact can be conditioned by following causes. According to [6.2, 6.3], the riblets arranged longitudinally deturbulize the flow and accelerate the transition if they are in the region of the development of Tollmien–Schlichting wave. These riblets arranged in the region

of rise and development of Λ structures essentially delay the transition to turbulence. In given tests, the path of riblets was long enough and intersected both the linear and non-linear areas of the transition development. Thus, the acceleration of the transition at the linear stage was compensated by delay of it in the non-linear stage of the transition development. This supposition are planned to verify in the following stage of the tests.

Apart from measurements of the laminar/turbulent transition, the profiles of $\bar{u}(y)$ and $u'(y)$ in the boundary layer behind the strings were measured. The measurements were carried out at u_∞ in the ranges from 10 to 22m/s in the cross-section $x=1235$mm i.e. at the aft cut of the floating element.
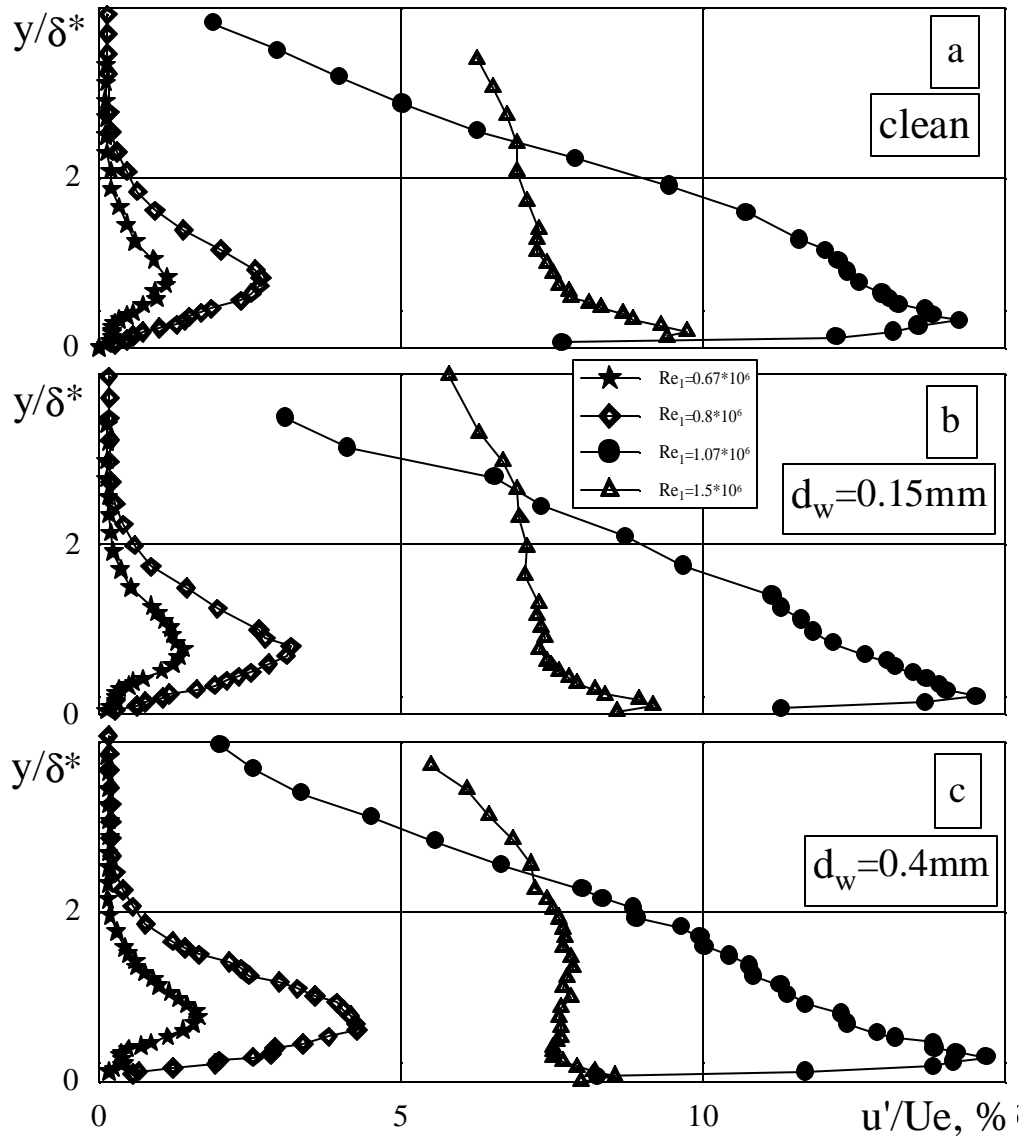

Fig. 7.5

In Fig. 7.4, the plot of formparameter $H = \delta^*/\delta^{**}$ as a function of Re_1 are presented both for the boundary layer on the smooth surface and on the surface with strings at d_w=0.15; 0.4mm; Δz_w=2mm.

It is seen that, in this range of Reynolds numbers, all three regimes of flow over the

floating element were realized: the laminar regime for which $H(\text{Re}_1 \approx 0.7 \cdot 10^6) \approx 2.6$, the transition one with $H(\text{Re}_1 \approx 10^6) \approx 1.9$ and the turbulent one for which $H(\text{Re}_1 \approx 1.5 \cdot 10^6) \approx 1.45$. The mutual position of functions $H(\text{Re}_1)$ for the smooth surface and that with the strings also testifies about insignificant displacement of the laminar/turbulent transition upstream in case the surface with the strings. It may be also noted the dependence $H(\text{Re}_1)$ fully conforms with the results of the balance measurements at these values of Reynolds numbers Re_1 (see plot of C_f vs Re_1 in Fig.7.1,a).

The distribution of pulsations $u'(y/\delta)$ in the boundary layer in the wake behind the strings is shown in Fig. 7.5. It is seen that intensity of pulsations slightly increased at the presence of strings at all the regimes of flow (from the laminar regime to the turbulent one). More detail analysis of the turbulent pulsations structure change (included the measurements of $v', w', \overline{u'v'}$) are planned to carry out in future.
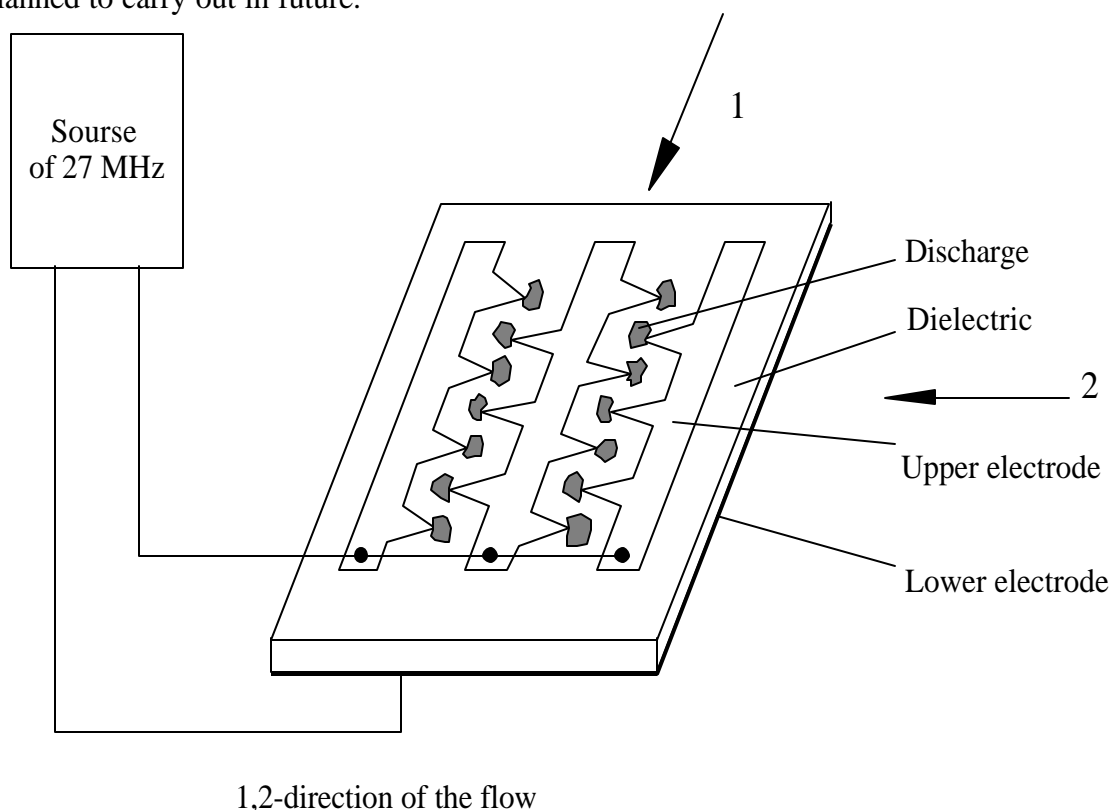

Sourse of 27 MHz

1

Discharge

Dielectric

2

Upper electrode

Lower electrode

1,2-direction of the flow

Fig. 8.1

8. DEVELOPMENT OF THE DISCHARGE GENERATOR

The analysis fulfilled at TsAGI showed that the economically profitable skin friction reduction with help of the near surface electrical discharges would be possible if the serious requirements to the values of effect and energetic expenditures were carried out. For example, the evaluation of the fuel effectiveness of this method for a subsonic transport aircraft that has the skin friction equal 50% of the total drag gives the value of the fuel economy of approximately 6% if the turbulent skin friction reduction is 20% and the expenditures on the electric discharges creation are about 1kW per 1m^2. The results of experiments with the model of fuselage presented above distinctly show that it is necessary, by the optimal way, to match the geometry of a body

and the place of the heat area arrangement to reach success in this direction. A number of aerodynamic experiments [1.2] shows that effective influence on the turbulent skin friction can be created by the system of small randomly deposited unevenness. On the other hand, it can be expected that the local many point discharges could carry out the function of such unevenness. Apart from that, the local character of the discharge burning must lead to reduction of the energy expenditures in comparison with the method of the distributed surface heat. The theoretical investigation that was carried out at TsAGI shows that the last method of the drag reduction is not effective at least at subsonic and low supersonic velocities.

a)

b)

Fig. 8.2

In the fulfilled work, the investigation on creation of discharges which we called many point ones was carried out at the 27 MHz electric field source use. The discharges were ignited as capacitive ones on the principal scheme shown in Fig. 8.1.

The basic difficulty of the HF discharge creation on the surface of a dielectric was significant density of the capacitive current that passed through the dielectric at $F = 27$ MHz.

This current going through the plasma as a current of conductivity gives off the Joule's energy and heats both the plasma and air. If this energy exceeds some threshold the destruction of the dielectric surface begins and also the system of electrode/dielectric breaks down. Therefore, the concept of the many point discharges use conforms with necessity of the reduction of the energy provided to the unit of area. In this case, at the moderate electric fields, the electron emission value is restricted by small dimensions of the discharge dots and also limited by the number of them on the unit of the surface. On the other hand, the use of an enough power source allows to serve a large area of a surface due to rising of the number of points at which the discharge ignites.
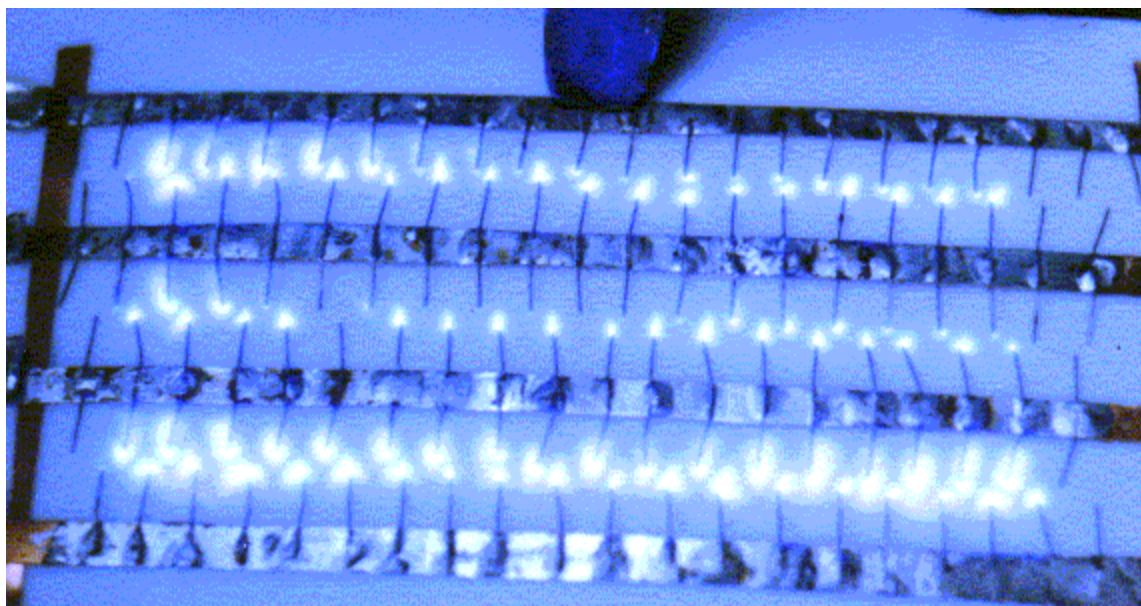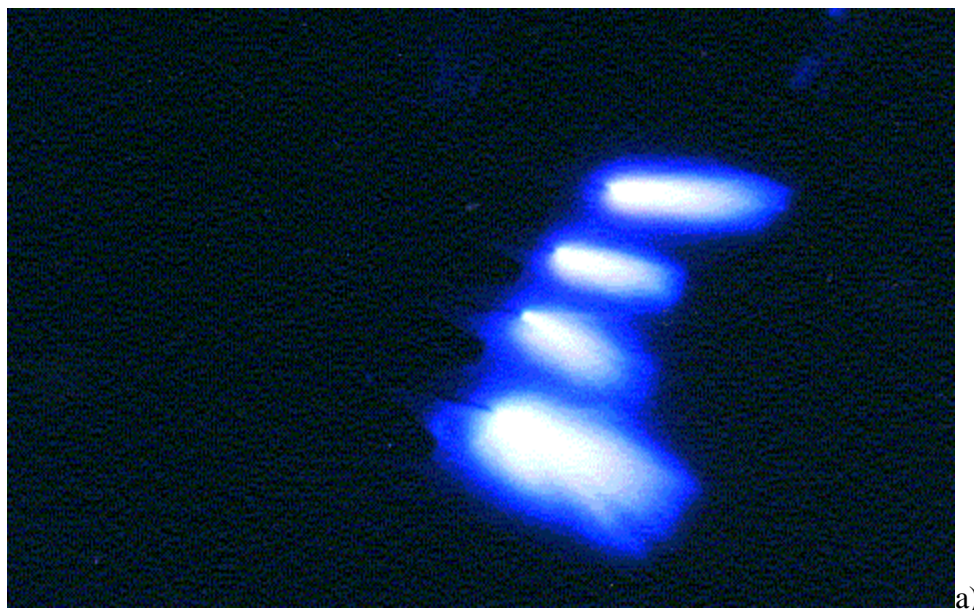

a)

b)

Fig. 8.3

All the basic experiments considered below were carried out at presence of the air flow with a velocity of about 10 – 20 m./s both for observation of peculiarities of the discharge burning at these conditions and cooling of the surface and the electrodes at which the discharge burnt that turned out to be important to prevent arising of the arc regime.

In the preliminary work, the answers were obtained for a number of technical and physical problems. In particular, the important role of the material of the insulator that separated upper and lower electrodes was elucidated. Such dielectric materials as textolite, teflon, plexiglass and high temperature rubber were tested. At textolite and rubber use, discharge actively spread on the surface of dielectric; the surface under the discharge scorched, became conducting and broken down. At plexiglass use and moderate fields, the discharge burnt near the electrode but the surface of plexiglass was quickly melted because of heating and also broke down.

The best results on endurance of the dielectric was obtained at use of teflon. At the moderate electric fields, the discharge burnt only near the points and destruction of the dielectric was minimum. Therefore the basic investigations were carried out at the teflon use.
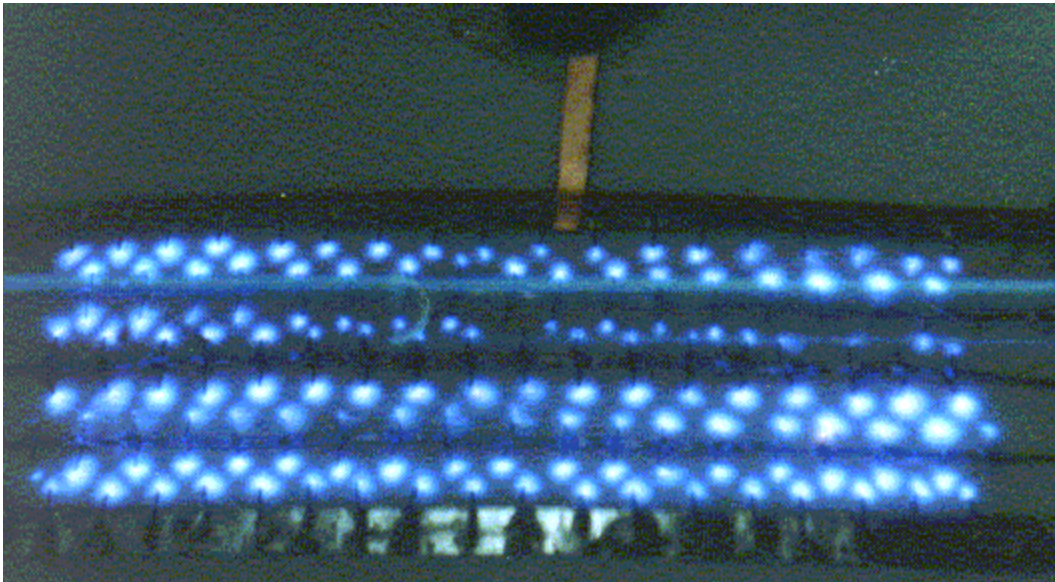

Fig. 8.4

The complex of investigations on choice of the materials of electrodes was fulfilled. The electrodes were manufactured of duralimin, titanium, stainless steel and copper. It turned out that the discharges on electrodes of titanium and stainless steel were inclined to transformation in an arc discharge, probably because of lower heat conductivity. Therefore, the basic experiments were made with electrodes of duralimin and copper.

The complex of experiments was also curried out to the end of choice of the geometry of electrodes. The problem consists in the neighboring plots of the metal surface can mutually screen the electric field near each other. Only in cases when such screening was not essential the decision of the discharge ignition problem was simple enough. For example, in Fig. 8.2 and 8.3, some results of the second stage of this treaty are presented. In particular, in Fig. 8.2.a, the photo of discharge is given for a line system of sharp teeth. In Fig. 8.2b, the photo of the discharge is presented for the system of electrodes that consisted of three rows of the teeth. In this case, the field near the point of each tooth depended on its geometry and a distance to the stripe of electrode bringing the following system of teeth. In this case, the discharges burnt better in the region where the neighboring plots of the electrode exerted weaker screening influence and did

not burn at those teeth where screening was essential (some upper inner teeth). In Fig. 8.3a, the photo of the discharges on the points of the one line system of thin wires is presented. In case of Fig. 8.3b, the discharges were realized in the multi electrode system of thin wires.
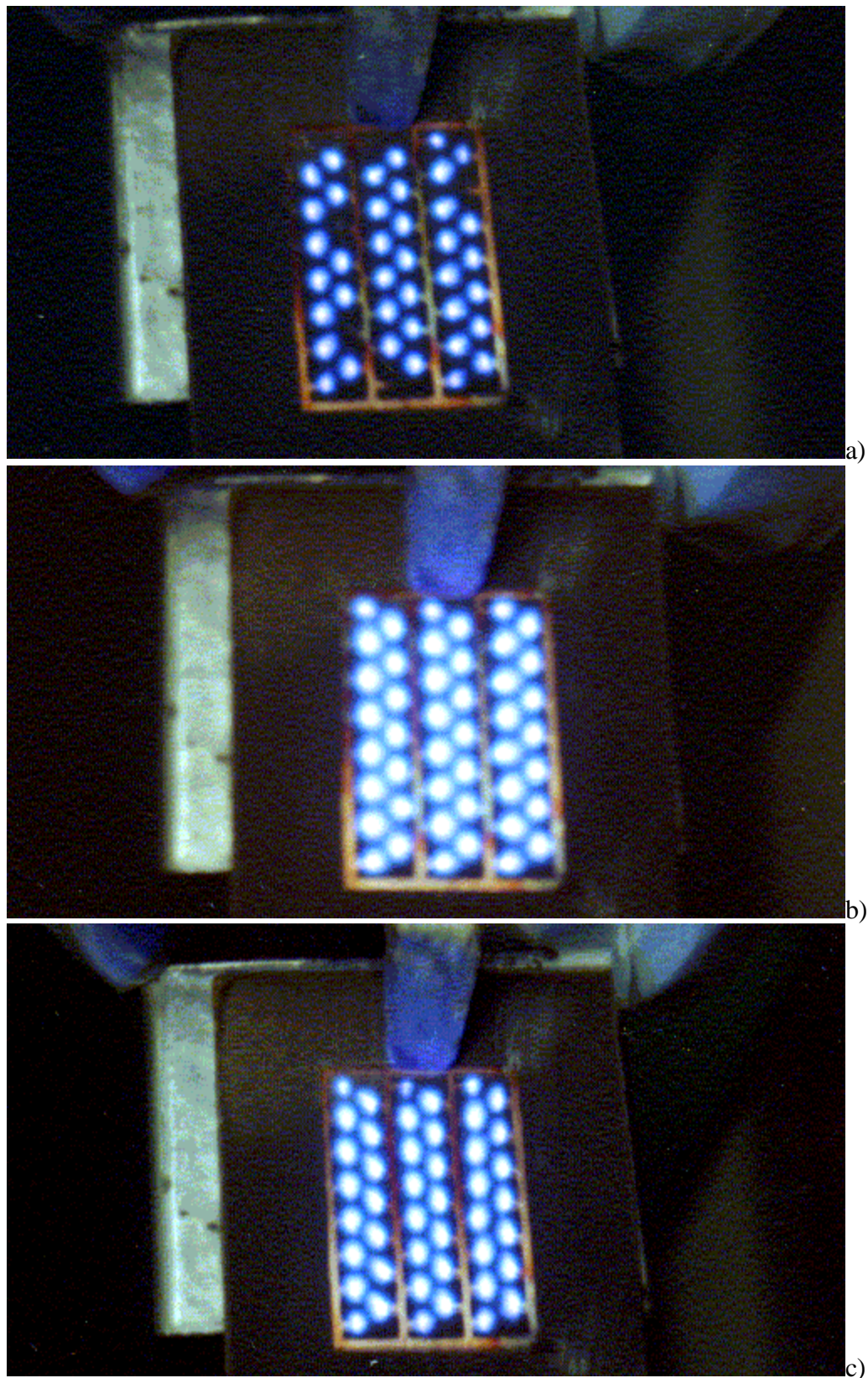

a)

b)

c)

Fig. 8.5

On the base of these results, the decision was accepted that the line point systems of

electrodes are the most perspective for creation of many point discharge on the large surface and the further work was mainly carried out in this direction.
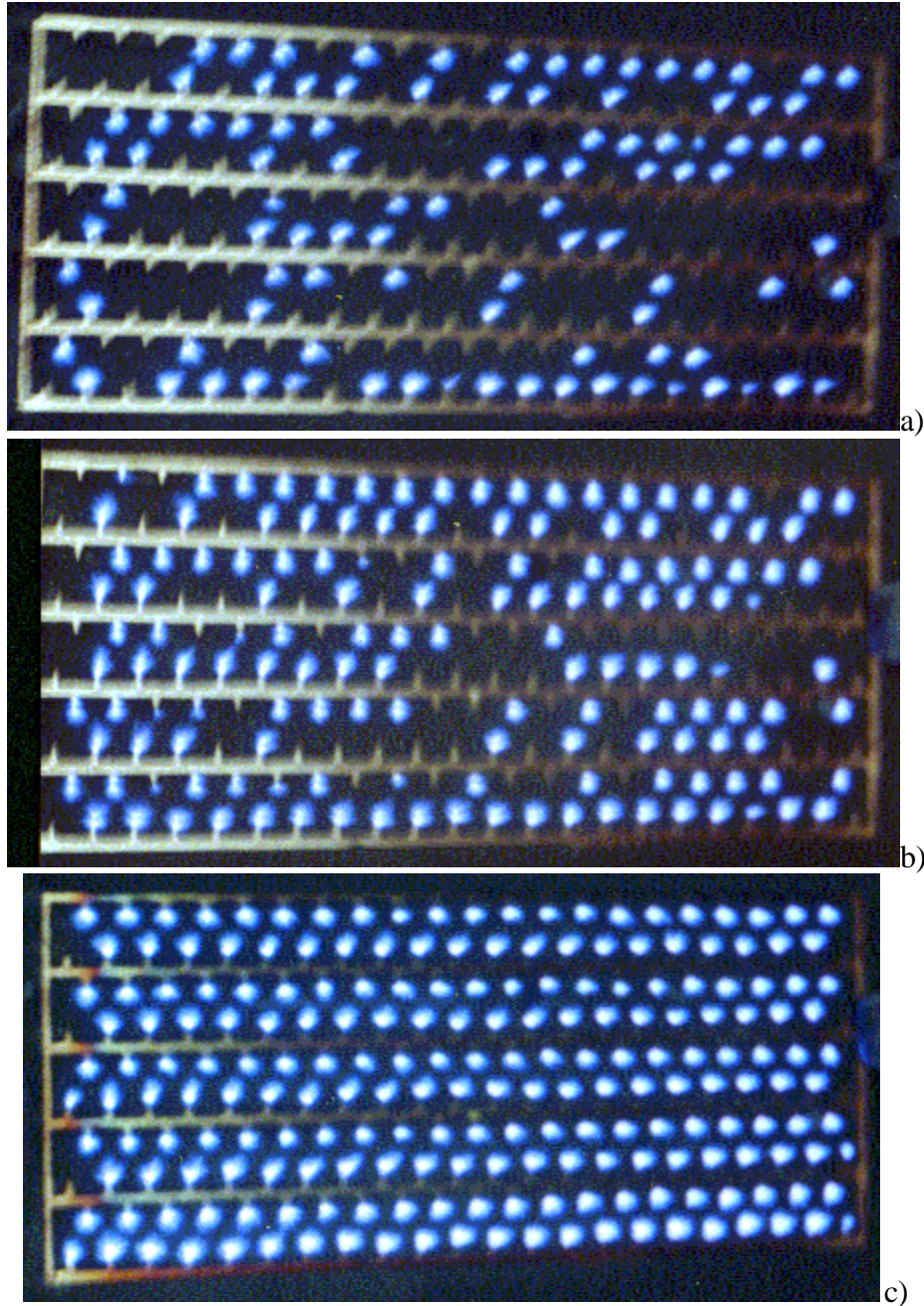

Fig. 8.6 (rotated clockwise 90°)

In Fig. 8.4, the local discharges in the multi line system of points manufactured of a thin copper wire are shown. Every crosswise wire had diameter of .2 mm and 2 mm – length. The extreme rows of these wires were soldered to copper strips; the inner wires were soldered to bearing copper wires of .4 mm – diameter. The discharges burnt in more than 100 points. The defect of such system consisted in difficulty of creation of strict geometry of the points arrangement at large number and high density of them since this system was not hard.

More perspective results were obtained with the electrodes in form of the line systems of sharp teeth that were manufactured of radiotechnical teflon with copper coating (Fig. 8.5 – 8.7). In fulfilled experiments, the thickness of dielectric was 1.5 mm. It was .1 mm for copper coating.

The step of strips was 9 mm. That of teeth along the strip equaled 5 mm. The height of a tooth equaled 2 mm. At this geometry, the maximum density of the discharge dots was 4.5 cm^{-2}.

In Fig. 8.5, the photographs of the many point discharge are shown for the variant of the system in which maximum number of points for the discharge ignition was 45. In Fig. 8.5a and 8.5b, the comparison of the discharges are given at two different levels of power input to the electrode system (the direction of air flow was crosswise to the strips). In case of Fig. 8.5a, the power was insufficient for the discharge ignition at all the points. Fig. 8.5b and Fig. 8.5c give comparison of the many point discharge burning at the level power input when the discharge ignition was realized at all points but, in the first case, the direction of the flow was crosswise to the strips and it was longitudinal in the second situation. It is seen that the discharge burning was identical at both cases. The estimation of the total active power supplied the plasma/electrode system in the last two cases gave the values about 100 – 130 W and the power density was about 9 – 11 W/cm^2.
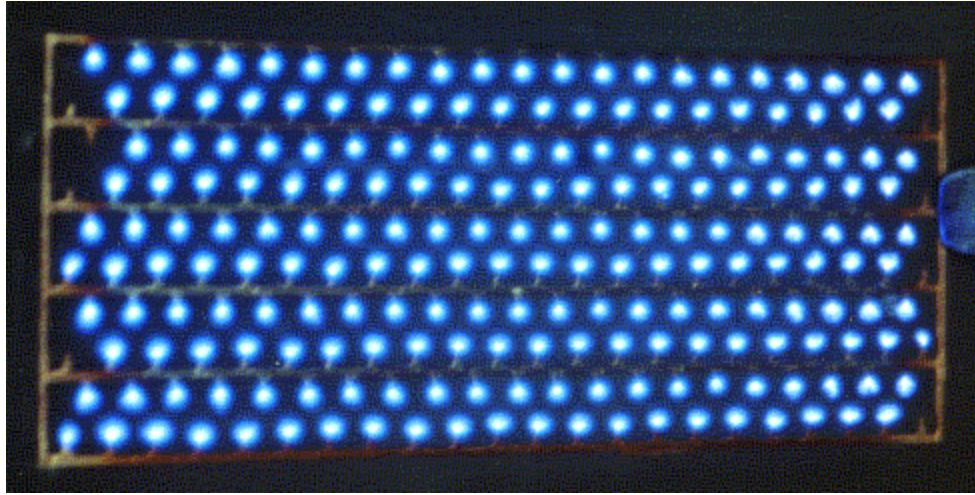

Fig.8.7. (rotated clockwise 90°)

In Fig.8.6 and 8.7, the view of the discharges is shown in the multiple-point system 45 by 110 mm in total size and maximum number of discharge dots equal 215. The structure of the electrode system was the same as in the case for Fig.8.5. The examples of the discharge burning at the direction of the air flow along the leading voltage strips and at the different levels of the power input are presented in Fig. 8.6 (the level of power rose from photo a to that c). In case of Fig. 8.6c, the discharge was realized practically at all the teeth. The photograph of the analogous discharge at the crosswise direction of the flow and the same level of power as for Fig.8.6c is shown in Fig.8.7. It is seen that the view of the discharge in both these cases practically coincides. However it can be noted that ignition of all system of the discharge at this geometry was reached at more high power than in the case of the geometry shown in Fig.8.5 and the dots of the discharge occupied some less area than at that geometry. The estimation of the total active power supplied to the discharge/electrode system for the case when discharge burnt on all the points gave values in the range of 350 –450 W and power density was about 7 – 9 W/cm^2. Let us note that the local active power on one dot led in the range from 1.5 to 2 W in the case of the large model (Fig.8.6,c, Fig.8.7) and it equaled 2.2 –2.9 W in the case of small model (Fig.8.5).

9. WIND TUNNEL EXPERIMENTS WITH FLAT PLATE RIBLET-LIKE DISCHARGE GENERATOR MOUNTED AT THE FLOATING ELEMENT

In frame of this contract fulfillment, the generator of high voltage pulses (HVPG–1) was worked out and manufactured for the experiments on plasma aerodynamics, in particular, in the low turbulent wind tunnel T–36I. The generator has got the regulated amplitude of the voltage U_d in the range from 4 to 12 kV; the frequency of following of pulses f_p and the duration of them $\Delta\tau_p$ are varied in the ranges from 3 to 20 kHz and from 5 to 50 μs, correspondingly. Apart from measurements of U_d, f_p, $\Delta\tau_p$, apparatuses of the check building in HVPG–1 allow to estimate the value of the power $\tilde{N}_d$ supplied to the discharge-electrode system. The cycle of the investigations on the choice of the characteristics of HVPG–1 providing the stable discharge burning was fulfilled.
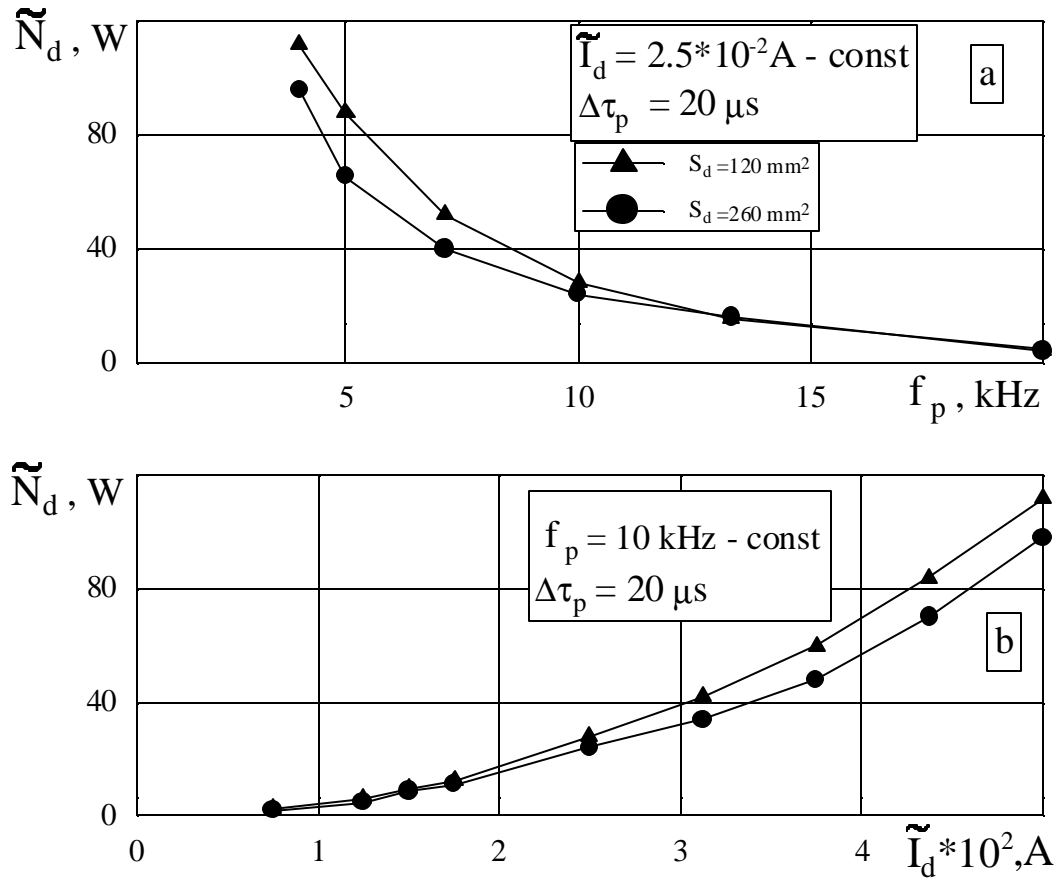

Fig. 9.1

For example, in Fig. 9.1, the dependence of power $\tilde{N}_d$ on the frequency f_p and on the mean value of the discharge current $\tilde{I}_d$ is shown. These characteristics relate to the discharge generators of "riblet" type manufactured in view of a row of nichrome wires. The wire had diameter equal .18 mm and was stretched with the step $\Delta z_W =4$ mm on the panel of glass – textolite. The generator having the discharge burning area $S_d =120$cm^2 was installed on the nose part of the flat plate (Fig. 9.2, position 3*) and that with $S_d \approx 260$cm^2 was arranged on the panel before the floating element of the balance (Fig.9.2, position 1*).

From the presented data, it is seen that the dependence $\tilde{N}_d\left(f_p\right)$ and $\tilde{N}_d\left(I_d\right)$ stay close in

these two cases in spite of the difference of the area occupied by the discharges about 2.2 times (the maximum difference of data did not exceed 15 %). This signifies that power input is the own characteristics o HVPG and changing the area which can be occupied by the discharge it is possible to control the density of power $\tilde{N}_d/S_d$ that influence on the flow.
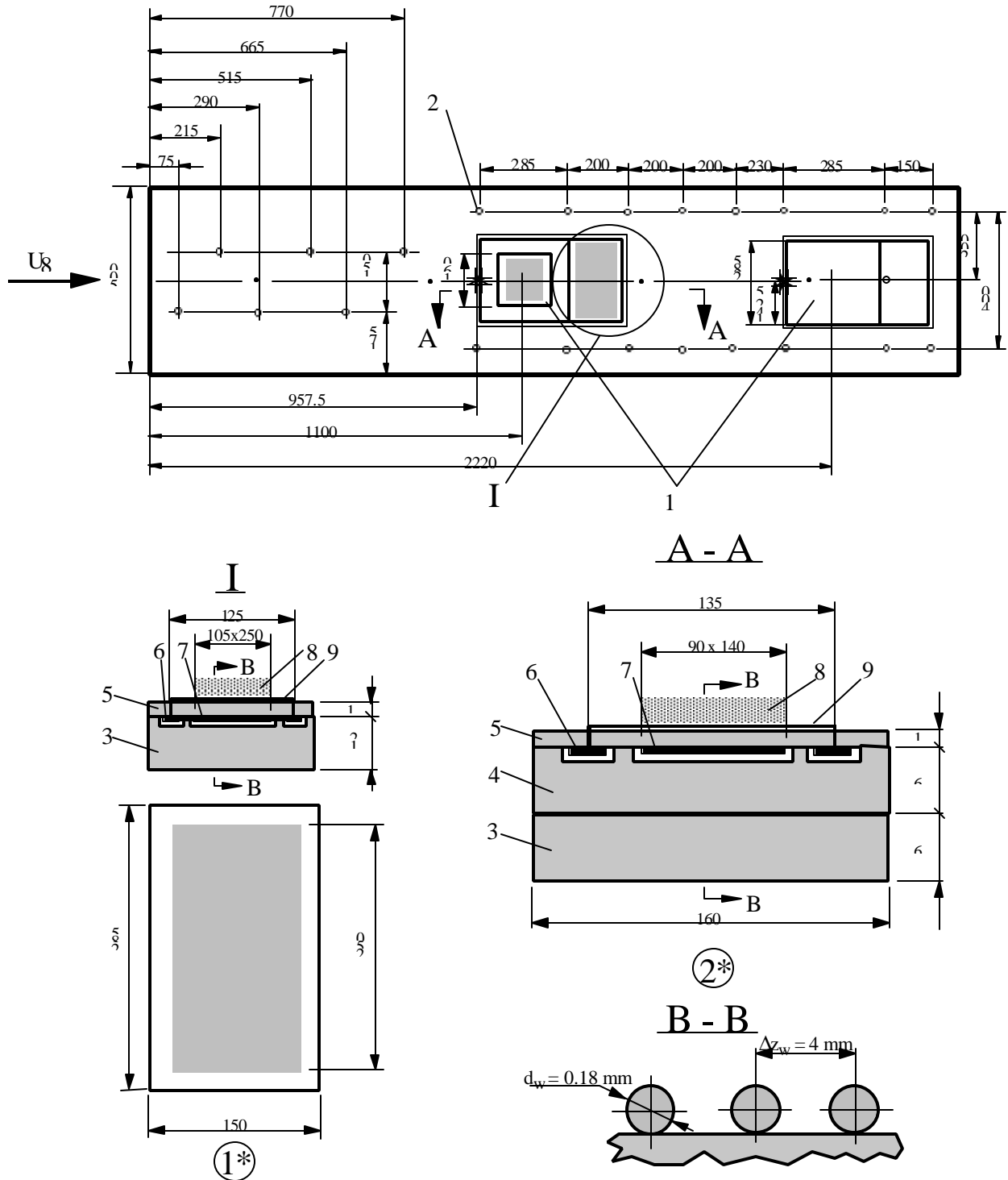

Fig. 9.2a 1- possible positions of floating element; 2- drain orifices; 3- base; 4- insulating washer; 5- insulator; 6- positive electrode; 7- negative (grounded) electrode; 8- discharge; 9- wire; 10- nozzle; 11- turbulizator; 12- origin of the test section; 13- test section; 14- diffuser; 15- model; 16- anemometer probe; 17- arrangement of micro-traverse; 18- flaps

9.1. Aerodynamic tests of flat plate models

The basic purpose of this stage of investigations was obtaining of preliminary knowledge about practical possibilities of the method of the electric discharge influence on flow over the model of a flat plate at the laminar, transitional and turbulent regimes of the flow. The balance and hot wire anemometric measurements were carried out in the test chamber of the wind tunnel T-36I that had the cross section of 350 by 500 mm and 2610 mm – length. The velocity U_∞ was varied in the range from 5 to 65 m/s. The experiments were fulfilled in two series.
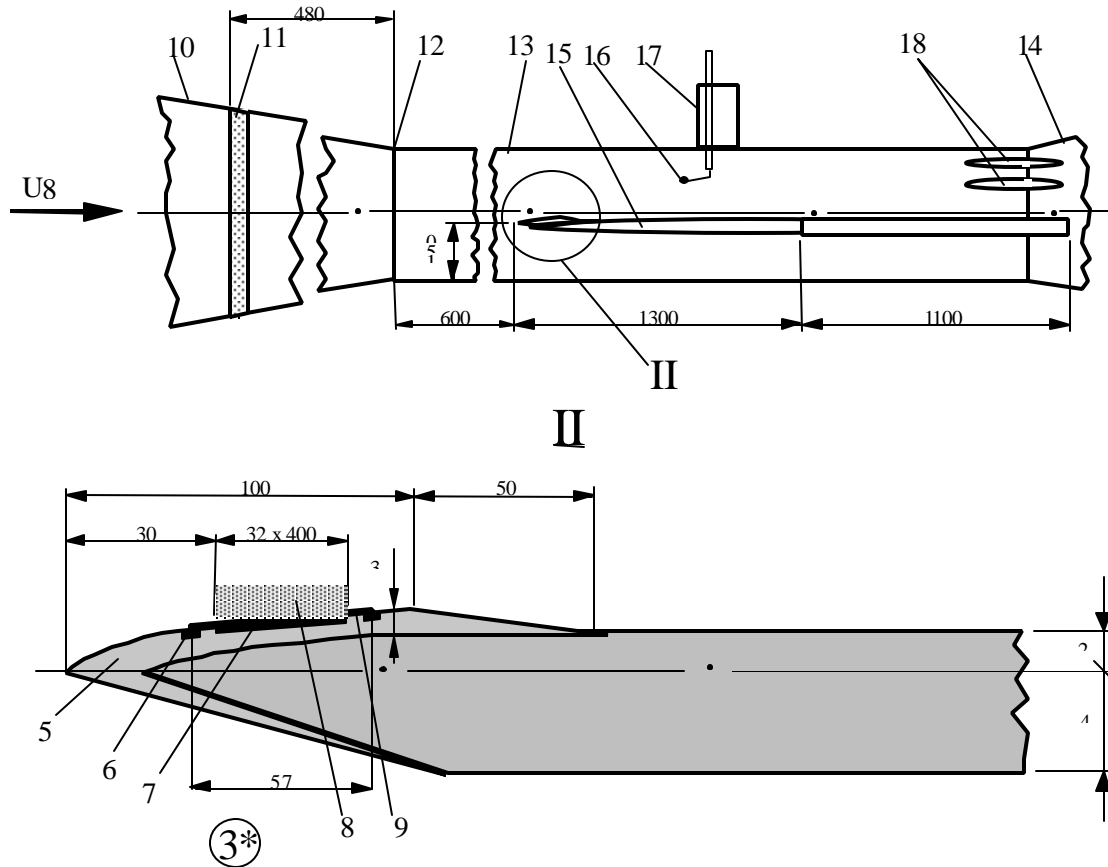
Fig.9.2b.

In the first series of tests, the lower wall of the wind tunnel was used as the model of a flat plate. The parameters of the boundary layer on the lower wall of the wind tunnel were measured in detail at the initial stages of the work. In the second stage, an all-metal plate .5 m by 2.4 m in size and 6 mm – thickness was used (Fig.9.2, b).

Three types of the discharge generators of the "riblet" type were manufactured for the experiments. The basic geometric parameters of the generators are given in Fig. 9.2. The streamlined surface was the set of unevenness in view of the strings that laid on the basic one and were flowed over in the longitudinal direction. In the case of the experiments with the lower wall use, the electrode systems were arranged either before the floating element of the balance (position 1* in Fig. 9.2,a) or directly on it (position 2* in Fig.9.2,a). In the case of the flat plate, the plasma generator was component of the model (position 3* in Fig.9.2,b). The discharge ignited on 85 % of the string length for the first plasma generator, on 65 % of the length of them

for the second one and on 50 % of that length in the case of the third generator.

The arrangement of the plasma generator on the flat plate requires more detail consideration. It was assembled on the panel of textolite of 3 mm – thickness and 150 mm – length. The upper surface of the nose part of the generator and, consequently, of the model that was faced to the flow was manufactured in view of a half-ellipsoid with ratio of the half axes 1:6. The small half-axis equaled 5 mm. The rear edge of the discharge generator had the form of a half- wedge on the length equal 50 mm. The lower part of the nose of the model was cut under the angle about $6^o30^{'}$ to its axis. The radius of the leading edge bluntness was about .6 mm.

At the tests, the flat plate was mounted horizontally, i.e. under the angle of attack equal zero. The leading edge was arranged at a distance of 600 mm from the origin of the test chamber of the wind tunnel. The distance of the flat plate from the upper part of it was 200 mm i.e. the flat plate divided the test chamber on two rectangular channels. The position of the line of braking on the nose part was regulated by changing of the upper channel drag at the expense of the angle of attack change of two flaps (l_f =100mm, h_f =3mm) that were installed over the flat plate near the rear edge of it (Fig.9.2,b).

Fig. 9.3

As it was noted above, in the first series of the tests, the lower wall of the wind tunnel was used as the model of a flat plate. The tests were carried out both with the turbulizator arranged in the nozzle of the wind tunnel (position 11 in Fig. 9.2,b) and without it. At the first stage of this series, the discharge generator No 1 was mounted flush to the surface of the lower wall before the floating element (position 1* in Fig. 9.2,a). The sizes of the floating element plate that perceived the skin friction of the flow was 285 by 285 mm. The distance from the nozzle cut to the center of the floating element plate equaled 1250 mm. The photo of the discharge burning at this geometry of the experiment is shown in Fig. 9.3. The goal of the tests was study of the possible influence

both the riblet system itself (measurements at $\tilde{N}_d = 0$) and the surface of it at the discharge presence on the skin friction downstream behind the plasma generator.
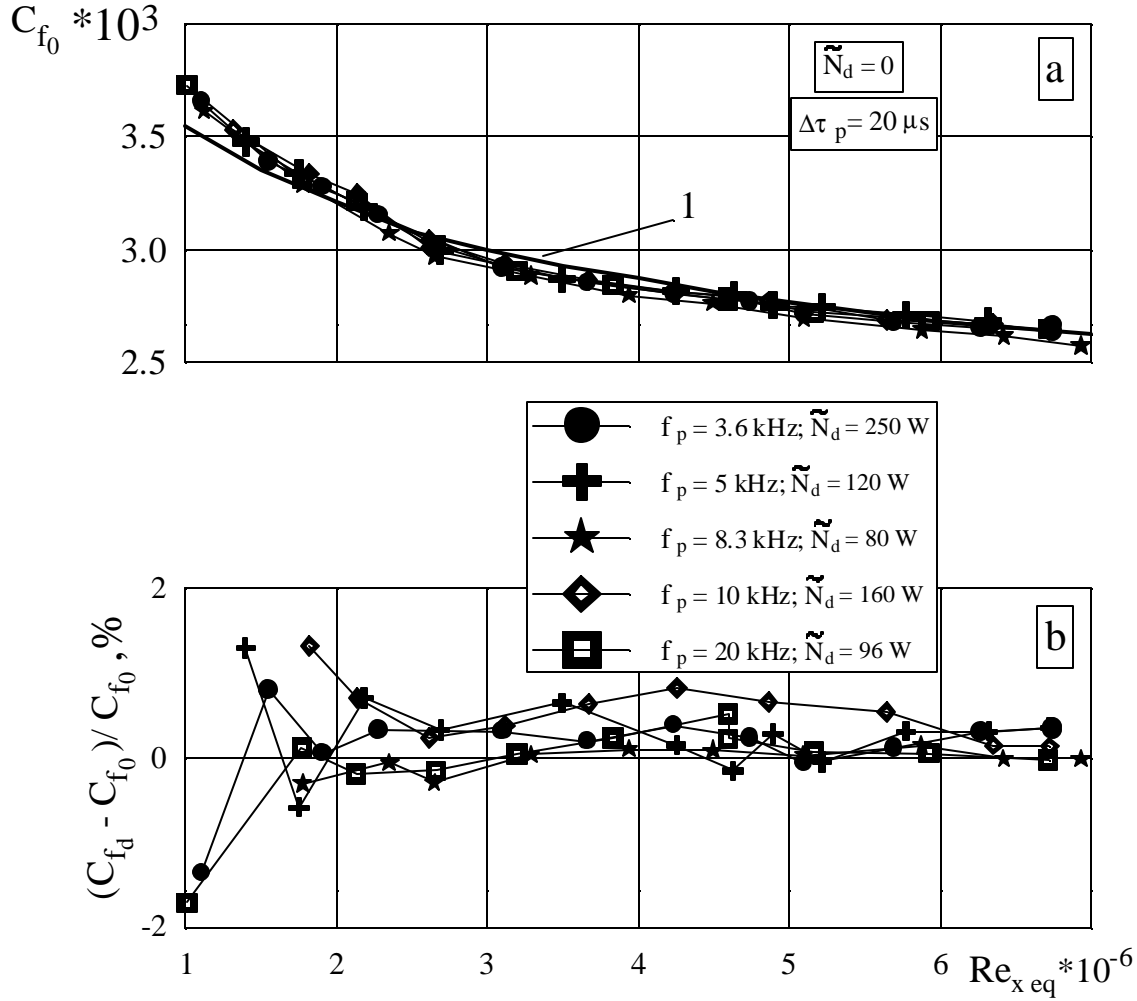

Fig. 9.4

The results of the tests at the turbulizator presence are given in Fig. 9.4,a in view of the dependence of the local skin friction coefficient C_f on Reynolds number $\mathrm{Re}_{Xeq} = U_\infty x_{eq}/\nu$ (where $x_{eq} = 1.72$m is the distance from the leading edge of the turbulizator to the floating element center). For comparison, the dependence $C_{f0}(\mathrm{Re}_{Xeq})$ is given here by the solid line 1. The last was obtained on the velocity profiles $\overline{u}(y)$ in the boundary layer, relations $C_f(\delta, \delta^{**}, etc.)$ known from the literature and also with help of results of the balance measurements for the smooth surface of the lower wall. From the presented data, it is seen that arrangement of the string generator before the floating element did not practically change the dependence $C_{f0}(\mathrm{Re}_{Xeq})$ i.e. the effect of "after action" was absent.

The results of determination of the skin friction downstream behind the discharge in these experiments are presented in Fig. 9.4,b as the dependence of the relative change of the friction coefficient $(C_{fd} - C_{f0})/C_{f0}$ on Reynolds number Re_{Xeq} (here and below, C_{fd} and C_{f0} are the values of the local friction coefficient at the discharge presence and without it). The range of the discharge parameters that were varied in the tests is also given in Fig. 9.4,b. From these results it is seen that the discharge ignition did not influence on the value of C_f downstream.

$$C_f*10^3$$

$d_w = 0.18 \text{ mm}; \Delta Z_w = 4 \text{ mm}$
$f_p = 8.3 \text{ kHz}; \Delta\tau_p = 52 \text{ μs}$

clean

$\tilde{N}_d = 0$

$\tilde{N}_d = 80 \text{ W}$

a

b

$(C_{f_d} - C_{f_0})/C_{f_0}, \%$
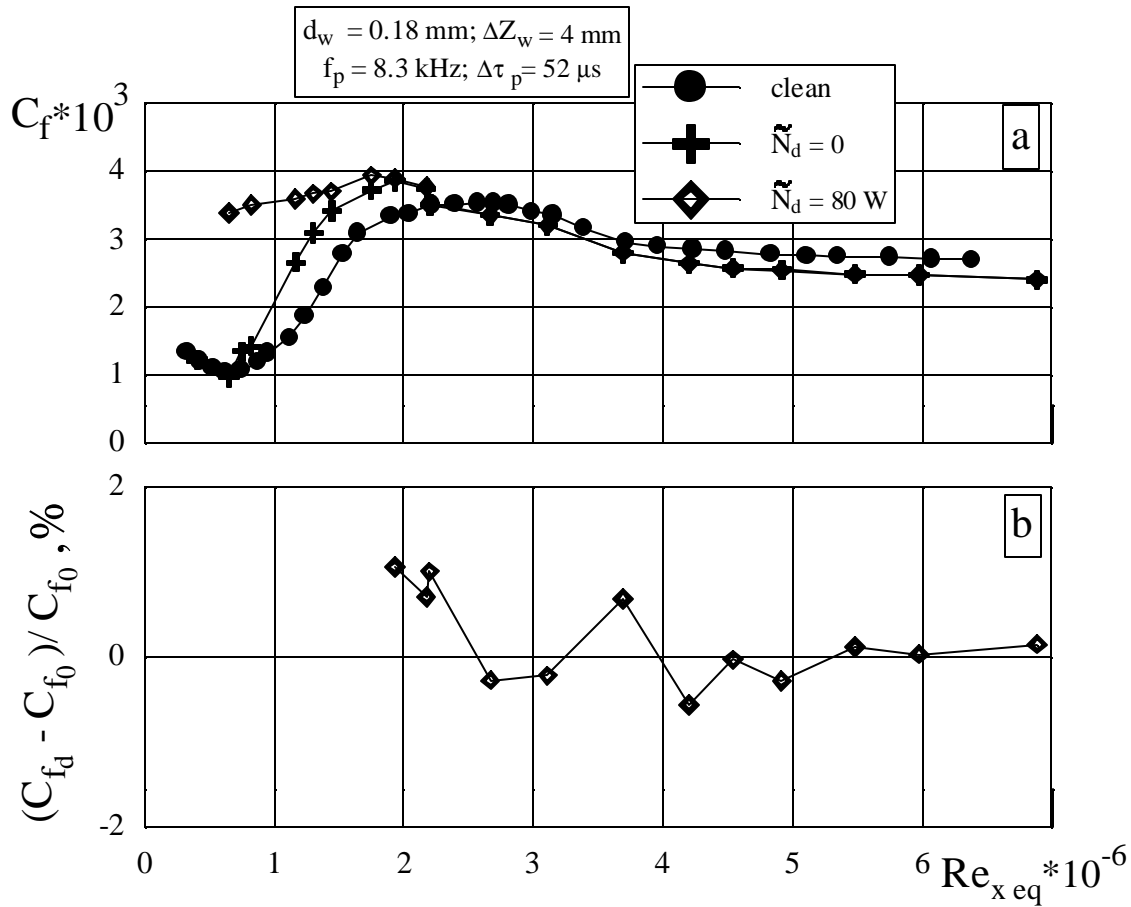
$Re_{x \, eq}*10^{-6}$

Fig. 9.5

The results of the tests in which the turbulizator was absent in the nozzle i.e. at the simulation of the laminar, transitional and turbulent regimes are shown in Fig. 9.5. It is seen that, at the plasma generator presence, the initial stage of the transitional area displaced upstream in comparison of the case of the smooth surface and the discharge increased this displacement. At the turbulent regime ($Re_{Xeq} > 2 \cdot 10^6$), the ignition of the discharge did not exert influence on the skin friction downstream behind the discharge generator in this variant of the experiment as well as in the previous one.

The photo of the discharge burning in this case is shown in Fig. 9.6. The results of the balance measurements are presented in Fig. 9.7. Here the dependence $C_f(Re_{Xeq})$ are plotted both at the discharge presence and without of it. From Fig. 9.7,a, one can see that, in case when the discharge was absent, the dependence $C_f(Re_{Xeq})$, at the initial stage of the transitional regime (i.e. in a zone where the coefficient of intermittence laid in the range $0<\gamma\leq.5$), displaced downstream (see the dependence $C_f(Re_{Xeq})$ marked (+) for regimes with the generator but in absence of the discharge and that in the case of the completely smooth surface marked (•)). At the turbulent regime ($Re_{Xeq} \geq 2 \cdot 10^6$), the dependence $C_f(Re_{Xeq})$ for the smooth surface and that with the plasma generator practically coincided.

The discharge ignition in this variant of the tests led to the transitional zone origin displacement upstream and did not influence on the skin friction at the turbulent regime as well as in the first variant experiments when the plasma generator was arranged before floating element.

The absence of this influence took place also at the modelling of the completely turbulent regime of the flow along the lower wall of the test chamber at the turbulizator installation on the walls of the wind tunnel nozzle (this dependence is marked by ($\star$) in Fig. 9.7,b).
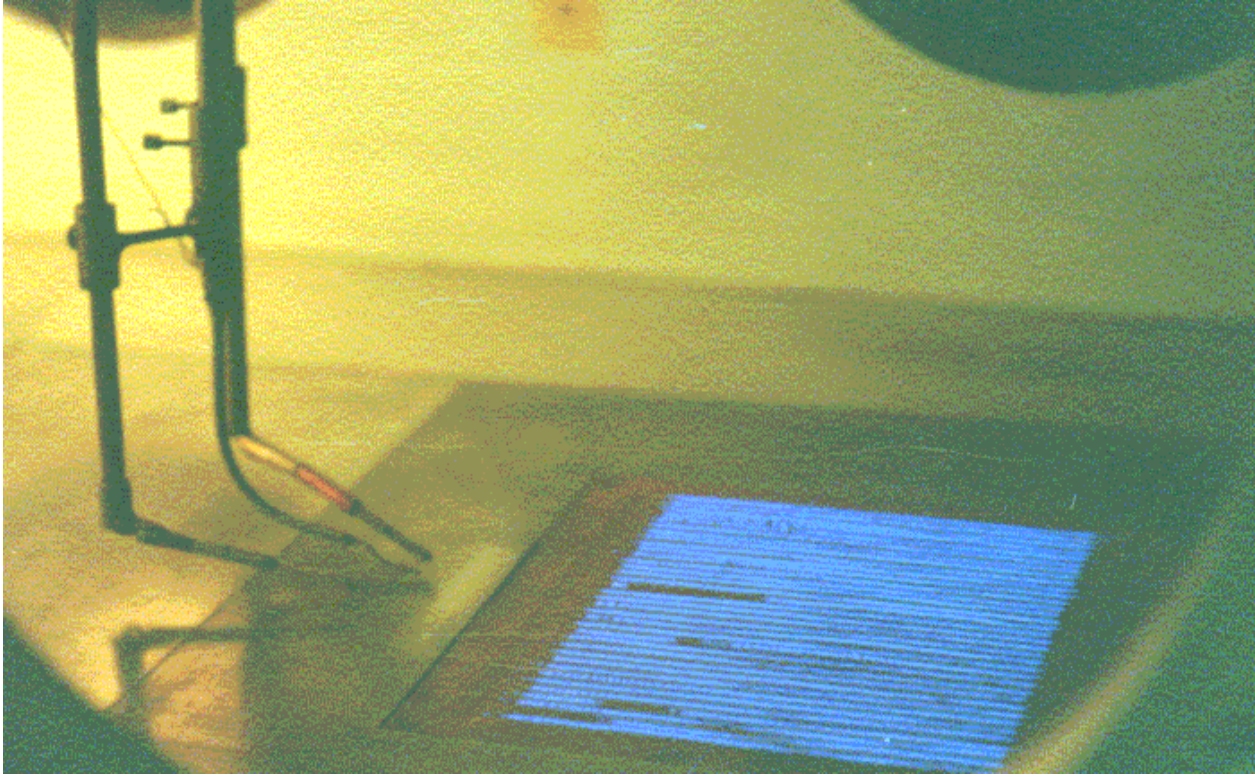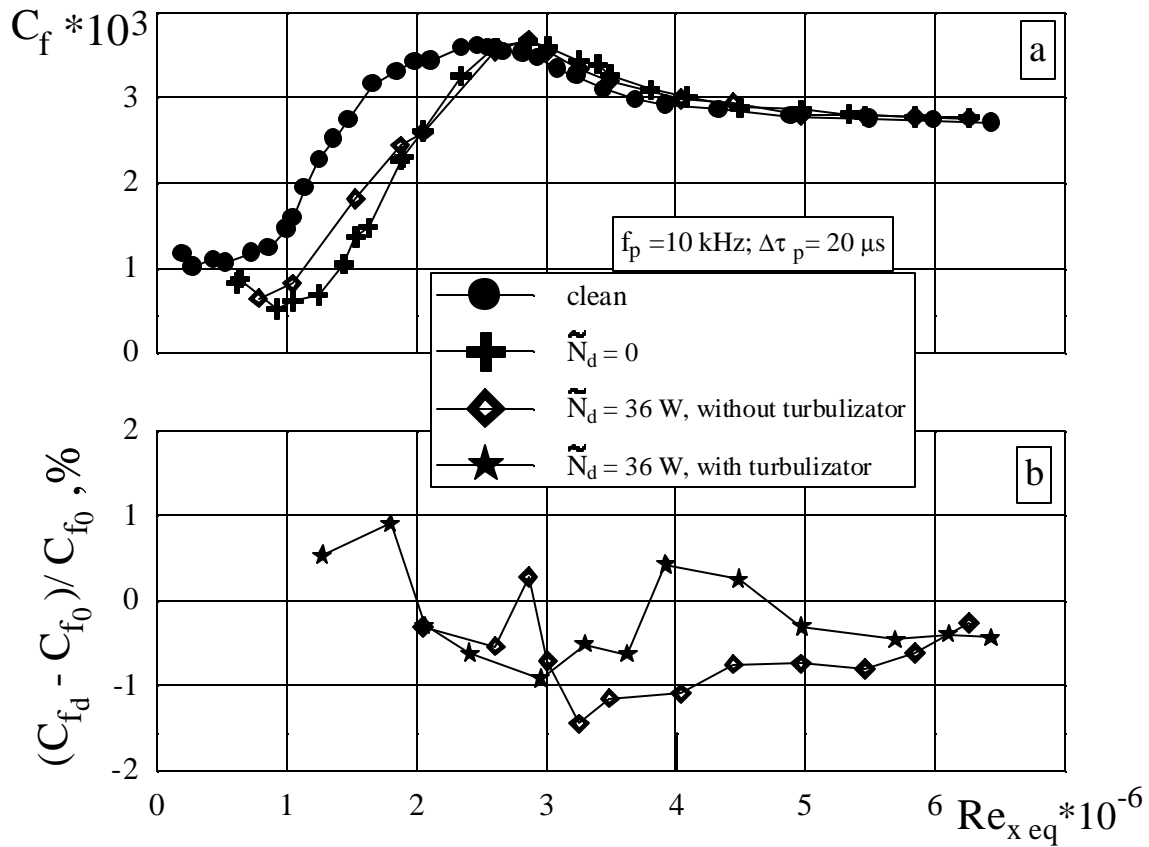

Fig. 9.6

Fig. 9.7

Fig.9.9

Fig. 9.10

In the papers [5.1, 5.2], it was shown that heating of the nose part of a plate can increase stability of the boundary layer, delaying the laminar/turbulent transition, and, consequently reduce the skin friction because of the increase in the laminar portion length. The basic purpose of the present tests were to obtain the first data about of possibilities of the laminar/turbulent transition control by means of heating of the boundary layer with help of the discharge in the concrete scheme of the discharge generator of the riblet type. In Fig. 9.9, the photograph of the

discharge at this variant of the experiment in the wind tunnel is given.

The velocity of the flow and the turbulent parameters were measured by the single filament probe of the hot wire anemometer of DISA which was arranged at a distance of 300 ÷ 600 mm from the leading edge of the model and at a height of .3 ÷.6 mm from the surface of it. As it was noted above, the position of the line of braking was regulated by means of change of the angle of attack of the flaps arranged near the rear edge of the model. This angle could vary from -20° to$+20^o$.

The results of the experiments showed the position of the line of braking exerted of strong influence on the boundary layer development. In case when this line was near the leading edge, a flow over the model had non-steady (intermitting) character, even at low vales of the unit number $Re_1 \approx (.3 \div .5) \cdot 10^6 m^{-1}$. The intermitting character of a flow over a plate was probably conditioned by the significant turbulization of the stream on the strings of the plasma generator and a positive gradient of the pressure in a zone of the rear edge of it (on the half- wedge, Fig. 9.5,b).

The tests showed some additional turbulizing influence of the discharge created at the strings on the boundary layer. For example, in Fig 9.10, the results of measurements of the dependence of the pulsation $u'/U_e(Re_1)$ and the mean velocity $\overline{u}/U_e$ on Re_1 are shown both at the discharge presence (◆) and without it (+). From the presented data it is seen that, in the case of the discharge ignition at the density of the power input of $\widetilde{N}_d/S_d \approx 1 W/cm^{-2}$, the complete turbulization of the flow took place beginning from numbers $Re_1 \approx .3 \cdot 10^6$ m^{-1}. One can be noted however that the results of these tests have got the preliminary character and can be prolonged at the change of the plasma generator installed on the leading edge of the plate. In the first turn, it is necessary to reduce the turbulizing influence of the strings action (by means of the decrease in the diameter of strings or transition to other types of electrodes) and also to get rid of the positive pressure gradient at the rear edge of the generator.

10. NUMERICAL INVESTIGATION OF DISCHARGE-INDUCED DRAG REDUCTION.

10.1. Outline of the simulated experiment

The experiment to be simulated [10.1] was carried out at the wind tunnel with open working section. Axial-symmetric model equipped by the plasma generator was mounted by means of vertical streamlined strut on the balance to measure drag force. Stream diameter at the working section was 1.2m. Flow velocity was varied in the range 10...70m/s. Turbulence intensity was less then 0.3%. The model axis was aligned with the axis of the stream. The strut has airfoil cross section with 0.2m chordwise dimension and 0.035m in thickness. There was 0.05m of the strut in the flow. The rest part was shielded by the dummy strut to avoid additional drag.

The model geometry consists of cylinder of 0.5m length and 0.1m diameter, head and rear sections are ellipsoidal with semi-axes 0.2m and 0.3m respectively. Total length of the model is 1m. The range of Reynolds number of the model was $0.75 \cdot 10^6 ... 5.3 \cdot 10^6$. As it was determined by

means of thermo-anemometer, the boundary layer was both laminar and turbulent at the different sections of the model. Because of high sensitivity of the method to temperature disturbances, the state of boundary layer was diagnosed only without the plasma. Further details of measurements can be found in [10.1].

10.2. Numerical simulation of the outer flow.

The flow out of the boundary layer is to be calculated at first as a background for the further boundary layer analysis and, at second, to predict qualitatively the behavior of flow separation zone at rear section of the model and its effect on the total drag force when thermal action of the plasma is turned on and off.

Fig.10.1.

The flowfield beyond the boundary layer (Fig.10.1) is calculated by solving numerically full system of the Euler equations for ideal compressible gas in 2D region. Care is taken to reduce the numerical drag force due to finite domain of calculations far below the expected physical drag. Also, the numerical viscosity is diminished by means of mesh and differencing scheme adjustment so as its effect of the flow velocity distribution along the model wall is less than some tenth of percentage.

Like a mesh is be used for the pressure drag analysis by means of Navier-Stokes equation with a suitable model of turbulence. The only difference concerns with fine enough division of boundary layer zones and separation-recirculation region.

10.3. Boundary layer flow stability and laminar-turbulent transition prediction.

When the laminar portion of the boundary layer is not small in comparison with the model length it is required to find the laminar-turbulent transition location. And then on the base of the assumption that the nonlinear part of the transition region is small in order to obtain the total friction drag one can calculate the friction forces in the laminar and turbulent portions of the boundary layer. In this situation the accurate prediction of the laminar-turbulent transition location is acknowledged to be one of the most important part of this study. In order to predict the laminar-turbulent transition location it is assumed to use the well known linear stability theory of

the local plane-parallel boundary layer flow and the e^N-method. On the base of the local parallel assumption it is assumed that the main undisturbed boundary layer flow parameters depend only on the coordinate normal to the streamlined body surface and all disturbed flow parameters can be represented by the sum of the stationary main flow and the infinitesimal amplitude disturbances $f = f_0 + f'$. In this assumption the all fluctuating parameters can be given using the normal mode form:

$$f'(t, x, y, z) = \hat{f}(y)\exp[i(\alpha x + \beta z - \omega t)] \tag{10.3.1}$$

Here $\hat{f}$ represents the complex amplitude functions of the disturbed flow parameters such as velocity components (u, v, w), density, pressure and etc., y is the surface normal coordinate and α, β are the corresponding streamwise and spanwise wave numbers, which are assumed to be real, and ω is the complex frequency of the disturbance. Thus we consider only temporal stability theory of the boundary layer flow.

Substituting the disturbed flow parameters (10.3.1) in the linearized Navier-Stokes equations for three-dimensional nonstationary compressible viscous flow and assuming that all disturbed functions (besides the disturbed pressure) tend to zero at the surface $y = 0$ and at the outer edge of the boundary layer when $y \to \infty$ one can obtain the eigen value problem for a ordinary differential equation system of the eighth order. This equation system is the analogue of the equation system obtained in [10.2]. The coefficients of the system of the differential equations obtained are also given in [10.2].

In order to find the transition point location it is assumed the e^N-method. In order to do this it is required to calculate the spatial disturbance increments σ of the small amplitude disturbance having the fixed nondimensional frequency F and then one can calculate the perturbation growth exponent N_F by the following formula:

$$N_F = \ln\left(\frac{A}{A_0}\right) = \int_{s_0}^{s} \vec{\sigma} d\vec{s}$$

Here A and A_0 are the amplitudes of the perturbations at the point s and s_0 respectively, s_0 is the point where the boundary layer loses stability with the respect to the perturbation having the frequency F. The nondimensional frequency $F = \omega_r \nu_\infty / u_\infty^2$ and spatial perturbation increment $\vec{\sigma}$ is calculated using the following transformation

$$\vec{\sigma} = \frac{\omega_i}{\left|\vec{V}_g\right|^2}\vec{V}_g, \quad \vec{V}_g = \left\{\frac{d\omega_r}{d\alpha}, \frac{d\omega_r}{d\beta}\right\}$$

Here ω_r is the real part of the complex frequency ω, the ω_i is the time increment growth of the perturbation, $\vec{V}_g$ is the group perturbation velocity. It is assumed that transition occurs at the point where reaches the critical values N^*. The above formulated problem was closed using the envelope method [10.3-10.4]. The direction of the spatial increment $\vec{\sigma}$ was defined as that of

the maximum disturbance growth increment $\max|\vec{\sigma}|$ for fixed frequency F. It is assumed to reduce the computer resource requirement by using the approximation formula for dispersion relationship. The amount of calculation can be reduced by using a quadratic approximation of the function $\omega_i(\alpha,\beta)$ and a linear approximation of the function $\omega_r(\alpha,\beta)$, both resulting in insignificant errors in N_F [10.2, 10.5].

10.4. Modeling of turbulent boundary layer.

Numerical calculations of turbulent boundary layer on axisymmetric model described above will be performed in Cartesian coordinates (x^*,y^*) since a boundary layer thickness is much less than the model radius. The x^* coordinate is directed along the model surface, and the y^* coordinate is normal to it.

Previously an ability of skin friction and heat transfer coefficients prediction in a compressible turbulent boundary layer on a heated surface has been tested for several turbulence models [10.6, 10.7]. Algebraic model of Cebeci-Smith [10.8], two second-order $k-\varepsilon$ models [10.9, 10.10] and four-order variable-Prandtl-number model [10.11] have been compared. A comparison of numerical results has been made with experimental research of a Mach 2.3 turbulent boundary layer on an isothermal flat plate with a wall temperature factor 1, 1.5, and 2 [10.12]. Chien's $k-\varepsilon$ model of turbulence [10.9] has been defined as optimal from point of view both accuracy of numerical results obtained and computational effectiveness. Namely this model will be used in present calculations of turbulent boundary layer.

For numerical simulation of compressible turbulent boundary layer it is convenient to introduce dimensionless variables (without superscript *) according to the following expressions:

$$x^* = l^* x, \quad y^* = \delta^* y, \quad \delta^* = l^* \delta(x), \quad u^* = u_\infty^* u_e u$$

$$v^* = u_\infty^* u_e \delta\left(V + \frac{yu}{\delta}\frac{d\delta}{dx}\right), \quad k^* = \frac{u_\infty^{*2}}{\mathrm{Re}^{1/2}}k, \quad \varepsilon^* = \frac{u_\infty^{*3}}{l^*}\varepsilon \qquad (10.4.1)$$

$$T^* = T_\infty^* T, \quad \rho^* = \rho_\infty^* \rho, \quad \mu^* = \mu_\infty^* \mu, \quad \mathrm{Re} = \frac{\rho_\infty^* u_\infty^* l^*}{\mu_\infty^*}$$

Here l^* is the characteristic length (the length of the experimental model), δ^* is the boundary layer displacement thickness which is defined during calculation procedure in each boundary layer section, u^* and v^* are the longitudinal and transversal velocity components, u_∞^* and u_e are the upstream flow velocity and dimensionless velocity on the model surface obtained from the solution of Euler equations according to the Section 2.2., k^* and ε^* are the kinetic energy of turbulence and the rate of its dissipation, T^*, ρ^* and μ^* are the gas temperature, density and dynamic viscosity. The subscript ∞ denotes the values in upstream flow.

The system of governing equations and boundary conditions for compressible turbulent boundary layer in dimensionless variables (10.4.1) takes the following form:

$$\frac{\partial \rho u}{\partial x} + \rho u \left(\frac{\delta'_x}{\delta} + \frac{u'_{ex}}{u_e} \right) + \frac{\partial \rho V}{\partial y} = 0, \quad \rho = \frac{1}{T} \tag{10.4.2}$$

$$\frac{1}{\delta^2 \operatorname{Re}} \frac{\partial}{\partial y} \left[(\mu + \mu_t) \frac{\partial u}{\partial y} \right] = u_e \left(\rho u \frac{\partial u}{\partial x} + \rho V \frac{\partial u}{\partial y} \right) + \left(\rho u^2 - \rho_e \right) u'_{ex} \tag{10.4.3}$$

$$\frac{1}{\delta^2 \operatorname{Re}} \frac{\partial}{\partial y} \left[\left(\frac{\mu}{\operatorname{Pr}} + \frac{\mu_t}{\operatorname{Pr}_t} \right) \frac{\partial T}{\partial y} \right] = u_e \left(\rho u \frac{\partial T}{\partial x} + \rho V \frac{\partial T}{\partial y} \right) -$$

$$-(\kappa - 1) u_e^2 M_\infty^2 \left[\frac{\mu + \mu_t}{\delta^2 \operatorname{Re}} \left(\frac{\partial u}{\partial y} \right)^2 + \rho_e u'_{ex} u \right] \tag{10.4.4}$$

$$\frac{1}{\delta^2 \operatorname{Re}} \frac{\partial}{\partial y} \left[\left(\mu + \frac{\mu_t}{\sigma_k} \right) \frac{\partial k}{\partial y} \right] = u_e \left(\rho u \frac{\partial k}{\partial x} + \rho V \frac{\partial k}{\partial y} \right) - \frac{\mu_t}{\delta^2 \operatorname{Re}^{1/2}} \left(\frac{\partial u}{\partial y} \right)^2 +$$

$$+ \rho \operatorname{Re}^{1/2} \varepsilon + \frac{2\mu}{\delta^2 \operatorname{Re}} \frac{k}{y^2} \tag{10.4.5}$$

$$\frac{1}{\delta^2 \operatorname{Re}} \frac{\partial}{\partial y} \left[\left(\mu + \frac{\mu_t}{\sigma_\varepsilon} \right) \frac{\partial \varepsilon}{\partial y} \right] = u_e \left(\rho u \frac{\partial \varepsilon}{\partial x} + \rho V \frac{\partial \varepsilon}{\partial y} \right) - C_{\varepsilon 1} \frac{\mu_t}{\delta^2 \operatorname{Re}^{1/2}} \frac{\varepsilon}{k} \left(\frac{\partial u}{\partial y} \right)^2 +$$

$$+ C_{\varepsilon 2} f_2 \rho \operatorname{Re}^{1/2} \frac{\varepsilon^2}{k} + \frac{2\mu}{\delta^2 \operatorname{Re}} \frac{\varepsilon}{y^2} \exp\left(-0.5 y^+ \right) \tag{10.4.6}$$

$$y = 0: \quad u = V = k = \varepsilon = 0, \quad T = T_w \tag{10.4.7}$$

$$y = y_e: \quad u = 1, \quad T = T_e, \quad k = \varepsilon = 0$$

$$\operatorname{Pr} = 0.72, \quad \operatorname{Pr}_t = 0.9, \quad \kappa = 1.4, \quad \mu = T^{3/2} \frac{1 + A_\infty}{T + A_\infty}, \quad A_\infty = \frac{114}{T_\infty^*}$$

$$\mu_t = C_\mu f_\mu R_t \mu, \quad R_t = \rho k^2 / \mu \varepsilon, \quad f_\mu = 1 - \exp(-0.0115 y^+) \tag{10.4.8}$$

$$f_2 = 1 - \frac{2}{9} \exp\left[-\left(\frac{R_t}{6} \right)^2 \right], \quad y^+ = y \frac{\rho}{\mu} \left[\delta \operatorname{Re} \left(\frac{\mu}{\rho} \frac{\partial u}{\partial y} \right)_{y=0} \right]^{1/2}$$

$$\sigma_k = 1, \quad \sigma_\varepsilon = 1.3, \quad C_\mu = 0.09, \quad C_{\varepsilon 1} = 1.35, \quad C_{\varepsilon 2} = 1.8$$

Here $()'_x$ denotes the derivative along the model surface.

To obtain the initial conditions for formulated parabolic boundary value problem the following procedure is used. At first a calculation of laminar boundary layer with given distributions of the wall temperature and outer flow velocity and temperature is carried out up to transition point defined according to the previous section. Numerical solution of the problem (10.4.2)-(10.4.7) starts from the obtained laminar profiles of velocity and temperature and zero profiles for the kinetic energy of turbulence and the rate of its dissipation. At the beginning only first four equations (10.4.2)-(10.4.4) are solved with the coefficient of turbulent viscosity defined as $\mu_t = f_{tr}(x)\mu_{ta}$, where $f_{tr}(x)$ is a liner transition function which varies from zero up to unity at a sufficiently short distance, and μ_{ta} is defined by algebraic model of turbulence of Cebeci-Smith [10.7].

When the function f_{tr} achieves the unity the equation for kinetic energy of turbulence (10.4.5) is involved in the solution procedure with $\mu_t = \mu_{ta}$ and initial zero profile of k. The kinetic energy of turbulence begins of positive in next boundary layer sections due to the third source term in the right side of the equation (10.4.5). When this function becomes positive in all y-grid points except $y = 0$ and $y = y_e$ the equation for dissipation rate (10.4.6) is involved in the solution also still with $\mu_t = \mu_{ta}$. Similar to k, ε increases gradually due to generation term with the coefficient $C_{\varepsilon 1}$. After several sections the dissipation rate of turbulence becomes positive across the boundary layer except the boundary points and then the coefficient of turbulent viscosity is calculated according to (10.4.8).

Efficient numerical method of the second-order accuracy [10.13] is used for solution of the formulated problem.

Local skin friction coefficient in turbulent boundary layer is calculated according to

$$C_f = \frac{2}{\rho_e u_e \mathrm{Re}\delta}\left(\mu\frac{\partial u}{\partial y}\right)_{y=0}$$

Calculated distributions both laminar and turbulent local skin friction coefficients along the model surface are integrated to obtain a total friction drag of the model.

10.5. Results and discussion

10.5.1. Inviscid flow

As stated above, the calculation of inviscid flow are destined to provide the detailed analysis of boundary layer flow with the air properties 'at infinity'. Here the final results of the calculations are presented (Fig.10.1) for the undisturbed air velocity $u_\infty = 50$m/s and ambient pressure and temperature $p_\infty = 10^5$Pa and $T_\infty = 20°$C respectively.

The curves (1) and (2) shows respectively the distributions of tangential velocity and its derivative along the surface curvilinear coordinate for the fuselage-like axisymmetric body. Some irregularities are seen near the joints of head and rear ellipsoidal sections with the cylinder because the mathematically precise description of the surface was used in present calculations. In

practice, such joints are usually refined slightly after this parts being assembled to avoid the second derivative singularities of the body shape. Thus we may do something like that to facilitate numerical procedure of boundary layer calculation.
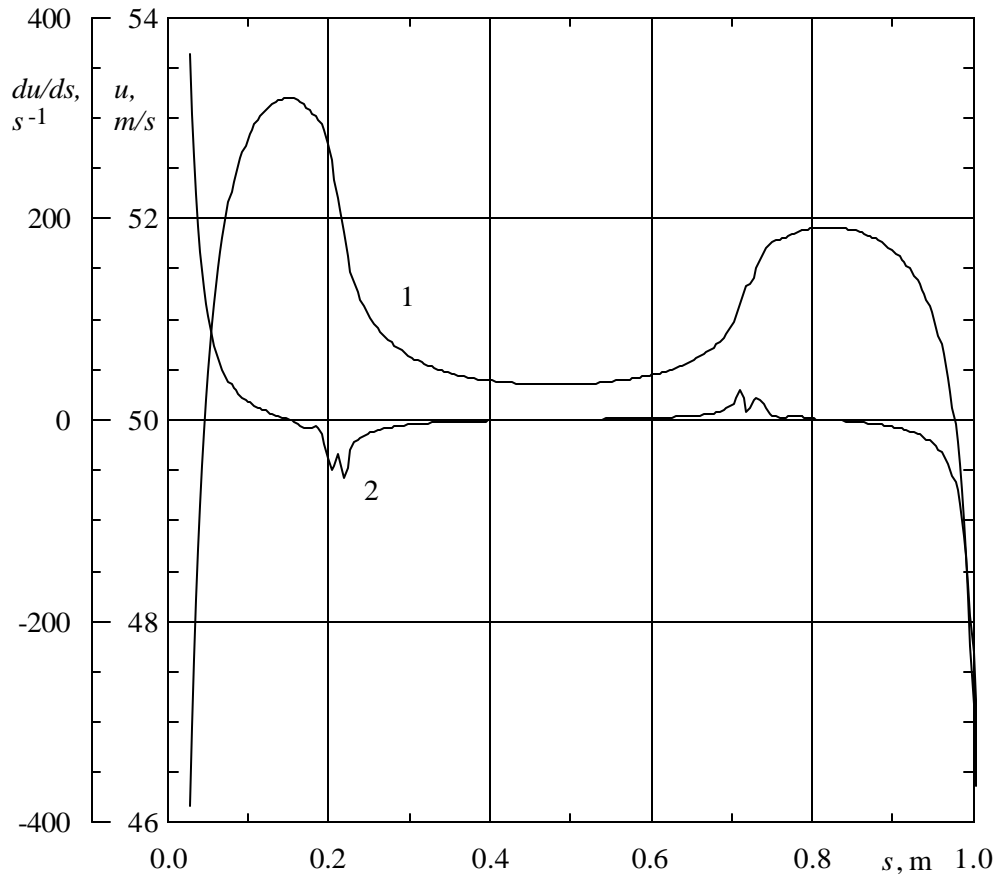

Fig.10.1.

For the purpose of this investigation the discretization of the flow field was made rather fine. Residual drag of the body due to numerical viscosity and non-infinite boundary location is less then 0.1% of the total drag. Most dependent on this inaccuracies is the minimum velocity over the middle of cylindrical section. Computational grid refinement was stopped when its effect on the velocity distribution has become invisible in the scale of Fig.10.1.

Also, a comparison was made with the results of current experiments in T-36I wind tunnel. Extremal point of the pressure distribution were reproduced rather well when taking into account essential interference of the closed working section. Nevertheless the noticeable quantitative difference remains, evidently owing to the restrictions of the two-dimensional approach.

10.5.2. Drag components in presence of heat release.

To sort out the phenomenon which may affect the drag when an energy is input elsewhere in the flow we solved full two-dimensional system of Navier-Stokes equations on the same grid as used for inviscid flow calculations except for the near-wall region where the grid step normal to the wall was diminished to about $\sqrt{\mathbf{n}_w/u'_w}$ ($\mathbf{n}_w$ - kinematic viscosity, u'_w - normal gradient of tangential velocity at the wall). Because the experiments shows that laminar-turbulent transition

takes place in the boundary layer, the turbulent Reynolds terms was included into equations everywhere in the computational domain by use of standard k-ε turbulence model modified to take into account near-wall effects (so-called "low-Re" or "near-wall" model [10.14]).
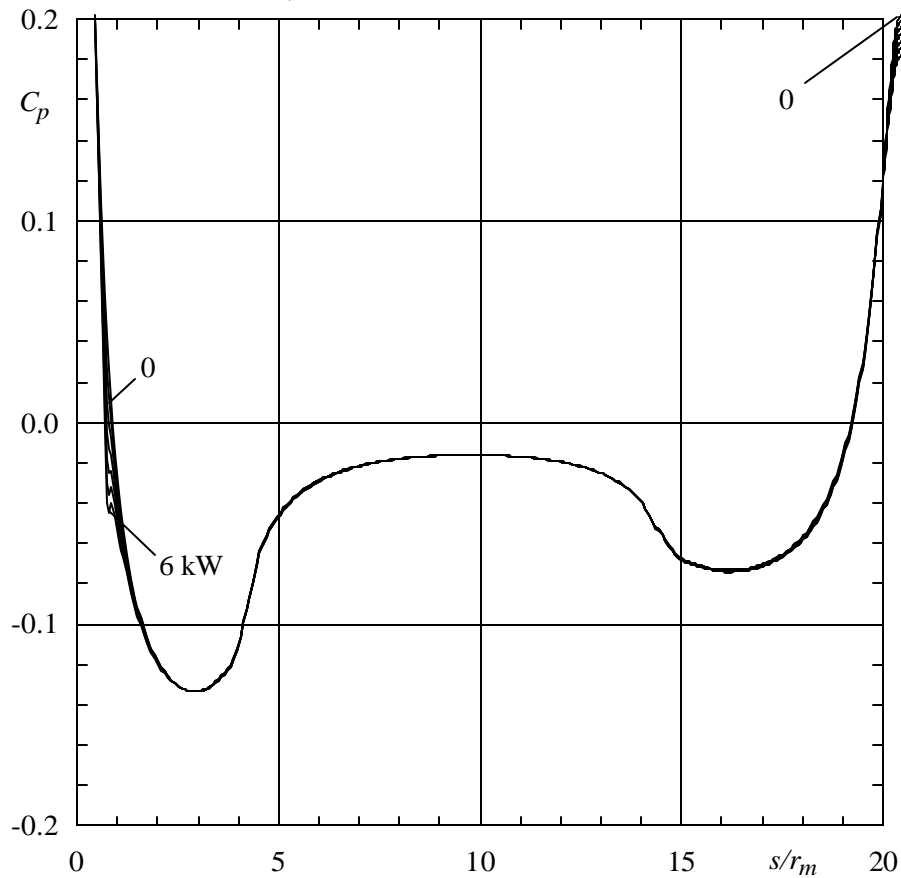

Fig. 10.2.

Turbulence characteristics were taken to be 0.3% intensity and 5mm scale length. This is rather low turbulence and its effect on the considered flow around the body is small.

General picture of the flow do not differ severely from that of inviscid flow. At the very end of the rear small region of reverse flow takes place. Drag coefficient equals to 0.142, the pressure contribution being fairly small value less then 6% of the total drag (the latter is appreciably less then the assessment of the work [10.1]).

Electric discharge was simulated by spatially homogeneous energy input in the nose region where the discharge generator was mounted in the experiments. The energy input region was assumed to be about 3.5cm along the surface from the center and about 5mm in thickness. Real energy source was a streamer sweeping at the frequency 200-600Hz around the model axis and randomly wandering in the space approximately specified above. Therefore the results of the calculation are only qualitative. Total power was varied from zero to 6 kW. The boundary condition for the temperature was adiabatic, i.e. the same as for inviscid flow without heat release. It implies firstly that the energy input acts long enough to let the model envelope heat over the thickness, and secondly that the heat conduction along the envelope is much less than the heat transport in the air.
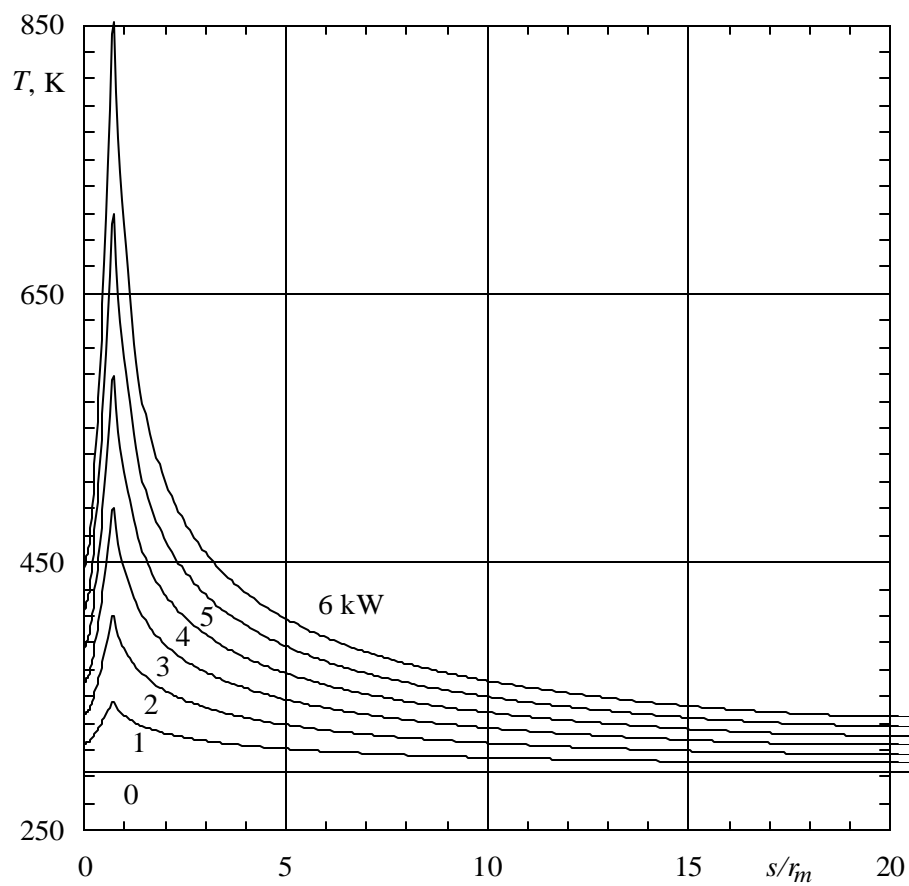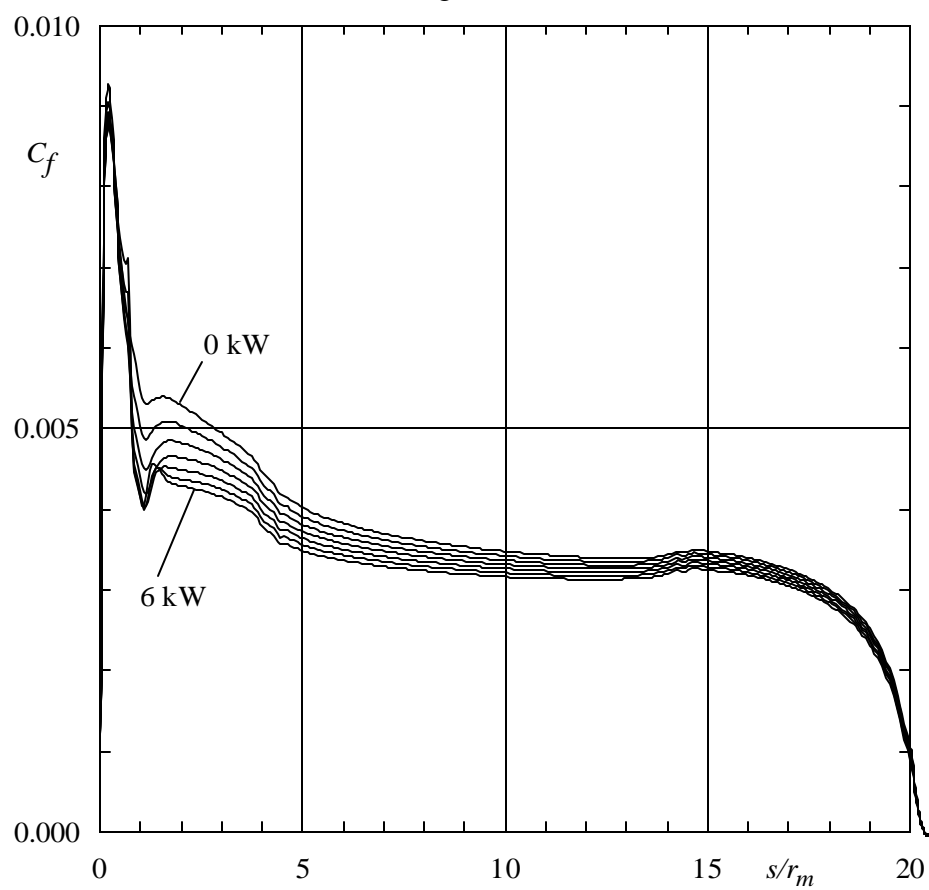
Fig. 10.3.

Fig. 10.4.

The distributions of the flow parameters on the model surface obtained at these assumptions are shown in Fig.10.2-10.4. Here

$$C_p = \frac{p_w - p_\infty}{q} ; \qquad C_f = \frac{t_w}{q} ; \qquad q = \frac{\rho_\infty u_\infty^2}{2} ,$$

p_w - air pressure, t_w - shear stress at the wall.

It can be seen that noticeable pressure variations due to air heating (Fig.10.2) are localized behind the region of heat release and at the rear recirculation region. Over the rest surface the pressure coefficient remains almost invariable. The sign of variations is positive (in the sense of contribution to the drag reduction) at the head region and negative at the rear. The skin friction (Fig.10.3) correlates with the wall temperature (Fig.10.2). Really, the distributions may be smoother because of neglected wall heat conduction which can be considerable near the temperature spike. The effect of air heating is positive over the entire surface.
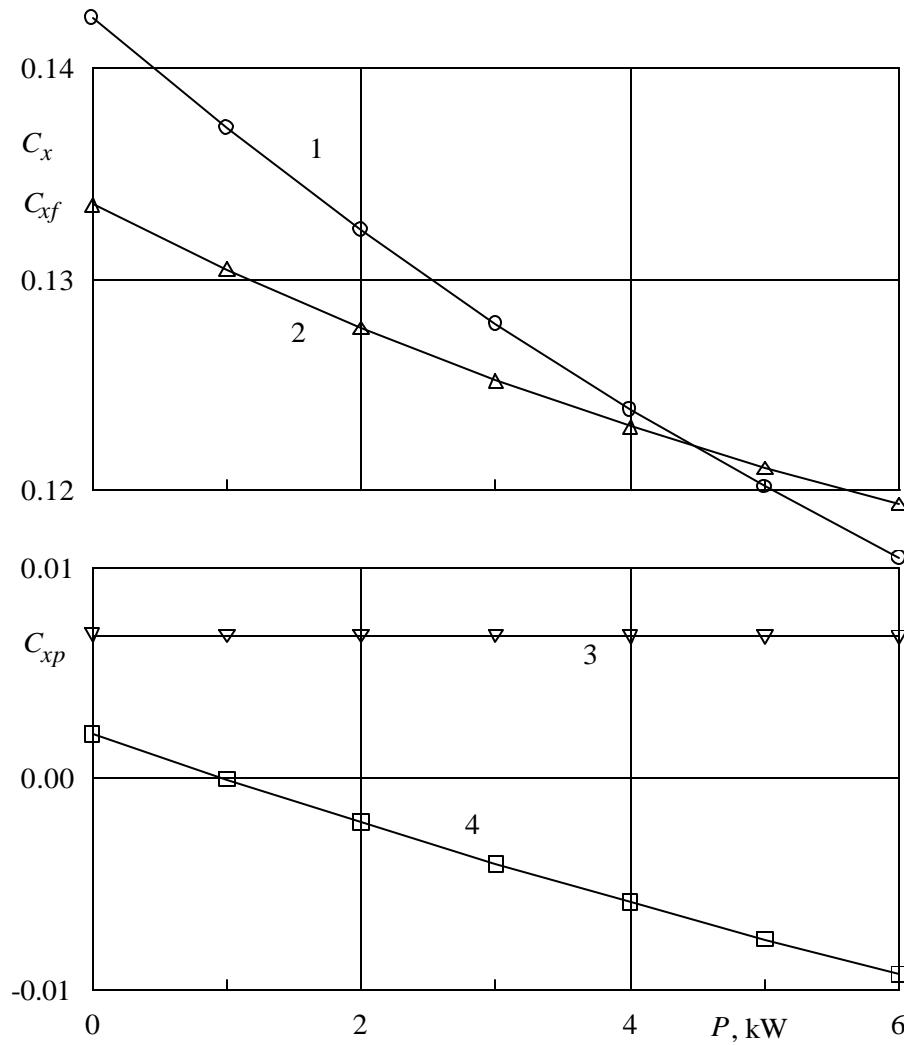

Fig. 10.5.

The total effect and its main components are presented in Fig.10.5. versus the power input. Here the curves 1-4 show respectively the total drag coefficient, skin friction component and pressure components of head and rear sections separately (environment pressure is excluded).

According to this calculations, drag reduction consists of nearly equal contributions of skin friction and head section pressure variations, while the rear section drag variation is negligible. The net drag reduction about 15% at P=5kW exceeds the value reached in the experiments [10.1]. This may be attributed to both incorrect definition of the energy source geometry and the straightforward computational model of boundary layer. More accurate analysis will be done at the next section. Here we just notice, that the simple thermal model of the discharge effect on the drag is able to explain under reasonable assumptions whole range of drag variations observed in experiments.

10.5.3. Influence of surface heating on the laminar-turbulent transition.

So, the calculations of the influence of the energy supply generated by electric discharge on the body drag were carried out in order to clarify the possible effect of the electric discharge generated near the model nose when it was switched off. Electric discharge was simulated by spatially homogeneous energy input in the model nose region where the discharge generator was mounted in the experiments. The energy input region was assumed to be about 3.5 cm along the surface from the center and about 5mm in thickness. Real energy source was a streamer sweeping at the frequency 200-600 Hz around the model axis and randomly wandering in the space approximately specified above. Therefore the results of the calculation demonstrated in previous section are rather qualitative. Total power was varied from zero to 6 kW.

As it was demonstrated by calculations the volumetric energy input to the turbulent viscous flow over the blunt axisymmetric body cased the diminishing of the local drag coefficient as well as the total body drag. It must be emphasized that in these calculations model surface is considered as adiabatic one, that is the electric discharge was assumed to be switch on for the extended period of time and the experimental model has a chance to heat and model surface can achieve the adiabatic temperature.

It should be noted that the duration of the experiments was not sufficiently large, electric discharge was switch on only the small period of time (approximately 0.5-1.5 sec.), then the electric discharge was switch off, but over the course of the experiment (its duration was approximately equal 3-5 sec.) the drag reduction was observed but the value of drag reduction was slowly diminished during the measurement from its maximum value to zero.

Thus, there is a good probability that in experiments the model surface have not time to reach the corresponding large temperatures when it becomes adiabatic one and the drag reduction was caused not only by the volumetric energy supply to the flow but, although, by the surface heating and the surface temperature distribution. Nevertheless, this investigation shows the detectable effect of the volumetric heat supply on the turbulent drag reduction of the model. But, when the Reynolds number is not sufficiently large and the initial free stream flow perturbations are not large too(this is the case when the electric discharge is switch off), some part of the boundary layer flow near the model nose must remain laminar one. In this case it is required to consider the influence of surface heating caused by the volumetric energy supply on the laminar

drag coefficient as well as its influence on the position of the laminar-turbulent transition in order to estimate and calculate the turbulent friction on the rest of body where the boundary layer is turbulent, and to calculate the total drag of the model. By this means, when the electric discharge will be switch off, it should be search the influence of the surface heating on the laminar boundary layer parameters and laminar-turbulent transition only.
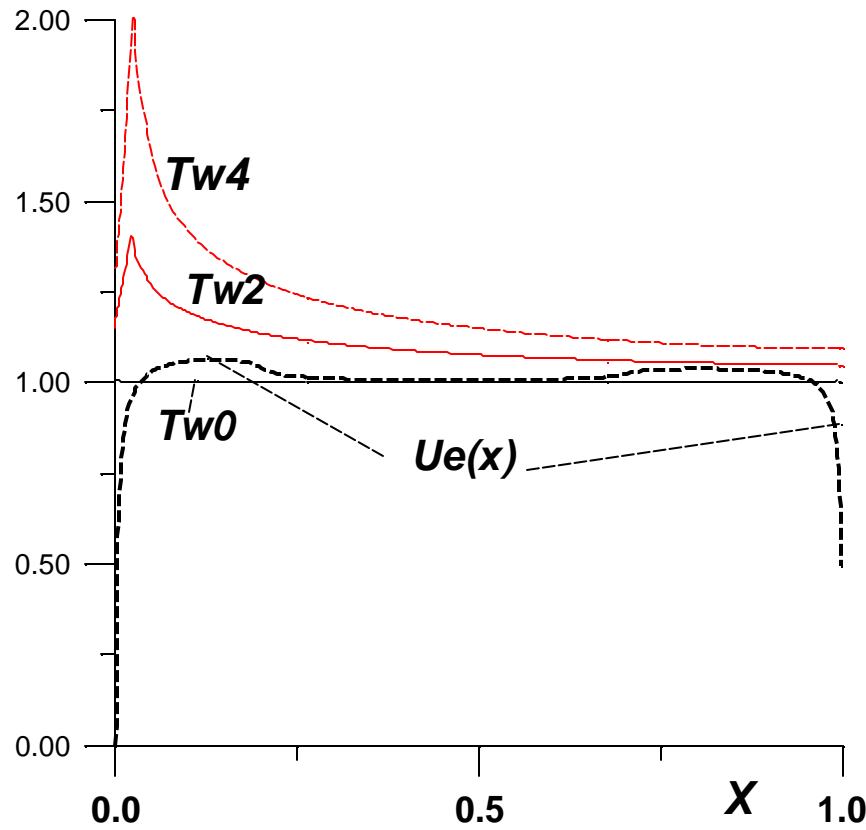

Fig.10.6. Distributions of the wall temperature and the external flow velocity.

It should be emphasized that the previous authors studies show that surface heating near the body leading edge can cause the laminar-turbulent transition delay and friction and drag reduction [10.15]. Of course, in order to obtain the total drag coefficient of the model it required to calculate not only laminar friction in boundary layer and laminar-turbulent transition position, but, although, to calculate the turbulent boundary layer flow and its skin friction coefficient along the rest of the body, where boundary layer must be considered as turbulent. In order to study the influence of the electric discharge heat supply on the laminar-turbulent transition and local skin friction coefficient, the numerical calculation of the laminar boundary layer flow were carried out using the inviscid flow parameters that were obtained by viscid flow calculation and demonstrated in previous report.

In view the fact that experimental data of temperature distribution along the model is absent, the required wall temperature distribution was taken from the mentioned above numerical calculation of the flow over the model with additional volumetric energy supply on the base of the full two- dimensional Navier-Stokes equations system with supplementary $k - e$ turbulence model equations. In case at assuming that for time moments or small time period after the moment, when electric discharge was off, the surface temperature distributions will be in close

agreement. The temperature distributions were obtained for different total energy input calculations and have been demonstrated in Fig. 10.3
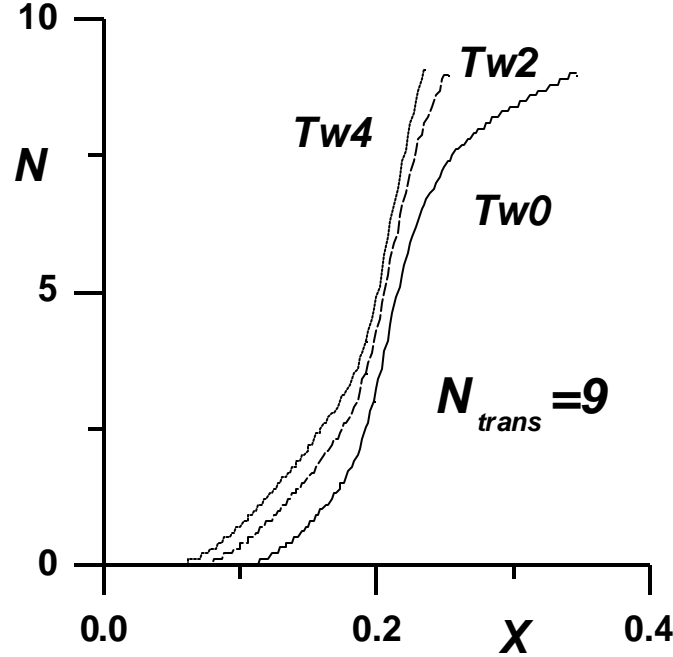

Fig.10.7. Integral increments of growth of linear disturbances.

The boundary layer calculation were carried out for the free stream velocity $u_\infty = 50$m/s and free stream pressure and temperature $p_\infty = 10^5$Pa and $T_\infty = 20°$C respectively. The non-dimensional temperature distributions for three different energy input that are 0kW, 2kW, and 4kW, designated as T_{W0}, T_{W2}, T_{W4}, as well as non-dimensional velocity distribution $U_e(X)$ along the model axis are presented on the Fig. 10.6.

Using the obtained boundary layer flow profiles the laminar-turbulent transition position was calculated on he base of the compressible boundary layer linear stability and well known e^N method [10.15, 10.16]. It is assumed that laminar-turbulent transition location corresponds to the N=9. The Fig.10.7. demonstrates the integral growth rates of the disturbances and laminar-turbulent transition location for different surface temperature distributions that correspond to the volumetric energy supply along the model axis 0kW, 2kW, and 4kW.

Thus, the calculation shows that for surface heating and surface temperature distributions that correspond to the these three different cases (no energy input, and two different energy input with 2kW, and 4kW) laminar-turbulent transition move to the leading edge of the model. Of course, in this case the laminar portion of the boundary layer will be decreased and, on the contrary, the portion of turbulent flow will be increased. In order to estimate the total drag of the model it is required to calculate the local and integral drag coefficient in the laminar and turbulent parts of the boundary layer.

10.5.4. Turbulent boundary layer and total skin friction

Numerical simulation of turbulent boundary layer is based on Chien's $k - e$ model of turbulence [10.9]. To obtain the initial conditions for turbulent boundary layer calculation the

following procedure is used. Numerical solution starts from laminar profiles of velocity and temperature in section corresponding to the beginning of laminar-turbulent transition. Then only first four equations of continuity, momentum, energy and state are solved with the coefficient of turbulent viscosity defined as $m_t = f_{tr}(x) \, m_{ta}$, where $f_{tr}(x)$ is transition function which varies from zero up to unity at a short distance, and m_{ta} is defined by algebraic model of turbulence of Cebeci-Smith [10.8].
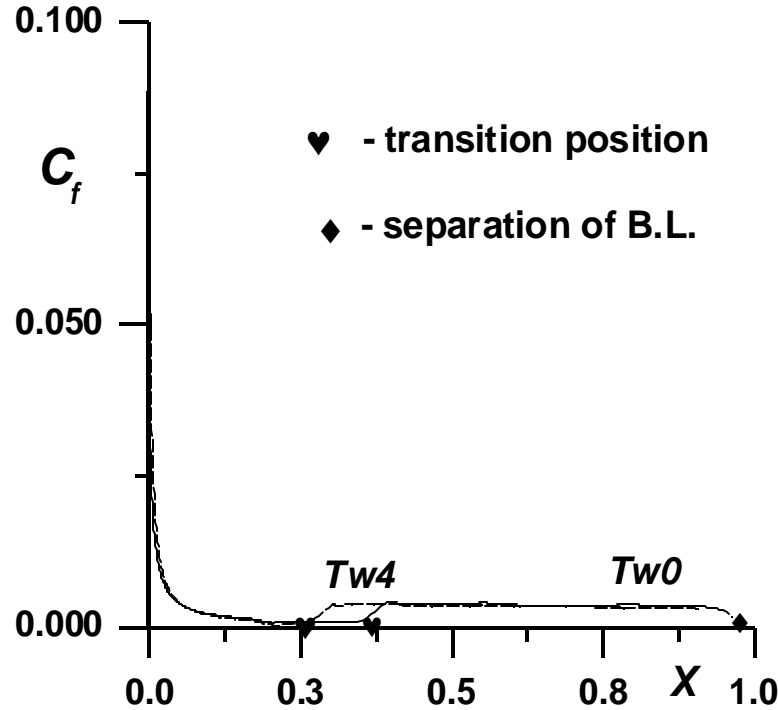

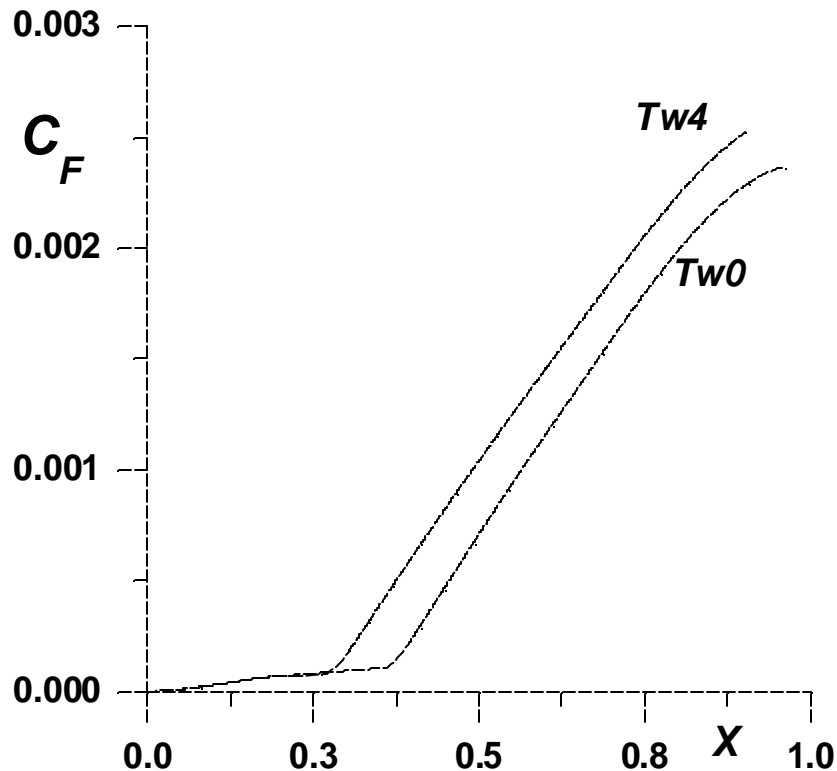Fig. 10.8. The local skin friction distributions.

Fig. 10.9. The total skin friction distributions.

When the function f_{tr} achieves unity the equation for kinetic energy of turbulence k includes in solution procedure with and initial zero profile of k. The kinetic energy of turbulence begins to grow in next boundary layer sections due to a source term in equation for k. When this function becomes positive in all y-grid points except $y=0$ and $y=y_e$ the equation for dissipation rate of turbulence e includes in the solution still with $m = m_{la}$. Similar to k, e increases gradually due to generation term in its equation. After several sections the dissipation rate of turbulence becomes positive across the boundary layer except the boundary points and then the coefficient of turbulent viscosity is calculated according to $k - e$ model [10.9].

The results of calculations of the local and total skin friction coefficients on the model surface both in laminar and turbulent parts of boundary layer are shown in Fig. 10.8 and Fig. 10.9 respectively for two surface temperature distributions T_{w0} and T_{w4} presented above. One can see that the total skin friction on heated surface is greater then on unheated one because of more earlier laminar-turbulent transition.

CONCLUSIONS

1. The analysis that was carried out in the frame of this work showed that the problem of the energy expenditure decrease at the attempts of the discharge methods use for aerodynamic characteristics improvement putted forward the boundary layer as a possible perspective field in this direction. In particular, the fulfilled estimations showed that the method of the influence on the laminar sublayer of turbulent flow with help of the local zones of the near surface heat output in the discharges could provide the sizes of the local unevenness that were necessary for the turbulent friction decrease. However the additional experimental verification of the method of the discharge zone localization in the gas flow is necessary.

2. For the axisymmetric model in form of fuselage that had the diameter d =100 mm, length equal 900 mm (at elongation of the tail part λ_{tail}=1.5) or 1000 mm (λ_{tail}=3), the experimental investigations have been carried out more than 15 configurations of the model with obstacles which imitated various types of the electrodes of discharge generators. On the base of the direct balance measurements at Re_d =(.8–4.2)·10^5, it was shown that the definite configuration electrodes arrangement near the scorn part of the model (at λ_{tail}=1.5) led, in the range of Re_d =(.8–1.6)·10^5, to decrease in the drag on 9–35 %.

3. The experimental study of nose part surface heating influence on the drag was carried out at various localization of zone of heating from positions of the possible analogous action of near surface discharges. These experiments show that the localization of the heated zone in the area of the negative pressure gradient causes the remarkable drag reduction. The balance measurements that were carried out for the model without the developed scorn zone of separation (λ_{tail}=3) showed that the local heating of the nose part, at $0 < X/L <$.035 in the zone of the negative pressure gradient, up to the surface temperature $\overline{T}_W$ =2 led to the drag decrease in 2 – 8 % at Reynolds numbers Re_L =(1.–4.2)·10^6 characteristic for the area of the transition.

4. The experiments at atmospheric pressure that were carried out on the local near surface discharges creation at the use of the source of energy of 27 MHz showed many point capacitive discharges could serve a large area of surface of a streamlined body. The experiments showed that the material of the dielectric that bore such discharges without essential destruction at moderate powers was teflon. The best results on the discharges burning were obtained on the electrodes that had got the geometry of the multi line system of the sharp points or teeth. In this case, the steady burning of the large number of the local near surface discharges was realized simultaneously. The maximum number of the discharge dots was more than 200 on the area of 100 mm by 45 mm at active power input about 350 – 450 W and the density of the discharge points equal 4.5 cm^{-2}. It can be noted that, at the further experiments, one can obtain corresponding results on the plates of larger sizes.

5. The first experiments on plasma aerodynamics of the boundary layer was carried out in the wind tunnel T – 36I with use of the generator of high voltage pulses which worked out in frame of this contract. It has got the regulated amplitude of the voltage in the range 4 – 12 kV; the frequency of following of pulses and the duration of them are varied in the ranges 3 – 20 kHz and 5 – 50 μs, correspondingly. The generator was connected to the electrode systems of the "riblet" types that were installed either on the lower wall of the wind tunnel before the floating element of the balance or on this element directly or on the model of the flat plate. The experiments were carried out both at the turbulent regime of a flow over a body and at the regime of the laminar/turbulent transition. The tests at the first regime showed that influence of the discharge on the skin friction was absent at the frequency of the pulses in the range 3.6 – 20 kHz and the density of power input equal 0 – 1 W/cm^2 . The balance and hot wire anemometric tests at the second regime showed that, at the initial stage of transition (intermittence coefficient equaled $0<\gamma\leq.5$), the plasma generator of investigated type in view of the strings stretched along a flow ($d_W^+ \approx 2\div15$, $\Delta z_W^+ \approx 50\div300$) laminarized the flow without discharge. At the density of power input equal or more than $.3 W/cm^2$, the discharge generator system exerted turbulizing influence on the flow. This result was also obtained in the hot wire anemometric tests for the flat plate on the leading edge of which the discharge generator was arranged.

6. For obtaining of possibility of the numerical determination of the parameters of the gas flow in a neighborhood of region of the heat generation and also at the simulating conditions of the "cold" tests, the asymptotically grounded simplification of the total Navier-Stokers equations was carried out. Corresponding calculations together with the data of the "cold" experiments are supposed to use for determination of the rational geometric parameters of the electrodes system.

7. Two variants of the boundary layer state on experimental model have been considered in theoretical research, namely, the fully turbulent boundary layer and laminar-turbulent boundary layer. The numerical evaluations of skin friction and drag coefficient have shown that at a presence of a laminar part of the boundary layer flow, a surface heating can lead to a

decrease of this part (at least for temperature distribution considered) and, as a consequence, lead to an increase of total skin friction and the total drag of the model considered. On the contrary, in the case of fully turbulent boundary layer, that was simulated numerically on the base of full two-dimensional Navier-Stokes equations system with taking into account the standard low-Reynolds number $k-\varepsilon$ turbulent shear stress model, an local volumetric energy supply and the corresponding increase of the surface temperature results in a remarkable drag reduction. Thus, the theoretical studies make possible to conclude that the total drag reduction induced by a near-wall electric discharge and observed in appropriate TsAGI's experiments at subsonic speeds can be explained by a skin friction reduction produced by the volumetric energy supply and associated surface heating in the fully turbulent boundary layer that begins almost immediately from the model nose.

8. The next experiments on development of discharge flow control should be accomplished in turbulent regimes at multi point surface discharge.

9. The qualitative analysis shows that for more effective flow (and drag) control at conditions of repetitively-pulsed electric field its temporal and space parameters should be correlated with properties of used electrode system

REFERENSES

1.1. A.V. Boijko, G.R. Grek, V.V. Kozlov Arising of Turbulence in Near Wall Flows // Nauka, 1999.

1.2. L. Sirovich, S. Karisson Turbulent drag reduction by passive mechanisms // Nature, 1997, V. 388/21 PP 753 – 755.

4.1. Chang P.K. Separation of Flow. Oxford. Pergamon Press. 1970.

4.2. Fluid Dynamic Drag. Ed. by Hoerner S.F. Washington. 1958.

4.3. Repik E.Y., Korobkina L.S. To the Question of the Choice of a Turbulizater Fixing Transition of a Laminar Boundary Layer to Turbulent One // Izvestia SO AN SSSR. 1988 Vol. 15. No 4 (in Russian).

4.4. Schlichting H. Boundary Layer Theory. New York. McGraw – Hill. 1968.

4.5. Winter K.G. An Outline of the Techniques Available for the Measurement of Skin Friction in Turbulent Boundary Layers // Progress in Aerospace Science. 1977. No. 18. Issue 1.

5.1. E. Coustols, A.M. Savill. Turbulent skin friction drag reduction by active and passive means. AGARD-R-786. Special Course on Skin Friction Drag Reduction. 1992.

5.2. A.V. Kazakov, M.N. Kogan, V.A. Kuparev About raising the stability of a subsonic boundary layer by heating of a surface near its leading edge // Dokl. AN SSSR,1985, V. 283. No2. PP.333-385.

5.3. A.V. Kazakov, M.N. Kogan Laminar-Turbulent Transition Delay by Intensive Local Surface Heating Near Flat Plate Leading Edge // High Temperature, 1996, V. 34, No 1, PP. 46-51.

6.1. I.A. Belov, V.M. Litvinov, A.V. Kazakov, M.N. Kogan, V.A. Kuparev Laminar Boundary Layer Stability and Delayed Transition on a Nonisothermal Surface // Izv. Acad. Nauk,

Mekh. Zhidk. Gaza, 1989, No 2 PP. 52-57.

6.2. G.R. Grek, V.V. Kozlov, S.V. Titarenko, G.B. Klingmann. The influence of riblets on a boundary layer with embedded streamwise vortex //Phys. Fluids A. – 1995. –Vol. 7(10). – P. 2504 –2506.

6.3. G.R. Grek, V.V. Kozlov, S.V. Titarenko An experimental study on the influence of riblets on transition // J. Fluid Mech. –1966. Vol. 315.-P. 31 – 49.

10.1. Efimov B.G., Kuznetsov Yu.E., et al. The experimental investigation of the influence the quasistatic plasma generator operation on the axisymmetric body drag in subsonic flow // Preprint TsAGI. 1992. No. 66. 36p.

10.2. Malik M.R., Orszag S.A. "Efficient computation of the stability of three-dimensional compressible boundary layer" // AIAA Paper ? 81-1277, 1981.

10.3. Srokowski A.J., Orszag S.A. "Mass flow requirements for LFC wing design" // AIAA Paper ? 77-1222, 1977

10.4. Kazakov A.V., Kuryachii A.P. "Effect of anisothermicity of the surface of the thin airfoil on the stability of the laminar boundary layer" // Izv. Akad. Nauk SSSR, Mekh. Zhidk. Gasa, 36, 1986.

10.5. Kazakov A.V. Kogan M.N., Kuparev V.A. "Optimization of laminar-turbulent transition delay by means of local heating of the surface" // Fluid Dynamics, Vol. 30, ? 4, 1995

10.6. Kuryachii A.P. About turbulent drag reduction due to local surface heating // 19th ICTAM, Kyoto, Japan, Aug. 25-31, 1996. Abstacts. P. 557.

10.7. Kuryachii A.P. Simulation of the thermal method for reducing turbulent friction // Fluid Dynamics. 1998. Vol. 33. No. 1. P. 48-55

10.8. Cebeci T., Smith A.M.O. Analysis of turbulent boundary layers. Academic Press: N.Y., 1974. 404 p.

10.9. Chien K.Y. Prediction of channel and boundary-layer flows with a low-Reynolds-number turbulence model // AIAA Journal. 1982. Vol. 20. No. 1. P. 33-38.

10.10. Zhang H.S., So R.M.C., Speziale C.G., Lai Y.G. Near-wall two-equation model for compressible turbulent flows // AIAA Journal. 1993. Vol. 31. No. 1. P. 196-199.

10.11. Sommer T.P., So R.M.C., Zhang H.S. Near-wall variable-Prandtl-number turbulence model for compressible flows // AIAA Journal. 1993. Vol. 31. No. 1. P. 27-35.

10.12. Carvin C., Debieve J.F., Smits A.J. The near-wall temperature profile of turbulent boundary layer // AIAA Paper. 1988. No. 136. 8 p.

10.13. Denisenko O.V., Provotorov V.P. Analysis of viscous gas flows at moderate Reynolds numbers // Proc. TsAGI. 1985. No. 2269. P. 111-127 (in Russian).

10.14. Speziale C.G., Abid R., Anderson E.C. A critical evaluation of two-equation models for near-wall turbulence // AIAA-Pap. 90-1481.

10.15. Kazakov A.V., Kogan M.N., Kuparev V.A. Stability of subsonic boundary layer on a flat palte with heating of the surface near the leading edge // Izv. Akad. Nauk SSSR, Mekh. Zhidk. Gaza, N 3, 1985